LAWRENCE
LIVERMORE
NATIONAL
LABORATORY

UCRL-ID-151578

Mechanistic Constitutive Models for Rubber Elasticity and Viscoelasticity

M. Puso

January 21, 2003

Disclaimer

This document was prepared as an account of work sponsored by an agency of the United States Government. Neither the United States Government nor the University of California nor any of their employees, makes any warranty, express or implied, or assumes any legal liability or responsibility for the accuracy, completeness, or usefulness of any information, apparatus, product, or process disclosed, or represents that its use would not infringe privately owned rights. Reference herein to any specific commercial product, process, or service by trade name, trademark, manufacturer, or otherwise, does not necessarily constitute or imply its endorsement, recommendation, or favoring by the United States Government or the University of California. The views and opinions of authors expressed herein do not necessarily state or reflect those of the United States Government or the University of California, and shall not be used for advertising or product endorsement purposes.

Auspices Statement

This work was performed under the auspices of the U.S. Department of Energy by University of California, Lawrence Livermore National Laboratory under Contract W-7405-Eng-48.

Mechanistic Constitutive Models for Rubber Elasticity and Viscoelasticity

By

MICHAEL ANTHONY PUSO
B.S. (University of California, Davis) 1987
M.S. (University of California, Davis) 1991

DISSERTATION

Submitted in partial satisfaction of the requirements for the degree of
DOCTOR OF PHILOSOPHY
in
Engineering

in the
GRADUATE DIVISION

of the
UNIVERSITY OF CALIFORNIA
DAVIS

Approved: Yannis F. Dafalias
Richard M Christensen

Committee in Charge

1994

ABSTRACT

Physically based models which describe the finite strain behavior of vulcanized rubber are developed. Constitutive laws for elasticity and viscoelasticity are derived by integrating over orientation space the forces due to each individual polymer chain. A novel scheme is presented which effectively approximates these integrals in terms of strain and strain invariants. In addition, the details involving the implementation of such models into a quasi-static large strain finite element formulation are provided.

In order to account for the finite extensibility of a molecular chain, Langevin statistics is used to model the chain response. The classical statistical model of rubber assumes that polymer chains interact only at the chemical crosslinks. It is known that such model when fitted for uniaxial tension data cannot fit compression or equibiaxial data. A model which incorporates the entanglement interactions of surrounding chains, in addition to the finite extensibility of the chains, is shown to give better predictions than the classical model. The technique used for approximating the orientation space integral was applied to both the classical and entanglement models.

A viscoelasticity model based on the force equilibration process as described by Doi and Edwards is developed. An assumed form for the transient force in the chain is postulated. The resulting stress tensor is composed of an elastic and a viscoelastic portion with the elastic stress given by the proposed entanglement model. In order to improve the simulation of experimental data, it was found necessary to include the effect of unattached or dangling polymer chains in the viscoelasticity model. The viscoelastic effect of such chains is the manifestation of a disengagement process. This disengagement model for unattached polymer chains motivated an empirical model which was very successful in simulating the experimental results considered.

TABLE OF CONTENTS

TITLE PAGE i
ACKNOWLEDGMENTS ii
ABSTRACT iii
INTRODUCTION 1
1. CLASSICAL MODEL FOR RUBBER ELASTICITY 4
    1.1 Introduction 4
    1.2 Development of the Classical Constitutive Model and Approximations 5
2. ENTANGLEMENT MODEL FOR RUBBER ELASTICITY 17
    2.1 Introduction 17
    2.2 Development of the Entanglement Constitutive Model 19
    2.3 Verification of Entanglement Model 24
    2.4 Approximation of Constitutive Model 27
    2.5 Analysis of Results from Entanglement Model 32
3. CONSTITUTIVE EQUATIONS USING VIRTUAL WORK 36
4. VISCOELASTICITY MODELS FOR RUBBER 43
    4.1 Introduction 43
    4.2 Topics from Rheology 44
    4.2 a Polymer Fluids 46
    4.2 b Polymer Melts 51
    4.3 Proposed Force Equilibration Viscoelasticity Model 64
    4.4 Thermodynamic Considerations 69
    4.5 Approximation of the Viscoelastic Backstress 70
    4.6 Comparison of Force Equilibration Viscoelastic Model to Experimental Results 75
    4.7 Evaluation of Results 83
    4.8 Two Network Theory 87
    4.9 Proposed Phenomenological Model 91
    4.10 Conclusions 93
5. FINITE ELEMENT IMPLEMENTATION 96
CONCLUSIONS AND RECOMMENDATIONS 103
REFERENCES 105
APPENDIX A 111
APPENDIX B 114
APPENDIX C 117
APPENDIX D 119

INTRODUCTION

With increased interest in the modeling of tire performance and elastomeric bearings and the development of mechanistic models for filled rubbers and polymer composites it seems that physically based constitutive models for the polymer matrix need be considered. Such models can provide better insight into the effects small filler particles or glass fibers may have on a polymer matrix or how the residual stresses evolve as the rubber passes from the melt stage to the vulcanized rubber in the tire forming process. Rheologists have made significant efforts in characterizing the behavior of polymers and in particular polymer fluids. Meanwhile, the mechanics community has been relatively unaware of the advances made in polymer science. In this work it was intended to draw concepts from the field of rheology and use them to provide polymer models that would be of interest to the mechanical or structural engineer. In this context the models would be based on a limited amount of statistical analysis and would be more intuitive. The constitutive models presented in this work are mainly extensions of theories given by rheologists but in a language comprehensible to an engineer.

The Neo-Hookean model for rubber provides a simple closed form constitutive law and in view of its simplicity gives reasonably good results. The original Langevin statistics model outlined by Treloar (1975) is based on the same kinematics as the Neo-Hookean model, but includes the effects of finite extensible chains. The constitutive equation for the Langevin statistics model is given by an integration over orientation space and can not be solved in closed form. Approximations such that chains are lumped in particular directions have been made. A series approach is used here to approximate the constitutive law. The nature of the expansion made provides a more accurate approximation than has been made in the past. In addition, the approximate constitutive law is in terms of the Cauchy Green tensor and strain invariance, hence no explicit calculation for the principle stretch and principle stretch axes is necessary.

It is known that this Langevin statistical model when fitted for uniaxial tension data cannot fit compression data. This discrepancy is seen to be severe for the data considered in this study* . A constitutive law that could model the behavior in both compression and tension and includes the effects of finite extensible chains was sought. A simple form of entanglement model was generalized such that it included finite extensible chains and fit the experimental data well. The same approximation technique that was used on the classical Langevin statistics model was used to get a closed form for the entanglement constitutive law.

A viscoelastic constitutive law based on the force equilibration concepts given by Doi and Edwards (1986) is proposed. In this model all the chains are assumed to be crosslinked and the viscoelasticity is due to a reconfiguration of chain sections after friction forces from the surrounding polymer network have carried the chain into a non-equilibrium position. An empirical form for the transient force in the chain is postulated. Again, the method for approximating the orientation space integrals proved useful in providing a closed form for the constitutive equation.

Predictions given by the force equilibration model of viscoelasticity compared to experimental data suggested the need to consider the unattached polymer chains. A two network theory is assumed; the network is composed of crosslinked and uncrosslinked chains acting independently. Doi and Edwards (1978) reptation model is used to capture the effects of the unattached chains while the elastic entanglement model is used to capture the effects of the crosslinked chains. In this model only the unattached chains contribute to the viscous stress while only the crosslinked chains contribute to the elasticity.

The two network model suggested a form for an empirical model which was very successful in simulating the experimental results considered. Perhaps, one of the biggest contributions mechanistic models can make is in suggesting phenomenological forms for constitutive equations.

---

* Actually the data for equibiaxial tension is considered here in lieu of compression. The rubber is nearly incompressible, hence results from equibiaxial tension can be considered equivalent to uniaxial compression after the stress is adjusted by a hydrostatic pressure.

1. CLASSICAL MODEL FOR RUBBER ELASTICITY

1.1 Introduction

Many constitutive models are available for modeling rubbery polymers in the large strain regime. Of them, the phenomenological Ogden's method (Ogden, 1972) seems to be the most proficient. These models, for the most part, are relied upon to capture the upturn in stress vs. strain seen at very high strain levels. The upturn is often attributed to the finite extensibility of the polymer chains although in some circumstances it is due to strain induced crystallization depending on the type of polymer considered. In addition to purely phenomenological methods are the so called statistical mechanics models. The Neo-Hookean method which relies on Gaussian statistics does not consider finite extensibility of the molecular chains. Treloar in numerous publications (Treloar, 1975 and 1979; Jones and Treloar, 1975; Vangerko and Treloar, 1978 etc.) , James and Guth (1943), Flory (1961) etc. have given attention to the Langevin statistical model of the polymer which incorporates the finite extensibility effects of deformation. But due to the complex nature of the Langevin function and kinematics it was difficult to arrive at any definitive method to apply the Langevin statistics in a constitutive model. Most of the methods used until recently lumped all the chains in particular orientations and solved the problems accordingly i.e. Flory's 'tetrahedral ' model and James and Guth's 'three chain' model. An eight chain model has also been proposed by Arruda and Boyce (1992). The draw backs of these models have been discussed at quite length. Treloar (1979) used Gauss point integration to incorporate the contributions from all chains to get results for shear and biaxial loading conditions.Wu and Van Der Giessen (1993) compared results from the three, and eight chain models to the numerical integration procedure given by Treloar (1979). The numerical integration procedure is not amenable to general boundary value problems using for instance a finite element procedure. A method which relies on a series expansion of the integral given by Treloar is proposed and can be used to solve generalized boundary problems. Because of the nature of the approximation technique used, the method yields good results for relatively high strains. The theory for rubber in this section does not incorporate effects due to entanglements. This theory will be referred to as the "classical theory" in contrast to the "entanglement model" presented in Section 2.

1.2 Development of the Classical Constitutive Model and Approximations

Rubber is composed of a network of long chain molecules which are connected at junction points by chemical crosslinks. It is commonly assumed that each junction point moves affinely and that each molecular chain vector **r** deforms as a material line. A typical molecular chain is shown in Fig. 1.2.1.

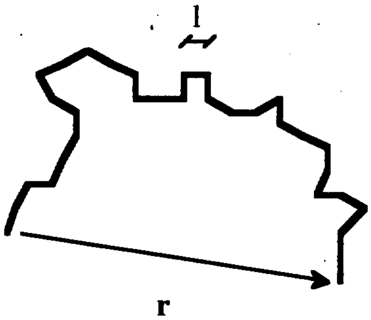

l = length of statistical link

N = number of statistical links per chain

$\mathbf{r}$ = chain vector

r = chain vector length

r_o = initial vector length of chain

Fig. 1.2.1 Typical molecular chain shown in bold along with important parameters

Based on some physical arguments as discussed in Treloar (1975),(1979) the initial chain length is $r_o = \sqrt{N}\, l$. Therefore $r = \lambda\, r_o = \lambda \sqrt{N}\, l$ where λ is the stretch of the chain vector.

Using Langevin statistics to describe the free energy in a polymer chain the following relation is given (Treloar, 1975) :

$$w(\lambda) = -T\, s(\lambda) = N\, k\, T \left(\frac{\lambda}{\sqrt{N}} L^{-1}\!\left(\frac{\lambda}{\sqrt{N}}\right) + \ln \left(L^{-1}\!\left(\frac{\lambda}{\sqrt{N}}\right) / \sinh L^{-1}\!\left(\frac{\lambda}{\sqrt{N}}\right)\right)\right) \qquad (1.2.1\ a)$$

$$L(\beta) = \coth(\beta) - 1/\beta \qquad (1.2.1\ b)$$

where s is the entropy, T is the temperature, L^{-1} is the inverse Langevin function and k is Boltzman's constant . Furthermore to calculate the total amount of free energy per unit volume due to all chains, Eq. 1.2.1 (a) is integrated over all possible orientations as such:

$$W(\lambda) = n\int_0^{2\pi}\int_0^{\pi} w(\lambda)\ C(\theta,\phi)\ \sin\theta\ d\theta\ d\phi \qquad \text{(-1.2.2)}$$

where n is the number of chains per unit volume* , θ and ϕ are the spherical coordinates of the current orientation of a given chain, $\lambda = \lambda(\theta,\phi)$, and $C(\theta,\phi)$ is the orientation distribution function (Wu andVan Der Giessen, 1993) such that $C(\theta,\phi)\sin\theta\ d\theta\ d\phi$ is the fraction of chains in a given direction.

The integral in Eq 1.2.2 is in terms of the variables (θ,ϕ) which represent the current orientation of chains. The initial orientation of a given chain may be represented by the spherical coordinates (Θ,Φ). The deformed and undeformed coordinates are interchangeable and the following transformations are used:

$$(\theta,\phi) = (\theta(\Theta,\Phi;t),\ \phi(\Theta,\Phi;t)) \qquad \text{(1.2.3 a)}$$

$$J = J\,(\Theta,\Phi) = \left|\frac{\partial(\theta,\phi)}{\partial(\Theta,\Phi)}\right| = \frac{\partial\theta}{\partial\Theta}\frac{\partial\phi}{\partial\Phi} - \frac{\partial\theta}{\partial\Phi}\frac{\partial\phi}{\partial\Theta} \qquad \text{(1.2.3 b)}$$

$$d\theta\ d\phi = J\ d\Theta\ d\Phi \qquad \text{(1.2.3 c)}$$

where J is jacobian. Using 1.2.2 and 1.2.3, a change of variables is made from current orientations (θ,ϕ) to initial orientations (Θ,Φ) giving:

$$W(\lambda) = n\int_0^{2\pi}\int_0^{\pi} w(\lambda)\ C(\theta,\phi)\ J\ \sin\theta\ d\Theta\ d\Phi \qquad \text{(1.2.4)}$$

Conservation of the number of chain vectors between the deformed and undeformed configuration requires that $C(\theta,\phi)\sin\theta\ d\theta\ d\phi = C(\Theta,\Phi)\sin\Theta\ d\Theta\ d\Phi$. Using (1.2.3 c) along with the assumption that the initial distribution of the chains is isotropic, i.e. $C(\Theta,\Phi) = 1/4\pi$, yields $C(\theta,\phi)\ J\sin\theta\ d\Theta\ d\Phi = (1/4\pi)\sin\Theta\ d\Theta\ d\Phi$. Hence, Eq. (1.2.4) becomes,

$$W(\lambda) = n\int_0^{2\pi}\int_0^{\pi} w(\lambda)\ \frac{\sin\Theta}{4\pi}\ d\Theta\ d\Phi \qquad \text{(1.2.5)}$$

---

* The rubber is assumed to be incompressible, hence no distinction is made between deformed and undeformed volume

Now the free energy in a chain $w(\lambda)$ is given by 1.2.1 while the average force in the chain is given by:

$$f(\lambda) = \frac{dw(\lambda)}{dr} = \frac{dw(\lambda)}{d\lambda}\frac{1}{\sqrt{N}\,l} = \frac{kT}{l}L^{-1}\left(\frac{\lambda}{\sqrt{N}}\right) \qquad (1.2.6)$$

where use of $r = \lambda\sqrt{N}\,l$ is made. Although Eq. 1.2.6 will not be needed explicitly, derivatives of the free energy "w" will be necessary and the inverse Langevin function will be necessary. There is no closed form for the inverse Langevin function. The function can only be found by numerically solving the inverse problem of Eq. 1.2.1 (b) or by a series representation which due to its infinite limit at $\lambda = \sqrt{N}$, converges very slowly at high extensions. A highly accurate approximation was sought for the inverse Langevin function to solve this problem. The approximation given by Eq. 1.2.7 is proposed and is plotted in Fig. 1.2.2 along with the numerical inverse to Eq. 1.2.1 (b).

$$L^{-1}\left(\frac{\lambda}{\sqrt{N}}\right) \approx \frac{3\frac{\lambda}{\sqrt{N}}}{1-\left(\frac{\lambda}{\sqrt{N}}\right)^3} \qquad (1.2.7)$$

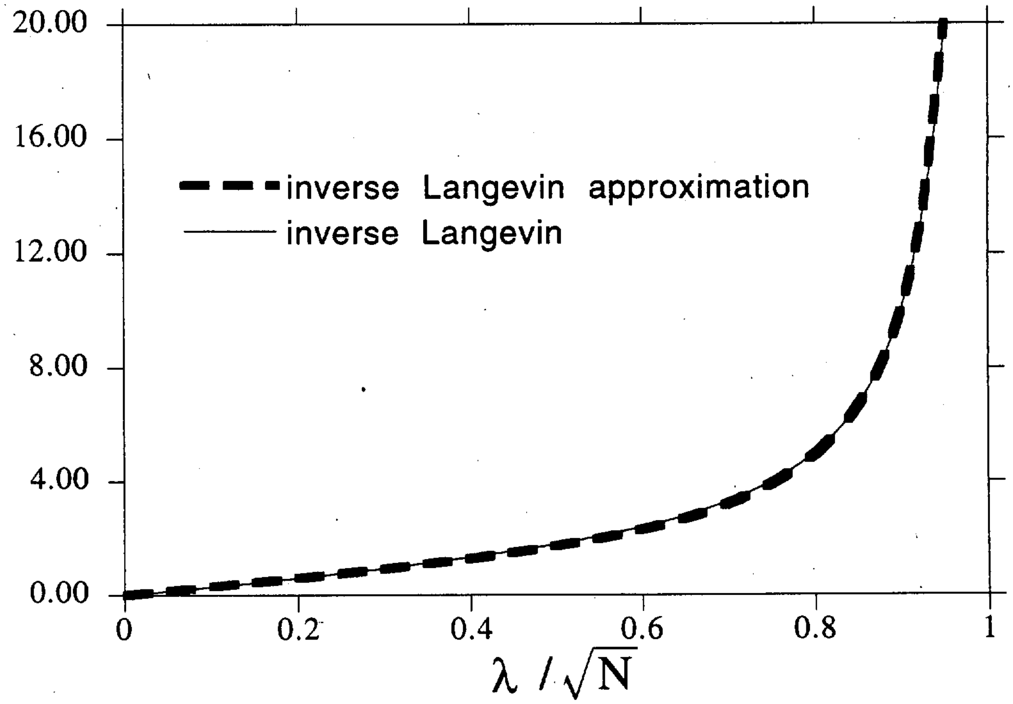

Fig. 1.2.2 Inverse Langevin from numerical solution to Eq. 1.2.1 (b) plotted with inverse Langevin approximation Eq. 1.2.7. Both functions go to infinity as $\lambda / \sqrt{N}$ goes to 1.

Integrating 1.2.7 gives the following approximation to Eq. 1.2.1 for the free energy of a stretched chain :

$$w(\lambda) \approx NkT\left(\frac{1}{2}\ln\left(\frac{1+\lambda/\sqrt{N}+(\lambda/\sqrt{N})^2}{(1-\lambda/\sqrt{N})^2}\right) - \sqrt{3}\,\mathrm{Tan}^{-1}\left(\frac{1+2\lambda/\sqrt{N}}{3}\right)\right) \qquad (1.2.8)$$

Substitution of 1.2.8 into 1.2.5 gives the following approximation for the total strain energy which is not integrable analytically.

$$W(\lambda) = NnkT\int_0^{2\pi}\int_0^{\pi}\left(\frac{1}{2}\ln\left(\frac{1+\lambda/\sqrt{N}+(\lambda/\sqrt{N})^2}{(1-\lambda/\sqrt{N})^2}\right) - \sqrt{3}\,\mathrm{Tan}^{-1}\left(\frac{1+2\lambda/\sqrt{N}}{3}\right)\right)\frac{\sin\Theta}{4\pi}\,d\Theta\,d\Phi$$

(1.2.9)

It is clear that the three chain method of James and Guth is a Gauss point approximation of Eq. 1.2.5 where six Gauss points are used and located on the Lagrangian principle axes of strain. Eq. 1.2.10 illustrates James and Guth's method.

$$W(\lambda) = \frac{n}{3}\left(w(\lambda_1) + w(\lambda_2) + w(\lambda_3)\right)$$

$$\sigma_i = \lambda_i \frac{\partial W}{\partial \lambda_i} + p$$

(1.2.10)

Where σ_i and λ_i are the principle stress and principle stretch respectively. Such a method gives the free energy as a function of principle stretches and has the appearance of Ogden's method. Methods in terms of principle stress are not the most efficient to implement into a finite element procedure. Furthermore, as shown in Van Der Giessen (1993), Treloar (1979) and further on here, the three chain method is much stiffer than the exact (numerical integration) solution to Eq. 1.2.5. The unit vector for the direction cosines of the chain vector **r** in the Lagrangian coordinate system is denoted **M** (see Fig. 1.2.3) such that

$$\mathbf{M} = (M_1, M_2, M_3) = (\sin\Theta\cos\Phi, \sin\Theta\sin\Phi, \cos\Theta) \qquad (1.2.11)$$

This convention (1.2.11) will be used throughout this work. It can be shown that the method by Arruda and Boyce results from a Gauss point integration of Eq 1.2.5 with eight Gauss points at the spherical coordinate positions $(\Theta,\Phi) \approx (54.74^\circ, 45^\circ), (54.74^\circ, 135^\circ), (-54.74^\circ, 45^\circ)$ etc. such that the directions cosines have the following values:

$$(\sin\Theta\cos\Phi, \sin\Theta\sin\Phi, \cos\Theta) = (\pm 1/\sqrt{3}, \pm 1/\sqrt{3}, \pm 1/\sqrt{3})$$

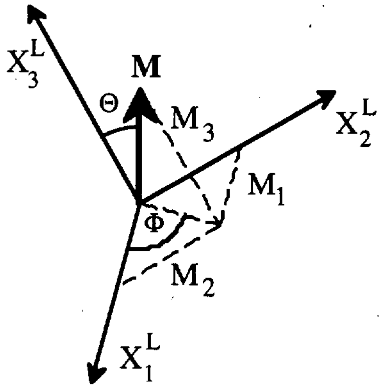

Fig. 1.2.3 The Lagrangian principle coordinate system with spherical coordinates (Θ,Φ) and unit vector $\mathbf{M} = (M_1, M_2, M_3) = (\sin\Theta\cos\Phi, \sin\Theta\sin\Phi, \cos\Theta)$

At this orientation $\lambda^2 = \mathbf{M}^T\,\mathbf{C}\,\mathbf{M} = I_1 / 3$ where **C** is the diagonal Green strain tensor in the principle coordinate system. Where I_1 and I_2 are the first and second invariants defined as such $I_1 = \mathrm{tr}\,\mathbf{C}$ and $I_2 = 1/2\,(\,(\mathrm{tr}\,\mathbf{C})^2 - \mathrm{tr}\,\mathbf{C}^2\,)$. Since the stretch $\lambda = \sqrt{I_1 / 3}$ at this orientation, the following is the Gauss point approximation for the strain energy and stress:

$$W(\lambda) = n\, w(\sqrt{I_1 / 3}) \qquad (1.2.12\text{ a})$$

$$S_{KL} = n \frac{\partial w(\sqrt{I_1 / 3})}{\partial I_1} \frac{\partial I_1}{\partial C_{KL}} + p\, F_{kK}\, F_{kL} \qquad (1.2.12\text{ b})$$

or, with $w(\lambda)$ given by Eq. 1.2.1 such that its derivative follows from Eq. 1.2.6, Eq. 1.12 (b) is rewritten,

$$S_{KL} = n\,k\,T \frac{1}{3} \frac{L^{-1}(\sqrt{I_1/3})}{\sqrt{I_1/3}} \delta_{KL} + p\, F_{kK}\, F_{kL} \qquad (1.2.12\text{ c})$$

where S_{KL} is the second Piola Kirchoff stress, p the pressure and F_{kK} the deformation gradient. As shown in Wu and Van Der Giessen (1993) and further on here the eight chain model tends to be rather soft compared to the exact solution to Eq. 1.2.2.

The solution proposed here yields Arruda and Boyce's eight chain model as a first approximation and becomes closer to the exact solution as terms are added. The method applies a Taylor series expansion about $\lambda^2 = I_1 / 3$ to any function of λ such as Eq. 1.2.8 yielding:

$$w(\lambda) = w(\sqrt{I_1/3}) + \left[\frac{\partial w(\lambda)}{\partial(\lambda^2)}\right]_{\lambda^2=\frac{I_1}{3}} (\lambda^2 - \frac{I_1}{3}) + \frac{1}{2}\left[\frac{\partial^2 w(\lambda)}{\partial(\lambda^2)^2}\right]_{\lambda^2=\frac{I_1}{3}} (\lambda^2 - \frac{I_1}{3})^2 +$$

$$\frac{1}{3}\left[\frac{\partial^3 w(\lambda)}{\partial(\lambda^2)^3}\right]_{\lambda^2=\frac{I_1}{3}} (\lambda^2 - \frac{I_1}{3})^3 + \frac{1}{4}\left[\frac{\partial^4 w(\lambda)}{\partial(\lambda^2)^4}\right]_{\lambda^2=\lambda^*} (\lambda^2 - \frac{I_1}{3})^4 \tag{1.2.13}$$

As noted before, the stretch $\lambda = \sqrt{I_1 / 3}$ (or $\lambda^2 = I_1 / 3$) in 8 orientations of the spherical coordinates (Θ,Φ) of the Lagrangian principle coordinate system where the direction cosines have the following values:

$$(\sin\Theta\cos\Phi, \sin\Theta\sin\Phi, \cos\Theta) = (\pm 1/\sqrt{3}, \pm 1/\sqrt{3}, \pm 1/\sqrt{3})$$

The energy $w(\lambda)$ could have been expanded about $\lambda = 1$ but more terms would be necessary to get good results. Now the stretch can be expressed in terms of the spherical coordinates by the following:

$$\lambda^2(\Theta,\Phi) = M_K C_{KL} M_L = \lambda_1^2 \sin\Theta\cos\Phi + \lambda_2^2 \sin\Theta\sin\Phi + \lambda_3^2 \cos\Theta \tag{1.2.14}$$

where M_K are the direction cosines, C_{KL} is the Green's strain tensor in the principle coordinate system and λ_i^2 are the ith principle stretches. Dropping the error term (last term) in 1.2.13 and substituting it into 1.2.5 gives,

$$W(\lambda) = n \int_0^{2\pi}\int_0^{\pi} \left[w(\sqrt{I_1/3}) + \left[\frac{\partial w(l)}{\partial (l^2)}\right]_{\lambda^2=\frac{I_1}{3}} (\lambda^2 - \frac{I_1}{3}) + \right.$$

$$\left. \frac{1}{2}\left[\frac{\partial^2 w(\lambda)}{\partial (\lambda^2)^2}\right]_{\lambda^2=\frac{I_1}{3}} (\lambda^2 - \frac{I_1}{3})^2 + \frac{1}{3}\left[\frac{\partial^3 w(\lambda)}{\partial (\lambda^2)^3}\right]_{\lambda^2=\frac{I_1}{3}} (\lambda^2 - \frac{I_1}{3})^3 \right] \frac{\sin\Theta}{4\pi}\, d\Theta\, d\Phi \tag{1.2.15}$$

The only dependence on orientation possessed by Eq. 1.2.15 is due to the λ terms; therefore, only these terms need be integrated over orientation space (unit sphere). Using 1.2.14 the following integrals are evaluated:

$$\frac{1}{4\pi}\int_0^{2\pi}\int_0^{\pi} \sin\Theta\, d\Theta\, d\Phi = 1 \tag{1.2.16}$$

$$\frac{1}{4\pi}\int_0^{2\pi}\int_0^{\pi} \lambda^2 \sin\Theta\, d\Theta\, d\Phi = \frac{\lambda_1^2 + \lambda_2^2 + \lambda_3^2}{3} = \frac{I_1}{3} \tag{1.2.17}$$

$$\frac{1}{4\pi}\int_0^{2\pi}\int_0^{\pi} \lambda^4 \sin\Theta\, d\Theta\, d\Phi = \frac{1}{15}(3\lambda_1^4 + 3\lambda_2^4 + 3\lambda_3^4 + \lambda_1^2\lambda_2^2 + \lambda_1^2\lambda_3^2 + \lambda_2^2\lambda_3^2)$$

$$= \frac{1}{15}(3 I_1^2 - 4 I_2) \tag{1.2.18}$$

$$\frac{1}{4\pi}\int_0^{2\pi}\int_0^{\pi} \lambda^6 \sin\Theta\, d\Theta\, d\Phi = \frac{1}{35}\left(2(\lambda_1^6 + \lambda_2^6 + \lambda_3^6) + 3(\lambda_1^4 + \lambda_2^4 + \lambda_3^4)(\lambda_1^2 + \lambda_2^2 + \lambda_3^2) + \right.$$

$$\left. 2\lambda_1^2\lambda_2^2\lambda_3^2\right) = \frac{1}{15}(5 I_1^3 - 12 I_1 I_2 + 8 I_3) \tag{1.2.19}$$

Using 1.2.16 - 1.2.19 the following integral identities are evaluated:

$$\frac{1}{4\pi}\int_0^{2\pi}\int_0^{\pi} (\lambda^2 - \frac{I_1}{3}) \sin\Theta \, d\Theta \, d\phi = 0 \qquad (1.2.20)$$

$$\frac{1}{4\pi}\int_0^{2\pi}\int_0^{\pi} (\lambda^2 - \frac{I_1}{3})^2 \sin\Theta \, d\Theta \, d\phi = \frac{4}{45} (I_1^2 - 3 I_2) \qquad (1.2.21)$$

$$\frac{1}{4\pi}\int_0^{2\pi}\int_0^{\pi} (\lambda^2 - \frac{I_1}{3})^3 \sin\Theta \, d\Theta \, d\phi = \frac{8}{945} (2 I_1^3 - 9 I_1 I_2 + 27 I_3) \qquad (1.2.22)$$

Substituting (1.2.8) into (1.2.15), taking the appropriate derivatives and using the identities given by (1.2.20) - (1.2.22), Eq. 1.2.15 is integrated giving:

$$W(I_1,I_2,I_3) = NnkT\left[\frac{1}{2} \ln\left(\frac{1 + (I_1/3N)^{1/2} + (I_1/3N)}{(1 - (I_1/3N)^{1/2})^2}\right) - \sqrt{3}\,\mathrm{Tan}^{-1}\left(\frac{1 + 2\,(I_1/3N)^{1/2}}{3}\right) + \right.$$

$$\left.\frac{3}{10}\,\frac{(I_1/3N)^{3/2}}{(1 - (I_1/3N)^{3/2})^2}\left(I_1 - 3\frac{I_2}{I_1}\right) + \frac{1}{70}\,\frac{(I_1/3N)^{3/2} + 5\,(I_1/3N)^{3/2}}{(1 - (I_1/3N)^{3/2})^3}\left(2\,I_1 - 9\,\frac{I_2}{I_1} + 27\,\frac{I_3}{I_1^2}\right)\right] \qquad (1.2.23)$$

Because of Eq. 1.2.20 the second term on the right hand side of (1.2.15) vanishes. If the rubber is considered incompressible the third invariant I_3 in (1.2.23) may be set equal to 1. The second Piola Kirchoff stress is calculated for isochoric deformations by the following formula:

$$S_{KL} = 2\left(\frac{\partial W}{\partial I_1} + \frac{\partial W}{\partial I_2} I_1\right)\delta_{KL} - 2\,\frac{\partial W}{\partial I_2} C_{KL} + p\,F_{kK}\,F_{kL} \qquad (1.2.24)$$

Where p is the pressure and F_{kL} is the deformation gradient. Substituing Eq. 1.1.23 into Eq. 1.2.24 and taking the derivatives with respect to the invariants gives the third order approximation for the second Piola Kirchoff stress, 3/10

$$S_{KL}=G\left[\frac{1}{(1-(I_1/3N)^{3/2})}+\frac{3}{10}\left(I_1+3\frac{I_2}{I_1^2}\right)\frac{(I_1/3N)^{3/2}}{(1-(I_1/3N)^{3/2})^2}+\frac{9}{5}\left(I_1-3\frac{I_2}{I_1^2}\right)\frac{(I_1/3N)^3}{(1-(I_1/3N)^{3/2})^3}+\right.$$

$$\frac{1}{70}\left(\frac{(I_1/3N)^{1/2}+12\,(I_1/3N)^2+5\,(I_1/3N)^{5/2}}{(1-(I_1/3N)^{3/2})^4}\right)\left(2\,I_1-9\,\frac{I_2}{I_1}+27\,\frac{I_3}{I_1^2}\right)+\frac{1}{210}\left(\frac{(I_1/3N)^{1/2}+5\,(I_1/3N)^2}{(1-(I_1/3N)^{3/2})^3}\right)\times$$

$$\left.\left(-11\,I_1+18\,\frac{I_2}{I_1}-81\,\frac{I_3}{I_1^2}\right)\right]\delta_{KL}+G\,\frac{9}{35\,I_1}\left[\frac{65\,(I_1/3N)^{3/2}-58\,(I_1/3N)^3}{(1-(I_1/3N)^{3/2})^3}\right]C_{KL}+p\,F_{kK}\,F_{kL} \qquad (1.2.25)$$

Where $G = n\,k\,T$ and n is the number of polymer chains per unit volume. Disregarding the third order contribution of the last term on the right hand sides of 1.2.23 (and 1.2.15), the second Piola Kirchoff stress is calculated using 1.2.24 to be:

$$S_{KL}=G\left[\frac{1}{(1-(I_1/3N)^{3/2})}+\frac{3}{10}\left(I_1+3\frac{I_2}{I_1^2}\right)\frac{(I_1/3N)^{3/2}}{(1-(I_1/3N)^{3/2})^2}+\right.$$

$$\left.+\frac{9}{5}\left(I_1-3\frac{I_2}{I_1^2}\right)\frac{(I_1/3N)^3}{(1-(I_1/3N)^{3/2})^3}\right]\delta_{KL}+G\,\frac{9}{5\,I_1}\left[\frac{(I_1/3N)^{3/2}}{(1-(I_1/3N)^{3/2})^2}\right]C_{KL}+p\,F_{kK}\,F_{kL} \qquad (1.2.26)$$

Eq. 1.2.25 represents the second order approximation of the stress. The first order approximation is merely the first term on the right hand side of 1.2.25 along with the pressure contribution,

$$S_{KL}=G\left[\frac{1}{(1-(I_1/3N)^{3/2})}\right]\delta_{KL}+p\,F_{kK}F_{kL} \qquad (1.2.27)$$

Which is seen to be the same expression as that from Arruda and Boyce's method (Eq. 1.2.12) after the approximation for the Langevin function is used (1.2.7). Eq. 1.2.25 is rather formidable, but the second approximation given by Eq. 1.2.26 is not too complicated and is easy to implement in a finite element procedure since it is a function of the invariants. Ogden's method and the three chain model (Eq. 1.2.10) require derivatives of the principle stretch with respect to the strain tensor to give the principle coordinate directions which makes them difficult and inefficient for finite element formulations.

The efficacy of the approximation methods is evaluated. An adaptive numerical integration scheme was used to get highly accurate approximations of the stress from Eq. 1.2.9. The details are described in Appendix A. The adaptive numerical integration gives results to an arbitrary degree of accuracy and hence will be considered the exact solution. Comparison of results for uniaxial loading (see Fig. 1.2.4 a) using the proposed series approximations, the exact numerical solution and the three chain model are shown in Fig. 1.2.5. The material parameters $G = 0.273$ and $N = 75$ were used. The stress "f" represents the force per undeformed area such that $f_1 = \sigma_1/\lambda_1$. Fig. 1.2.5 shows that the 3 chain model (1.2.10) is clearly too stiff. The first, second and third order approximations are given by (1.2.27), (1.2.26) and (1.2.25) respectively. Up until $\lambda_1 \approx 4$, the first, second and third order approximation schemes are coincident. For $4 < \lambda_1 < 7$ the first order approximation begins to deviate considerably from the exact solution whereas the second and third order approximations are close to the exact. For $\lambda_1 > 7$ the series approximations diverge from the exact solution. Although it should be noted that these results are at a relatively high strain since the limiting strain is $\lambda_1 = \sqrt{75} \approx 8.66$.

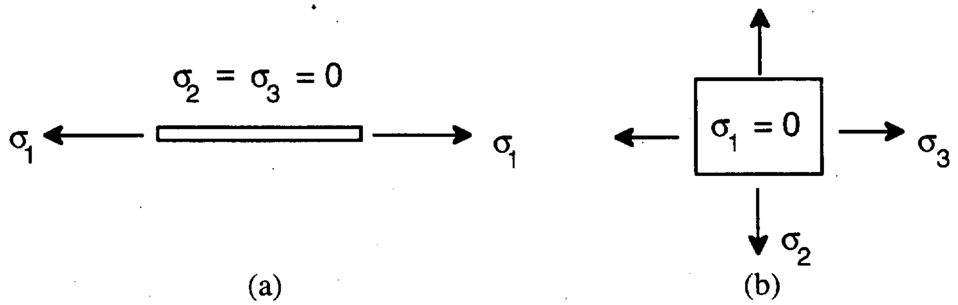

Fig 1.2.4 (a) Uniaxial tension (b) Equibiaxial tension ($\sigma_2 = \sigma_3$)

In Figs. 1.2.6 and 1.2.7 uniaxial and equibiaxial data (Fig. 1.2.4) from James et. al. (1975) is simulated using the exact numerical solution and the series approximation. The stress "f" is the force per undeformed area such that $f = \sigma_1/\lambda_1$ for uniaxial tension and $f = \sigma_2/\lambda_2$ for equibiaxial tension (cf. Fig. 1.2.4 b). The material parameters G = 0.4 and N = 50 were used to model the data. Good fits to the uniaxial data in Fig. 1.2.6 are acheived by the second and third order methods. Again the first order method tends to be too flexible (≈ 20% error at $\lambda_1 = 5$). The second and third order approximations are again very close to the exact solution for equibiaxial tension. For both uniaxial and equibiaxial tension, the second order approximation is nearly as good or better than the third order approximation. It is seen that the equibiaxial stretch data in Fig. 1.2.7 cannot be fitted using the classical theory and its approximations. This is the failure of the classical theory. In Section 2 an entanglement model is developed which seems to give good fits to the experimental data.

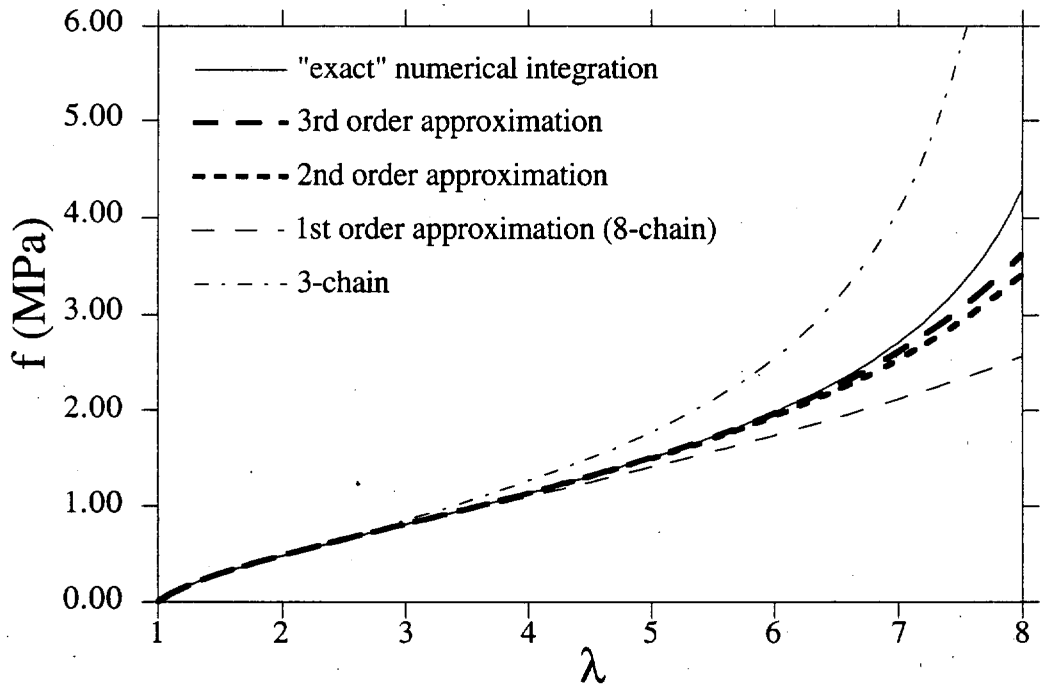

Fig. 1.2.5 Force per undeformed area f versus stretch for uniaxial tension. The three different approximation techniques are compared to the "exact" numerical integration. The material parameters G = 0.273 and N = 75 were used.

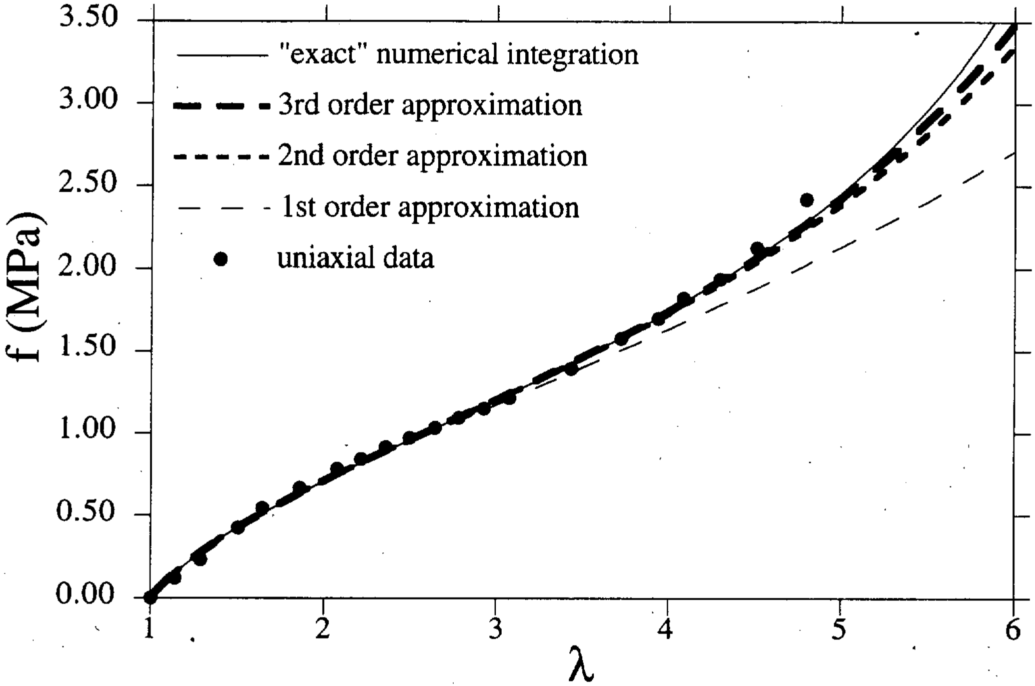

Fig. 1.2.6 Force per undeformed area f versus stretch for uniaxial tension. The three different approximation techniques are compared to the "exact" numerical integration. The experimental data is given by James et. al. (1975). The material parameters G = 0.4 and N = 50 were used.

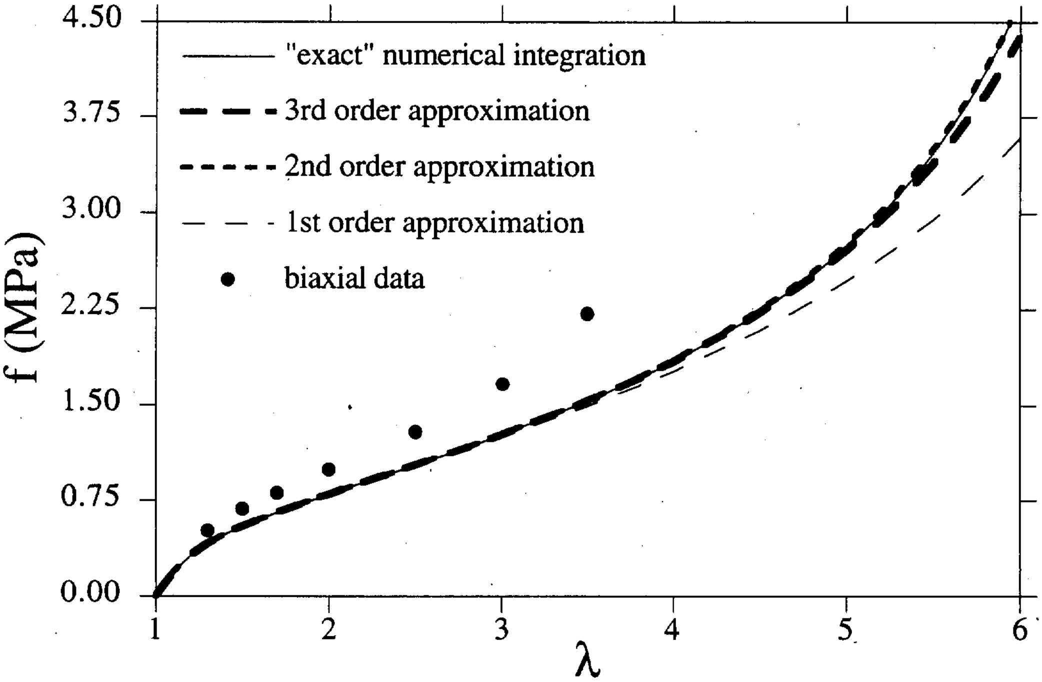

Fig. 1.2.7 Force per undeformed area f versus stretch for equibiaxial tension. The three different approximation techniques are compared to the "exact" numerical integration. The experimental data is given by James et. al. (1975). The material parameters G = 0.4 and N = 50 were used.

2. ENTANGLEMENT MODEL FOR RUBBER ELASTICITY

2.1 Introduction

In the classical theory of rubber elasticity, chemical crosslinks deform affinely and the polymer chains between the crosslinks stretch according to the relative displacement of the crosslinks. The polymer chains are otherwise unaffected by the surrounding network. It is apparent that this theory is insufficient in characterizing much of rubber behavior. For example, it was shown in Figs. 1.2.6 and 1.2.7 that the classical theory could match experimental data for uniaxial tension, but could not additionally simulate equibiaxial tension data at very large stains. There are many other theories of rubber elasticity, but most do not consider effects due to finite extensibility of the polymer chains.

One of the first attempts to modify the classical affine network model of rubber elasticity was the phantom network model (James and Guth,1947; Mark and Erman,1988) in which the crosslinks (except on the surface) were allowed to fluctuate in time without being hindered by the neighboring chains (hence the term phantom network). This theory yielded the same form for the free energy as the classical theory along with a front factor which depended on the functionality of the network (i.e. tetrafunctional):

$$\Delta A = f\,k\,T\,(\lambda_1^2 + \lambda_2^2 + \lambda_3^2 - 3)$$

where ΔA is the difference in free energy and f is the front factor. The crosslinks deformed affinely in the average but the configurational entropy was increased due to lack of constraint. Flory (1977) claimed that the junctions could not fluctuate freely because of the topological restraints of the surrounding network. He proposed the so called constrained junction theory.

Rheologists have suggested that deviations from classical theory may be due to topological constraints on the chain itself as opposed to just constraints on junction fluctuations (Higgs and Gaylord, 1989). Edwards (1977) and Doi and Edwards (1978) were among the first to model the constraining effects of the surrounding molecules on a polymer chain. Doi and Edwards, in work pertaining to polymer melts, argued that the polymer chain was confined to a tube like region or a 'cage' and fluctuates about a primitive chain (Fig. 2.1.1).

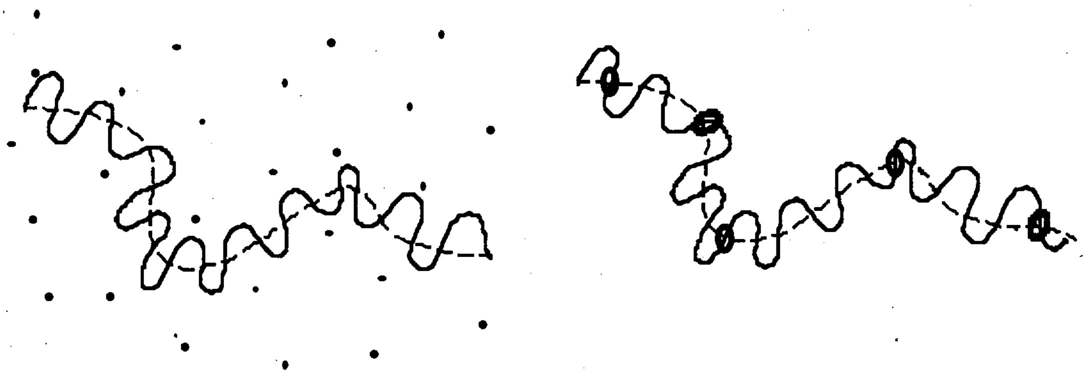

(a) (b)

Fig. 2.1.1 (a) Chain confined to cage formed by surrounding molecules. (b) The slip link model. The polymer molecule is shown as the solid line, the primitive chain is shown as the dotted line and primitive chains of surrounding molecules are shown as dots.

The primitive chain is defined as the average location in time of the chain atoms. It is assumed that the polymer chain remains inside a tube or cage like region formed by the surrounding primitive chains, since the polymer molecules cannot penetrate each other. The cage reduces the number of allowable configurations of the polymer chain, whereas in the classical theory, the polymer chain is allowed to attain all configurations between crosslinks. When the rubber or melt is deformed, it is assumed that the primitive chain is deformed affinely. To simplify the problem, Doi and Edwards introduced so called slip links to capture the topological constraints. The polymer chain is allowed to move freely between slip links. The portions of the chain between slip links are considered subchains and it is assumed that the slip links deform affinely. In the course of deformation, the number of polymer segments between slip links varies such that the tension in each subchain of a given chain is equivalent. This is called chain equilibration by Doi and

Edwards. Marrucci (1979) and Graessley (1981) applied this slip link model to crosslinked polymers. In Marrucci's interpretation, the slip links are just trapped entanglements and the distance between slip links can be defined as the distance between entanglements.

2.2 Development of the Entanglement Constitutive Model

The slip link model was originally derived for the Gaussian range of deformations but can be easily generalized to the non-Gaussian range. In the following, a derivation along the lines of Marrucci's will be given to incorporate the non-Gaussian behavior into the slip link model. The main assumptions in the theory are:

a) The tension in each subchain is the same for all subchains of a given polymer molecule.

b) All network junctions, either crosslinks or entanglements (or slip links), move affinely with the imposed deformation.

Fig. 2.2.1 (a) shows an entangled chain in the undeformed state. The chain has crosslinks at points A and E and trapped entanglements at points B,C and D. Upon deformation (Fig. 2.2.1 b) points A,B,C and D have deformed affinely according to assumption (b) such that line segments AB and CD have shortened and line segments BC and DE have lengthened.

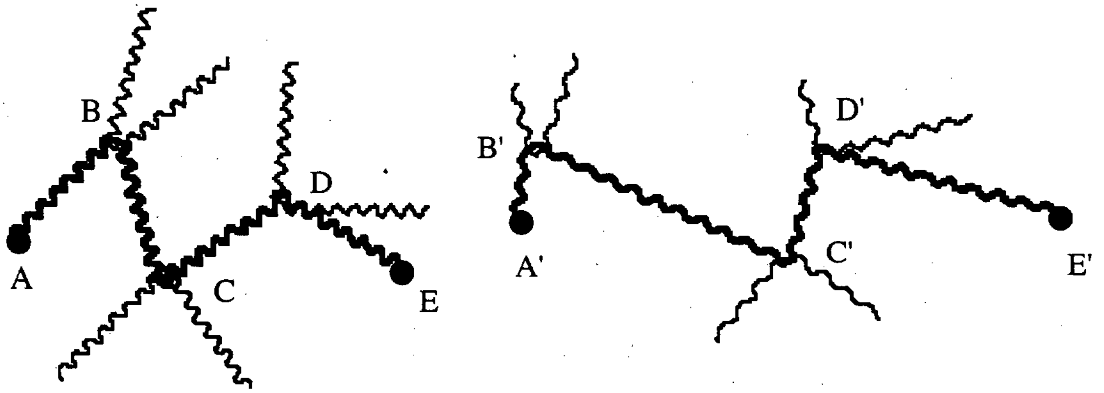

(a) (b)

Fig. 2.2.1 a) Entanglement network in undeformed configuration; b) in deformed configuration. The polymer chain, shown in bold, has crosslinks at A and E and trapped entanglements at B,C and D.

In order for assumption (a) to be satisfied the number of links in subchains A'B' and C'D' have reduced while the number of links between subchains B'C' and D'E' have increased. In the undeformed state it is assumed that all the subchains are of equal length r_o and have N_o statistical links (or monomers links). The undeformed subchain represents a random walk of step length l such that $r_o = \sqrt{N_o}\, l$. After deformation, the ith subchain (Fig. 2.2.2) is of length r_i and contains N_i statistical links.

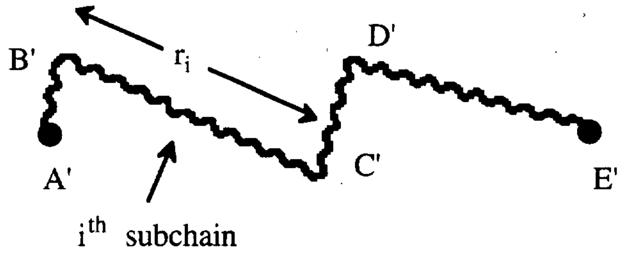

Fig. 2.2.2 i^{th} subchain of polymer chain of length r_i with N_i statistical links.

The polymer chain is composed of N statistical links and n_s subchains such that:

$$\sum_{i=1}^{n_s} N_i = n_s N_o = N \tag{2.2.1}$$

The mean square length of a subchain with N_i sublinks in a relaxed state is $\sqrt{N_i}\, l$ and the length of the stretched chain is

$$r_i = \Lambda_i \sqrt{N_i}\, l \tag{2.2.2}$$

where Λ_i represents the stretch of the ith subchain. Λ_i should not be confused with λ_i which is the stretch of the ith line segment between the entanglement points. For example, in Fig. 2.2.2 λ_i = B'C' / BC where B'C' is the affinely deformed line segment BC, while Λ_i is the stretch of a subchain with N_i links which occupies B'C'. The force in the ith subchain is described by the following relation (Treloar, 1972):

$$f_i = \frac{kT}{l} L^{-1}\left(\frac{r_i}{r_i^{max}}\right) = \frac{kT}{l} L^{-1}\left(\frac{\Lambda_i \sqrt{N_i}\, l}{N_i\, l}\right) = \frac{kT}{l} L^{-1}\left(\frac{\Lambda_i}{\sqrt{N_i}}\right) \tag{2.2.3}$$

where k is Boltzmann's constant, T the absolute temperature, l the length of the statistical link and L^{-1} is the inverse Langevin function. According to assumption (a) the force in all the subchains is equal; therefore for all i,

$$f_i = f \quad \text{and} \; \frac{\Lambda_i}{\sqrt{N_i}} = K \text{ (constant)} \qquad (2.2.4)$$

It remains to relate the constant K to the continuum mechanics of deformation. Now using Eq. 2.2.1 and $\Lambda_i = \sqrt{N_i}\,K$ from Eq. 2.2.4, the cumulative length of the subchains is:

$$\sum_{i=1}^{n_s} r_i = \sum_{i=1}^{n_s} \Lambda_i \sqrt{N_i}\, l = \sum_{i=1}^{n_s} K\ N_i\, l = K\, n_s\, N_o\, l \qquad (2.2.5)$$

The undeformed length between line segments was assumed to be $\sqrt{N_o}\, l$; therefore, according to the affine deformation assumption :

$$\sum_{i=1}^{n_s} r_i = \sum_{i=1}^{n_s} \lambda_i \sqrt{N_o}\, l = \lambda^{avg}\, n_s \sqrt{N_o}\, l \qquad (2.2.6)$$

where λ^{avg} is the average stretch over all sublinks. Because only uniform deformation is considered (i.e. the deformation gradient is independent of position), the stretch λ_i is only a function of the spherical coordinates θ and ϕ. The average stretch can be described by:

$$\lambda^{avg} = \sum_{i=1}^{n_s} \lambda_i \frac{1}{n_s} = \sum_{m=1}^{\tilde{N}} \lambda(\theta_m, \phi_m) \frac{\tilde{n}_m}{n_s} \qquad (2.2.7)$$

where $\tilde{n}_m$ represents the number of subchains in the (θ_m, ϕ_m) direction and $\tilde{N}$ is the total number of orientations. Now if it is assumed that the chain is highly entangled such that there are many subchains and that the undeformed distribution of subchains is isotropic the following approximation can be made:

$$\lambda^{avg} = \sum_{m=1}^{\tilde{N}} \lambda(\theta_m, \phi_m) \frac{\tilde{n}_m}{n_s} \approx \frac{1}{4\pi} \int_0^{2\pi}\!\!\int_0^{\pi} \lambda(\Theta, \Phi) \sin\Theta \, d\Theta \, d\Phi \qquad (2.2.8)$$

where the integral is over the unit sphere and the variables Θ and Φ represent the orientation of the undeformed line segments. It seems reasonable that 2.2.8 is still a good approximation even when the chain is not highly entangled; say for instance a chain containing three subchains in the directions of the principle axes of stretch. The operator $\langle\cdot\rangle$ is standard notation for the average quantity over orientation distribution space such that:

$$\langle\lambda\rangle = \frac{1}{4\pi}\int_0^{2\pi}\int_0^{\pi} \lambda(\Theta,\Phi)\sin\Theta \, d\Theta \, d\Phi \tag{2.2.9}$$

Using Eq. 2.2.5, 6, 8 and 9 gives:

$$K\, n_s\, N_o\, l = \langle\lambda\rangle\, n_s \sqrt{N_o}\, l \tag{2.2.10}$$

or

$$K = \frac{\langle\lambda\rangle}{\sqrt{N_o}} \tag{2.2.11}$$

Therefore, the force in the chain can be calculated using Eq. 2.2.3, 4 and 11 such that:

$$f = \frac{kT}{l}\, L^{-1}\left(\frac{\langle\lambda\rangle}{\sqrt{N_o}}\right) \tag{2.2.12}$$

It remains to find the stress versus strain constitutive relation from Eq. 2.2.12. The easiest way to do this is to derive the free energy function for the solid by summing the contributions from all the polymer chains. The free energy of the ith subchain with length r_i force is defined by the relation:

$$w_i = \int_0^{r_i} f_i\,(r_i)\, dr_i \tag{2.2.13}$$

Using $r_i = \Lambda_i \sqrt{N_i}\, l$ from Eq. 2.2.2 and equating Eq. 2.2.4 and 2.2.11 gives:

$$\Lambda_i = \frac{\sqrt{N_i}}{\sqrt{N_o}}\langle\lambda\rangle \quad \text{and} \quad r_i = \frac{N_i}{\sqrt{N_o}}\langle\lambda\rangle\, l \tag{2.2.14}$$

Using Eq. 2.2.12, 13 and 14 and the fact that $f_i = f$ gives the free energy of the ith subchain in terms of $\langle\lambda\rangle$.

$$w_i = kT\, N_i \int_0^{\langle\lambda\rangle / \sqrt{N_o}} L^{-1}\left(\frac{\langle\lambda\rangle}{\sqrt{N_o}}\right) d\left(\frac{\langle\lambda\rangle}{\sqrt{N_o}}\right) \tag{2.2.15}$$

Using Eq. 2.2.1 and 2.2.15, the free energy of all the subchains is summed to get the free energy for the jth polymer chain:

$$w_j^{chain} = \sum_{i=1}^{n_s} w_i = kT\, n_s N_o \int_0^{\langle\lambda\rangle / \sqrt{N_o}} L^{-1}\left(\frac{\langle\lambda\rangle}{\sqrt{N_o}}\right) d\left(\frac{\langle\lambda\rangle}{\sqrt{N_o}}\right) \qquad (2.2.16)$$

The force in the polymer chain (Eq. 2.2.12) is not dependent on the orientation (i.e. the spherical coordinates) of the chain (unlike the classical theory) and hence all the polymer chains have the same force. The total free energy W is found by summing the contribution of all n polymer chains:

$$W(\langle\lambda\rangle) = \sum_{i=1}^{n} w_j^{chain} = G\, N_o \int_0^{\langle\lambda\rangle / \sqrt{N_o}} L^{-1}\left(\frac{\langle\lambda\rangle}{\sqrt{N_o}}\right) d\left(\frac{\langle\lambda\rangle}{\sqrt{N_o}}\right) \qquad (2.2.17)$$

where $G = n\, n_s\, kT$. To calculate the stress tensor it is necessary to take the gradient of the free energy with respect to the Green's Strain tensor C_{ij} as such:

$$\frac{\partial W}{\partial C_{ij}} = \frac{\partial W}{\partial\langle\lambda\rangle} \frac{\partial\langle\lambda\rangle}{\partial C_{ij}} \qquad (2.2.18)$$

Now $\lambda(\Theta,\Phi) = \sqrt{M_i\, C_{ij}\, M_j}$, where $M_i = M_i\,(\Theta,\Phi)$ is the unit vector along a subchain in the undeformed reference configuration as defined in Eq. 1.2.11. Using Eq. 2.2.9, the derivative of the average stretch with respect to the strain is taken as follows:

$$\frac{\partial\langle\lambda\rangle}{\partial C_{ij}} = \frac{1}{4\pi} \int_{\Omega} \frac{\partial}{\partial C_{ij}} \sqrt{M_k\, C_{kl}\, M_m}\, \sin\Theta\, d\Theta\, d\Phi = \frac{1}{4\pi} \int_{\Omega} \frac{1}{2} \frac{M_i M_j}{\lambda} \sin\Theta\, d\Theta\, d\Phi$$

(2.2.19)

Using Eq. 2.2.17,18 and 19, the Cauchy stress for an incompressible rubber is found to be:

$$\sigma_{kl} = 2\, F_{ki} \frac{\partial W}{\partial C_{ij}} F_{lj} + p\, \delta_{kl} = G \sqrt{N_o}\; L^{-1}\left(\frac{\langle\lambda\rangle}{\sqrt{N_o}}\right) F_{ki} \left\langle \frac{M_i M_j}{\lambda} \right\rangle F_{lj} + p\, \delta_{kl} \qquad (2.2.20\ a)$$

The incompressibility assumption can be relaxed by adding a hydrostatic (bulk) contribution to the strain energy formula Eq. 2.2.17. An alternate form of Eq. 2.2.20 (a) is given:

$$\sigma_{kl} = G\sqrt{N_o}\;L^{-1}\Big(\frac{\langle\lambda\rangle}{\sqrt{N_o}}\Big)\Big\langle \frac{u'_k\,u'_l}{\lambda}\Big\rangle + p\,\delta_{kl}$$

$$= G\sqrt{N_o}\;L^{-1}\Big(\frac{\langle\lambda\rangle}{\sqrt{N_o}}\Big)\Big\langle \lambda\, m_k\, m_l\Big\rangle + p\,\delta_{kl}, \qquad (2.2.20\text{ b})$$

where $u'_k = F_{ki}\,M_i = \lambda\,m_k$ is the deformed unit vector M_k such that $\lambda = (u'_k\,u'_k)^{1/2}$ and m_k is the unit vector along the deformed subchain.

As with the classical theory, the entanglement model relies on two parameters to model elastomer behavior. In the entanglement model the parameter G depends on the total number of subchains and temperature and N_o is the average number of crosslinks between entanglements.

2.3 Verification of Entanglement Model

Numerous investigators have compiled ample experimental data for rubber strained into the non-Gaussian region of behavior (Treloar, 1944; Obata, 1970; Jones and Treloar, 1975; James et. al., 1975; Vangerko and Treloar, 1978; etc.). Results from these tests show that elastomers strained into this region share much qualitative behavior, but that the classical theory using Langevin statistics is insufficient in simulating the experimental data (Treloar and Riding, 1979; Wu and Van Der Giessen, 1993; etc.) In particular, Treloar and Riding (1979) showed that for chosen values of G and N the classical theory could fit uniaxial tension data but not additionally fit the uniaxial compression data. For the class of incompressible materials (which rubber is often assumed to belong) the equibiaxial tension test is equivalent to the uniaxial compression test. Plots which show the tensile stress from the equibiaxial tensile test, as opposed to the uniaxial compressive force, tend to magnify the discrepancy between the classical theory and the actual behavior. As seen from the results of the classical theory shown in Fig. 1.2.7, the equibiaxial tension appears to be grossly underestimated. The entanglement model using Eq. 2.2.20 is used to simulate the same experimental data (James et. al., 1975) for uniaxial tension and equibiaxial tension along with additional pure shear data (see Fig. 2.3.1). Analytical solutions of Eq. 2.2.9 and 2.2.20 are given in Appendix B for uniaxial and equibiaxial deformation. For pure shear deformation Eq. 2.2.20 (see also B.10) was integrated numerically using the procedure outlined in Appendix A.

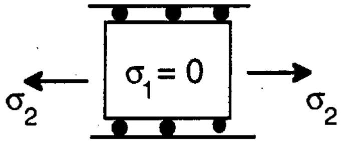

and $\lambda_3 = 1$

Fig. 2.3.1 Pure shear deformation

Eqs. B.4, B.6 and B.10 are used to simulate uniaxial tension, equibiaxial tension and pure shear data given by James et. al. (1975) and Treloar (1944). The results are shown in Figs. 2.3.2 and 2.3.3 in terms of the force per undeformed area f and stretch. The uniaxial tension is in the 1 direction such that $f = \sigma_1/\lambda_1$ (cf. Fig. 1.2.4 a) while for the equibiaxial and pure shear deformation the stress plotted is in the 2 direction such that $f = \sigma_2/\lambda_2$ (cf. Fig. 1.2.4 b and Fig. 2.3.1) . The following material parameters were used to fit the data:

Data from James et. al. (1975)	Data from Treloar (1944)
$G = 0.53$	$G = 0.4$
$N_o = 20$	$N_o = 22$

Table 2.3.1

The entanglement model appears to give good results for the different deformations for both James et. al. (1975) and Treloar's data. In order to illustrate the effect of the finite extensible chains, Fig. 2.3.3 also shows a uniaxial curve for the entanglement model with infinitely extensible chains, i.e. $N_o \rightarrow \infty$. Further analysis is made in Section 2.5

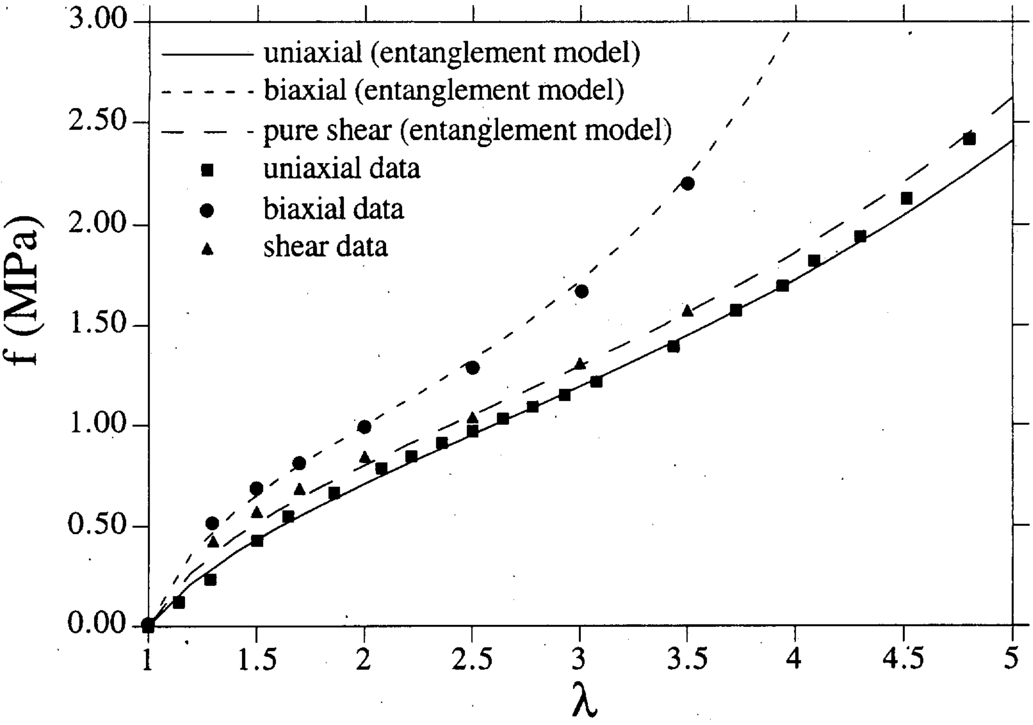

Fig. 2.3.2 Force per undeformed area for uniaxial tension, biaxial tension, and pure shear. The results by the entanglement model Eq. 2.2.20 are given for G = 0.53 and $N_o = 20$. The data is taken from James et. al. (1975).

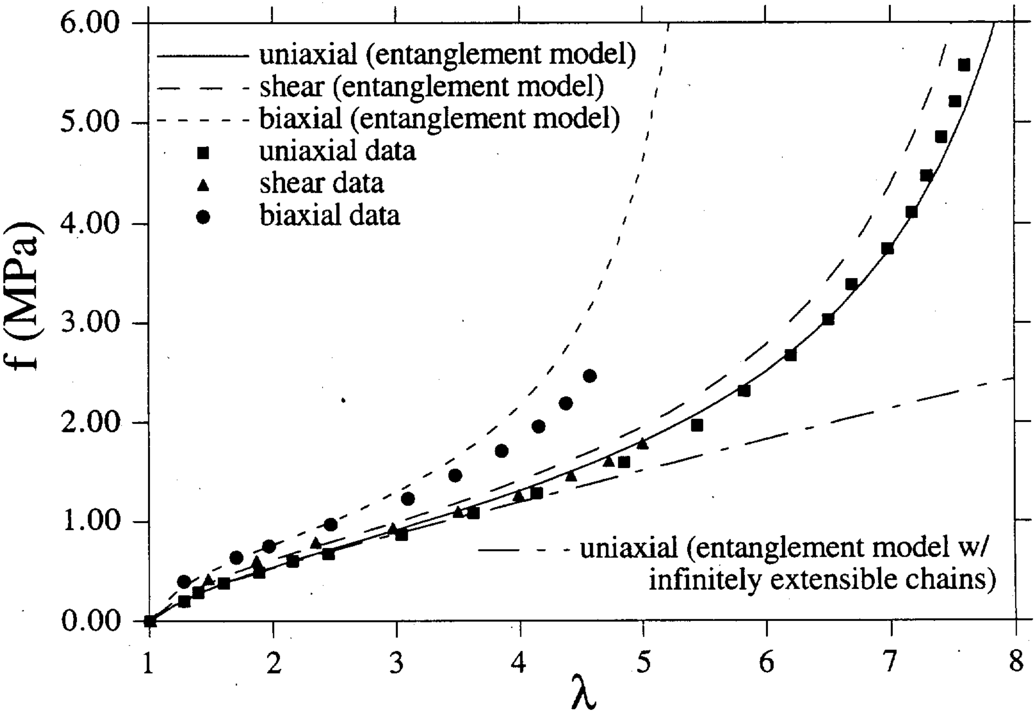

Fig. 2.3.3 Force per undeformed area for uniaxial tension, biaxial tension, and pure shear. The results by the entanglement model Eq. 2.2.20 are given for G = 0.4 and $N_o = 22$. The data is taken from Treloar (1944).

2.4 Approximation of Constitutive Model

The form of the constitutive relation Eq. 2.2.20 is not amenable to general boundary value problems due to the integral over the orientation distribution space. Methods similar to those introduced in Section 1 are used to find a viable approximation to Eq. 2.2.20. The first step in providing the approximation is to get an approximation for the average stretch. A Taylor series expansion about the stretch $\lambda^2 = I_1 / 3$ is used as follows:

$$\lambda(\Theta,\Phi) \approx \sqrt{I_1/3} + \left[\frac{\partial\lambda}{\partial(\lambda^2)}\right]_{\lambda^2=\frac{I_1}{3}} (\lambda^2(\Theta,\Phi) - \frac{I_1}{3}) + \frac{1}{2}\left[\frac{\partial^2\lambda}{\partial(\lambda^2)^2}\right]_{\lambda^2=\frac{I_1}{3}} (\lambda^2(\Theta,\Phi) - \frac{I_1}{3})^2$$

$$= \sqrt{I_1/3} + \frac{1}{2}\left(\frac{I_1}{3}\right)^{-1/2} (\lambda^2(\Theta,\Phi) - \frac{I_1}{3}) + \frac{1}{8}\left(\frac{I_1}{3}\right)^{-3/2} (\lambda^2(\Theta,\Phi) - \frac{I_1}{3})^2 \qquad (2.4.1)$$

where $\lambda^2(\Theta,\Phi) = M_i\, C_{ij}\, M_j$ where $M_i = M_i\,(\Theta,\Phi)$ are the direction cosines and C_{ij} is the Green's strain tensor. The approximation of Eq. 2.4.1 is shown in comparison to the exact value of $\lambda(\Theta,\Phi)$ with $\Phi = 0$ (i.e. x-y plane in Fig. 2.4.1) for uniaxial extension λ_1 in the 2D parametric plot of Fig. 2.4.2 (a).

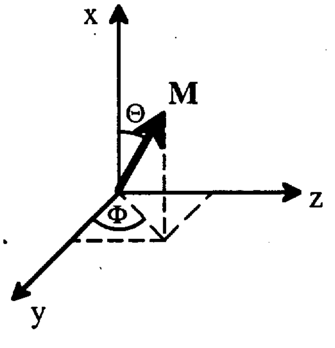

Fig. 2.4.1 Coordinate system used in Fig. 2.4.2 and 2.4.3

The unusual form of the plot (a figure eight) is due to the fact that the parameters (Θ,Φ) refer to the undeformed configuration. Using the transformation $\lambda^{-2}(\theta,\phi) = m_i\, B^{-1}_{ij}\, m_j$, where B^{-1}_{ij} is the inverse Finger tensor and $m_i = m_i(\theta,\phi)$ are the direction cosines in the deformed coordinates, in the first part of Eq. 2.4.1 gives the approximation for $\lambda\theta,\phi)$ and yields the more familiar strain ellipsoid plot shown in Fig. 2.4.2 (b). Similar type plots are shown in Figs. 2.4.3 (a) and (b) for simple shear ($\gamma = 2$) in the x-y plane.

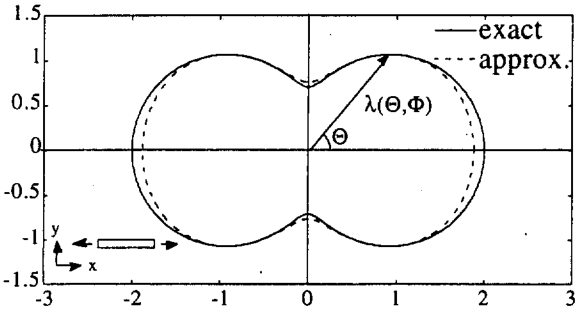

Fig. 2.4.2 (a) 2D parametric plot of $\lambda(\Theta,\Phi)$ in x-y plane for uniaxial extension in the x direction.

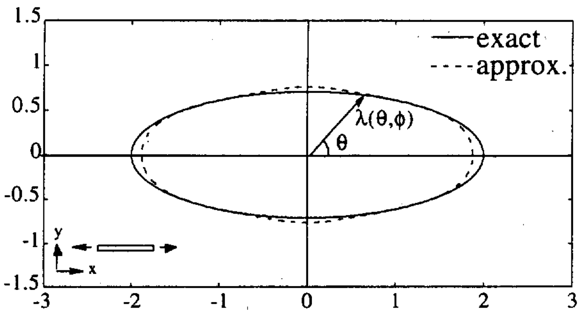

Fig. 2.4.2 (b) 2D parametric plot of $\lambda(\theta,\phi)$ in x-y plane for uniaxial extension in the x direction.

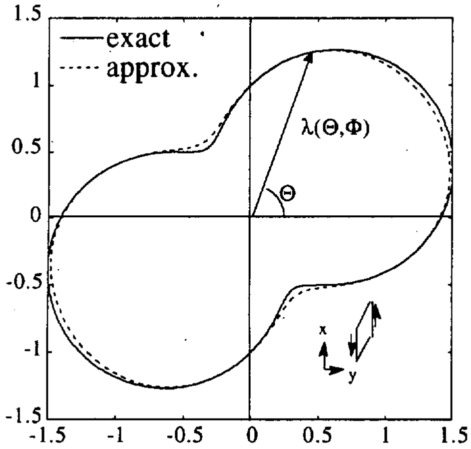

Fig. 2.4.3 (a) 2D parametric plot of $\lambda(\Theta,\Phi)$ in x-y plane for simple shear in the x direction.

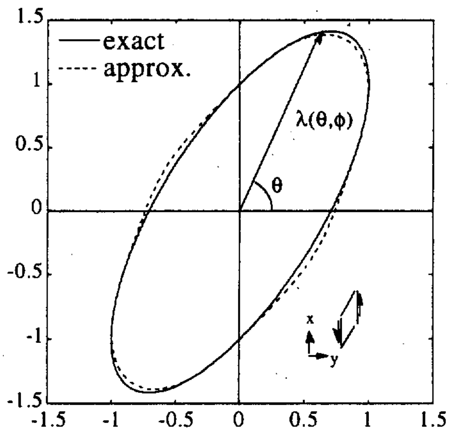

Fig. 2.4.3 (b) 2D parametric plot of $\lambda(\theta,\phi)$ in x-y plane for simple shear in the x direction.

Results shown in Figs. 2.4.2-3 show that Eq. 2.4.1 is a good approximation. To get the approximation for the average strain $\langle\lambda\rangle$, Eq. 2.4.1 is integrated over the orientation space as such:

$$\langle\lambda\rangle = \sqrt{I_1/3} + \frac{1}{8\pi}\left(\frac{I_1}{3}\right)^{-1/2}\int_0^{2\pi}\!\!\int_0^{\pi}\left(\lambda^2 - \frac{I_1}{3}\right) d\Theta\, d\Phi + \frac{1}{32\pi}\left(\frac{I_1}{3}\right)^{-3/2}\int_0^{2\pi}\!\!\int_0^{\pi}\left(\lambda^2 - \frac{I_1}{3}\right)^2 d\Theta\, d\Phi \qquad (2.4.2)$$

Substituting the integral identities given by Eqs. 1.2.20 - 1.2.22 into Eq. 2.4.2 gives the following for the average strain:

$$\langle\lambda\rangle \approx \frac{\sqrt{3}}{10}\left(3I_1^{1/2} + \frac{I_2}{I_1^{3/2}}\right) \qquad (2.4.3)$$

Because the second integral in Eq. 2.4.2 vanishes, Eq. 2.4.3 provides a high order approximation in a simple form. In figure 2.4.4 (a), the approximation Eq. 2.4.3 is compared to the exact solution Eq. B.3 for uniaxial tension and compression. In Fig. 2.4.4 (b), Eq. 2.4.3 is compared to the numerical quadrature solution of Eq. B.9 for pure shear deformation where λ is the maximum principle stretch.

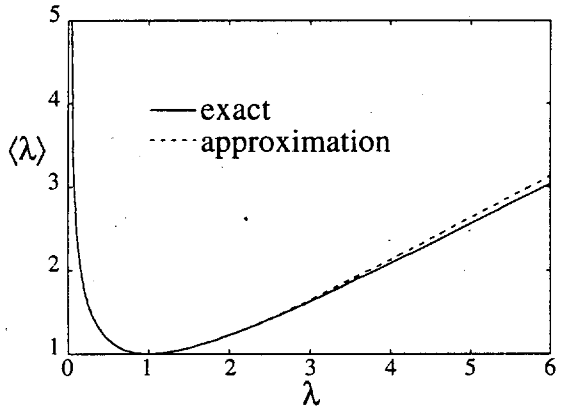

Fig. 2.4.4 (a) average stretch $\langle\lambda\rangle$ for uniaxial deformation.

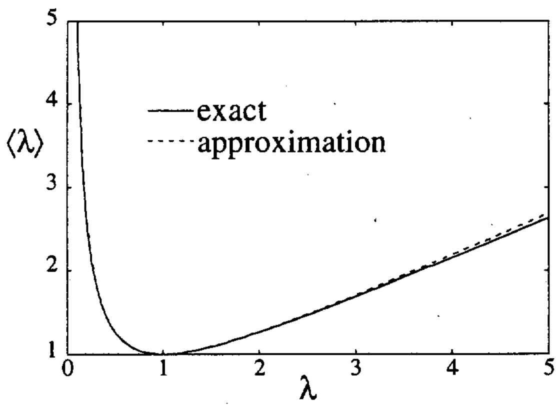

Fig. 2.4.4 (b) average stretch $\langle\lambda\rangle$ for shear deformation where λ is the maximum stretch.

The approximation for the average shear gives good results over a wide range of strains. The tensor in Eq. 2.2.19 can be approximated by taking the appropriate derivatives of Eq. 2.4.3 and the derivatives of strain invariants as follows:

$$\frac{\partial\langle\lambda\rangle}{\partial C_{ij}} = \frac{\partial\langle\lambda\rangle}{\partial I_1}\frac{\partial I_1}{\partial C_{ij}} + \frac{\partial\langle\lambda\rangle}{\partial I_2}\frac{\partial I_2}{\partial C_{ij}} = \frac{\sqrt{3}}{4}\left(I_1^{-1/2} - \frac{3}{5}\frac{I_2}{I_1^{5/2}}\right)\delta_{ij} - \frac{\sqrt{3}}{10}I_1^{-3/2}C_{ij} \qquad (2.4.4)$$

Substituting Eq. 2.4.4 into Eq. 2.2.20 (a) and making the appropriate tensor multiplications gives the approximate form for the Cauchy stress tensor shown in 2.4.5:

$$\sigma_{ij} = G\sqrt{N_o}\;L^{-1}\!\left(\frac{\langle\lambda\rangle}{\sqrt{N_o}}\right)\left(\frac{\sqrt{3}}{2}\left(I_1^{-1/2} - \frac{3}{5}\frac{I_2}{I_1^{5/2}}\right)B_{ij} - \frac{\sqrt{3}}{5}I_1^{-3/2}B^2_{ij}\right) + p\,\delta_{ij} \qquad (2.4.5)$$

probably correct

where B_{ij} is the Finger tensor and Eq. 2.4.3 is used for $\langle\lambda\rangle$. Using the approximation for the inverse Langevin function (Eq. 1.2.7) gives a closed form expression entirely in terms of strain and strain invariants:

$$\sigma_{ij} = \frac{3\ G\ \frac{\sqrt{3}}{10}\left(3I_1^{1/2} + \frac{I_2}{I_1^{3/2}}\right)}{1 - \left(\frac{1}{\sqrt{N_o}}\frac{\sqrt{3}}{10}\left(3I_1^{1/2} + \frac{I_2}{I_1^{3/2}}\right)\right)^3} \left(\frac{\sqrt{3}}{2}\left(I_1^{-1/2} - \frac{3}{5}\,\frac{I_2}{I_1^{5/2}}\right) B_{ij} - \frac{2\sqrt{3}}{5} I_1^{-3/2} B_{ij}^2\right) + p\,\delta_{ij} \tag{2.4.6}$$

Eq. 2.4.6 is used to model the same data given by James et. al. (1975) for uniaxial, biaxial and pure shear deformation. The results are shown using the force per undeformed area as in Fig. 2.3.2. For the results in Fig. 2.4.6 a slightly different value of G (0.50) than that of Fig. 2.3.2 (0.53) was used to get the best fit of the data. The following material parameters were used to fit the data using Eq. 2.4.6 (compare to Table 2.3.1).

Data from James et. al. (1975)	Data from Treloar (1944)
$G = 0.50$	$G = 0.4$
$N_o = 20$	$N_o = 24$

Table 2.4.1

James et. al. (1975) provides additional data for biaxial deformation for the same rubber sample. The biaxial tests (Fig. 2.4.5) were made such that λ_2 was varied for different values of λ_1 and the family of curves are plotted as $(\sigma_1 - \sigma_2)$ versus λ_2 (Fig. 2.4.7). Again, the same rubber was used by James et. al. (1975) for the uniaxial, equibiaxial, pure shear and biaxial tests (Figs. 2.4.6 and 2.4.7), hence the same material parameters were used.

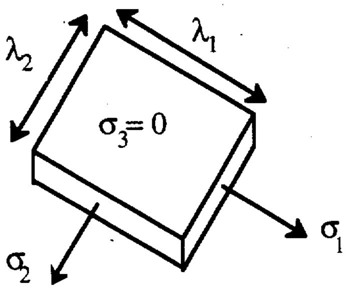

Fig. 2.4.5 Biaxial deformation

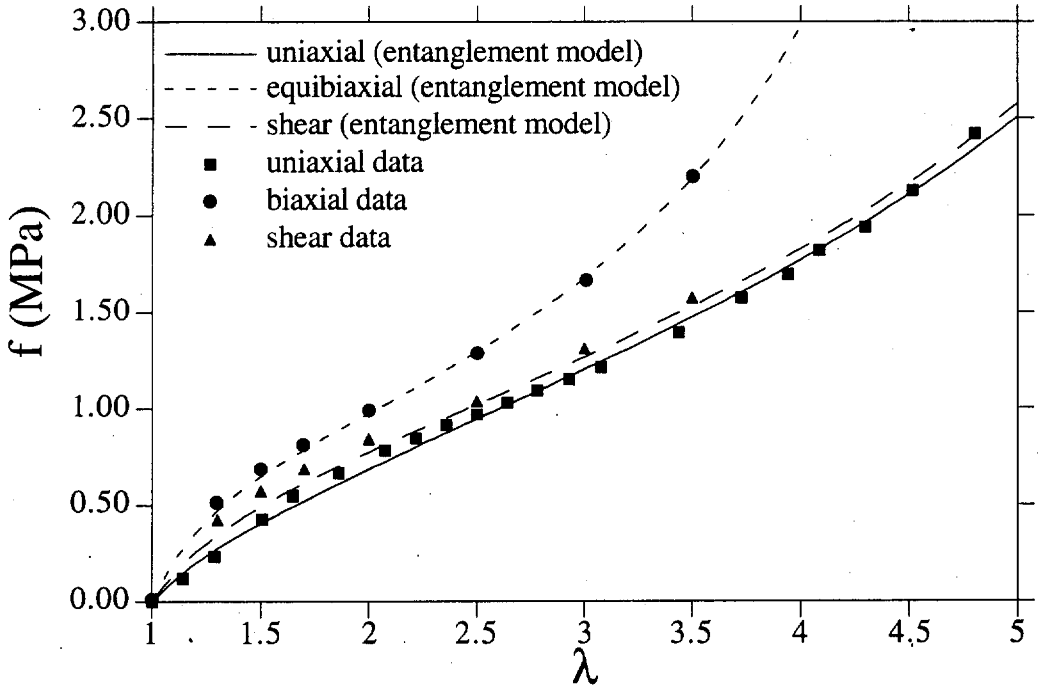

Fig. 2.4.6 Force per undeformed area for uniaxial tension, biaxial tension, and pure shear. The results by the entanglement model approximation Eq. 2.4.6 are given for $G = 0.53$ and $N_o = 20$. The data is taken from James et. al. (1975).

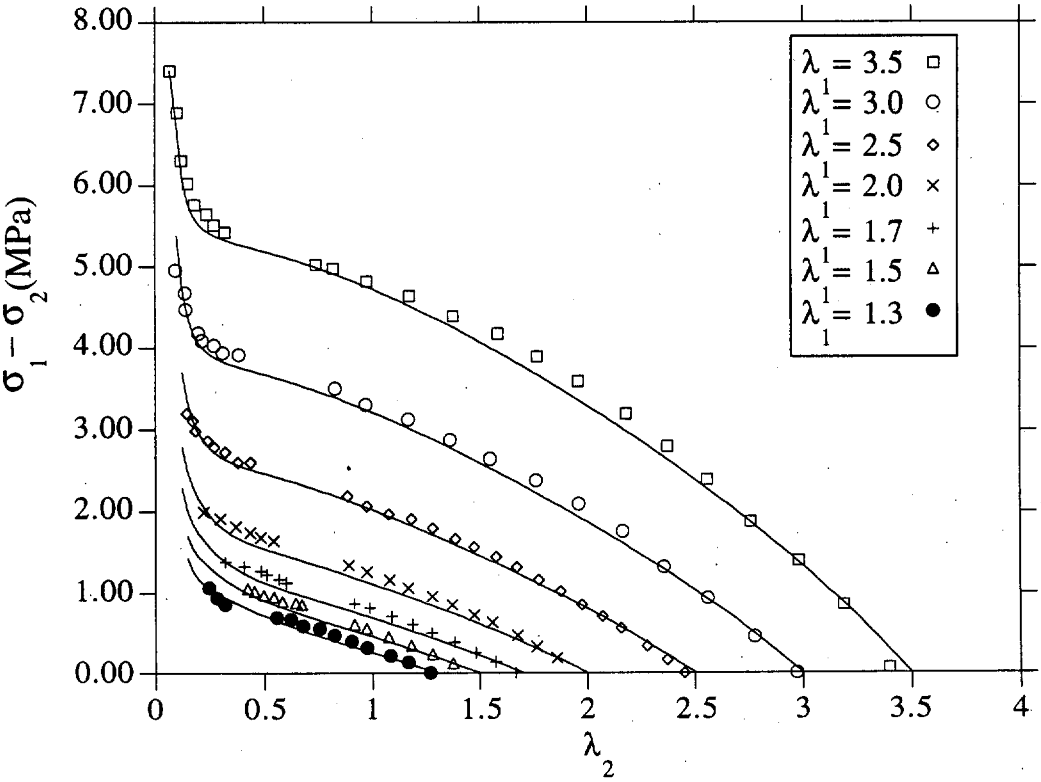

Fig. 2.4.7 The principle Cauchy stress difference for biaxial loading. The solid lines represent results by the entanglement model approximation Eq. 2.4.6 using $G = 0.53$ and $N_o = 20$. The data is taken from James et. al. (1975).

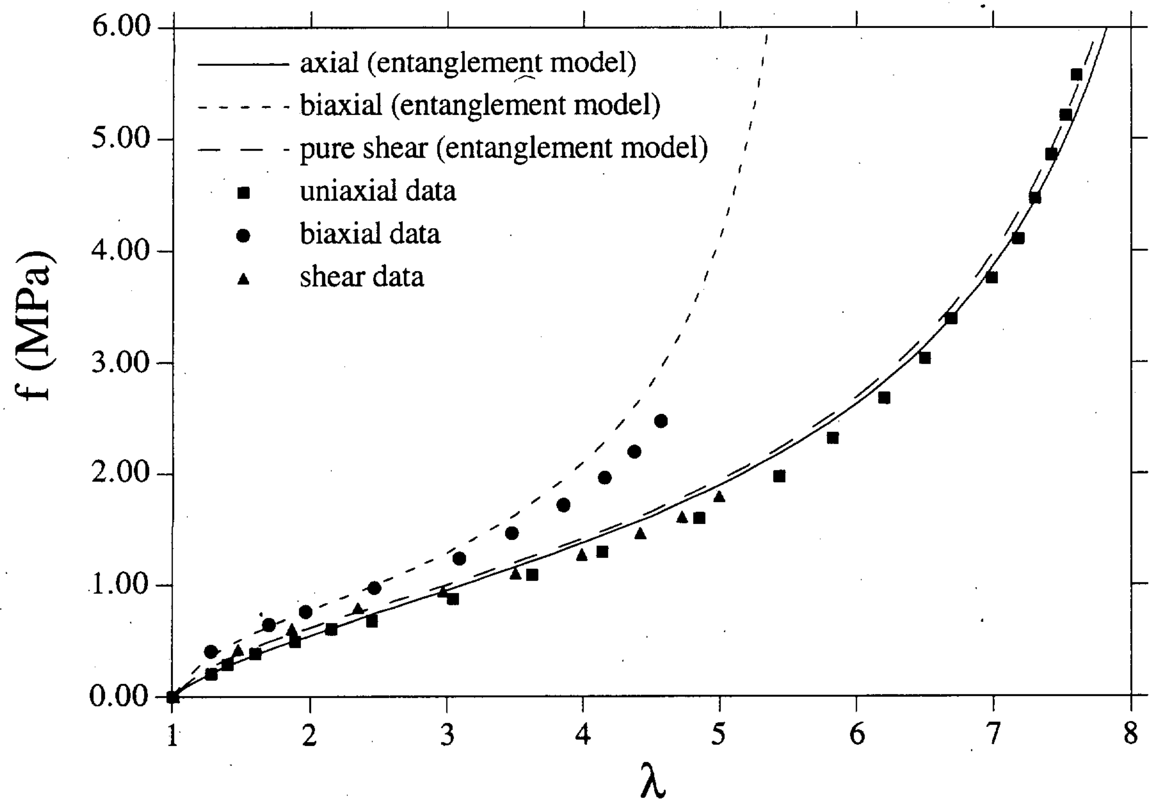

Fig. 2.4.8 Force per undeformed area for uniaxial tension, biaxial tension, and pure shear. The results by the entanglement model approximation Eq. 2.4.6 are given for G = 0.4 and N_O = 24. The data is taken from Treloar (1944).

The data given by Treloar (1944) is also modeled using Eq. 2.4.6 with results shown in Fig. 2.4.8. The material parameters used are shown in Table 2.4.1. This time a slightly different value for N_O was used than that used in Section 2.3. With Eq. 2.4.6, N_O = 24 was used. With Eq. 2.2.20, N_O = 22 was used.

The different values of G and N_O used to model the experimental data can be considered very small. It is concluded that Eq. 2.4.6 in terms of invariants and strain is successful in approximating Eq. 2.2.20.

2.5 Analysis of Results from Entanglement Model

From comparison of results by the classical theory Figs. 1.2.6 and 1.2.7, the entanglement model shows better quantitative agreement for the equibiaxial tension data particulary at the higher strains. The classical theory tends to predict much lower values of stress in equibiaxial tension not only for the data shown (James et. al. 1975), but for all data surveyed (Treloar and Riding, 1979; Obata, 1970; Jones and Treloar, 1975; Vangerko and Treloar, 1978; etc.). In fact results shown in Figs. 2.3.3 and 2.4.8 for Treloars data show that the entanglement model tends to over estimate the equibiaxial stress. Results for the additional biaxial data (Fig. 2.4.7) show that the entanglement model is valid over a wide range of loading conditions. Results from Treloar and Riding (1979) show that the classical theory gives poor quantitative results at low values of λ_2 for biaxial deformation test results like those seen in Fig. 2.4.7 .

It is particularly impressive that a two parameter model (G and N_0) is capable of modeling such a broad range of data. In all the results shown using the entanglement model, G and N_0 are merely chosen to best fit the uniaxial data and the remaining test data fit naturally. In fact G is chosen by matching the data at small strain and N_0 is chosen to model the upturn at high strains. In James et. al.(1975) third and fourth order Mooney Rivlin type strain energy functions with 6-8 determinable coefficients were used to model the biaxial data shown in Fig. 2.4.7. Values for the coefficients were found by least square fits of the biaxial data and the results were comparable to that given by the entanglement model. But it was further shown that in uniaxial tension beyond the value of $\lambda_1 = 3.5$ the results of the Mooney Rivlin model were poor. Unreasonable results may occur whenever a strictly phenomenological model is deformed beyond the range of values and outside the types of loading used to find its coefficients.

Ogden's method also relies on six determinable parameters to get good results. Moreover, Ogden's method is consistent with the Valanis-Landel hypothesis that the strain energy function is expressible by a sum of separate but identical functions of λ_1, λ_2, and λ_3 i.e.

$$W(\lambda_1, \lambda_2, \lambda_3) = w(\lambda_1) + w(\lambda_2) + w(\lambda_3) \qquad (2.5.1)$$

The difference in principle stresses using this form of free energy is found by Eq. 2.5.2 such that,

$$\sigma_1 - \sigma_2 = \lambda_1 \, w'(\lambda_1) - \lambda_2 \, w'(\lambda_2) \qquad (2.5.2)$$

Constitutive laws which are consistent with the Valanis-Landel hypothesis and, hence Eq. 2.5.2 will yield parallel $\sigma_1 - \sigma_2$ curves for biaxial stretch loading of the type seen in Fig. 2.4.7. The strain energy for the entanglement model is not separable as in (2.5.1), but for the range of stretches $1.3 < \lambda_1 < 3.5$, $0.2 < \lambda_2 < 3.5$ the entanglement model gives results which are close to parallel. Biaxial data from Vangerko and Treloar (1978) over a broader range of stretches shows $\sigma_1 - \sigma_2$ curves converging at very high stretchs suggesting that the Valanis Landel hypothesis may be invalid at these high stretch ratios.

The entanglement model given by Doi and Edwards, Marruci and Graessley and generalized here for non-Gaussian deformations is admittedly crude. One of the objections to the model is that the subchains between entanglements are considered fixed after deformation has occurred. That is the number monomers (or statistical links) between the subchain does not vary in time. In reality the chain wriggles back and forth across the entanglement. More sophisticated hoop models (Higgs and Gaylord, 1990) and tube models (Gaylord et. al., 1987) have been developed which consider this and other effects but do not consider finite extensibility. Another objection to the model is the affine deformation assumption for the crosslinks and entanglements. Again, a more sophisticated model exists (Ball et. al. 1980) where non-affine deformation is considered. The entanglement model used here is an exaggerated case such that in the undeformed configuration it is assumed that a given chain between crosslinks possesses an infinite number of subchains oriented isotropically between entanglements. As mentioned in the development of the model, it is more likely that a given polymer chain has a few subchains oriented in a few directions between entanglements. Even so, the chain experiences deformation in multiple directions. In the classical theory, the chain is only influenced by the displacement of the crosslinks in a given direction and is not concerned with the deformation of the neighboring chains. From experimental evidence it may be assumed that the exaggerated entangled state may be closer to reality than the chain oblivious to its surroundings.

3. CONSTITUTIVE EQUATIONS USING VIRTUAL WORK

In the case of inelastic deformations, the stresses, in general, cannot be determined by the gradient of a free energy function and an alternative method must be used to derive the macroscopic stress from the microstructure. The method developed here equates the external virtual work of the macroscopic stress to internal virtual work of the microstructural elements. It could be used to find the expression for the stress in polymer networks, fiberous composites, crystal plasticity etc. such that the sources of internal virtual work reflect the relevant mechanisms involved in the material. The expression for the stress tensor arrived at using this virtual work approach is actually the same expression used by rheologists. Rheologists develop their expression by a different approach.

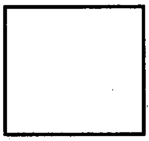

Undeformed Unit Cell
Volume = V

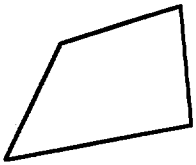

Deformed Unit Cell
Volume = v

Considering the unit cell above such that only homogenous deformations are applied, the rate of external virtual work is given by:

$$\delta W_{ext} = \sigma_{ij}\, \delta d_{ij}\, v \tag{3.1}$$

where σ_{ij} is the Cauchy stress, v is the deformed volume of the unit cell, and δd_{ij} is the virtual rate of deformation gradient given by

$$\delta d_{ij} = \delta \frac{1}{2}\left(\frac{\partial v_i}{\partial x_j} + \frac{\partial v_j}{\partial x_i} \right) \tag{3.2}$$

such that $x_i = x_i(t)$ is the current coordinate position and v_i is the velocity. It remains to specify the internal virtual.

Consider the segment of polymer chain or fiber in Fig. 3.1 in the current deformed configuration. The current length of the fiber $\Delta\mathbf{x} = \lambda\, l_o\, \mathbf{m}$ where l_o is the original undeformed length, λ is the stretch and $\mathbf{m}$ is the unit vector in the current direction of the fiber. For convenience, it is assumed the force $\mathbf{f} = f\,\mathbf{m}$ on each chain end is the same*. The magnitude f depends on the stretch λ and the stretch history such that $f = f(\lambda)$.

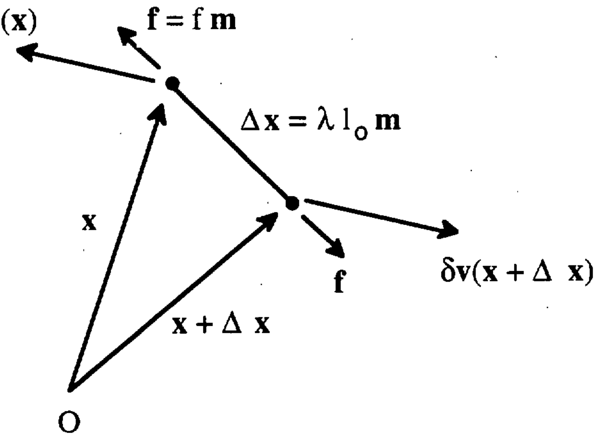

Fig. 3.1 Deformed fiber undergoing a virtual deformation

The rate of internal virtual work for the given fiber is defined as:

$$\delta W^{f}_{int} = \mathbf{f} \cdot (\delta\mathbf{v}(\mathbf{x} + \Delta\mathbf{x}) - \delta\mathbf{v}(\mathbf{x})) \qquad (3.3)$$

where $\delta\mathbf{v}$ is the virtual velocity. It is assumed that the chains or fibers deform affinely such that the endpoints of the line segment are embedded in the continuum. Furthermore only homogenous deformations of the fiber are considered; therefore,

$$\delta v_i(\mathbf{x} + \Delta\mathbf{x}) - \delta v_i(\mathbf{x}) = \delta\left(\frac{\partial v_i}{\partial x_j}\right)\Delta x_j \qquad (3.4)$$

Substituting, 3.4 into 3.3 gives:

---

* This assumption can be relaxed such that force is different at each end amounting to a distributed force acting along the length of the chain. In which case the element shown in Fig. 3.1 would be a differential element and an integration along a total length would be necessitated. Furthermore, for fibers a moment and a shear force could be incorporated at the end the element but is not necessary for a polymer chain.

$$\delta W^f_{int} = f\,\lambda\, l_o\, m_i m_j\, \delta\left(\frac{\partial v_i}{\partial x_j}\right) = f\,\lambda\, l_o\, m_i m_j\, \delta d_{ij} \tag{3.5}$$

Now δW^f_{int} (Eq. 3.5) represents the virtual work of one fiber of given orientation **m**.To get the total amount of internal virtual work, the contribution of the virtual work of all the fibers will be summed. It is recognized that all fibers with identical orientations in spherical coordinates (θ,φ) (cf. Fig. 3.2) will have the same stretch, stretch history and consequently the same force.

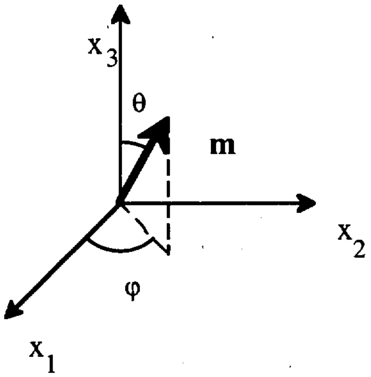

Fig. 3.2 Orientation of unit vector **m**

The number of fibers in a given orientation (θ,φ) of the unit cell is given by the relation (Van Der Giessen et al. 1993):

$$dn_t = n_t\, C(\theta,\varphi)\, V \sin\theta\, d\theta\, d\varphi \tag{3.6}$$

where n_t is the number of fibers per unit undeformed volume, $C(\theta,\varphi)$ is the orientation distribution function, and V is the undeformed volume of the unit cell. Using Eqs. 3.5 and 3.6 and integrating over all possible orientations the total internal virtual work is expressed as:

$$\delta W_{int} = \int_0^{2\pi}\int_0^{\pi} \delta W^f_{int}\, dn_t = \int_0^{2\pi}\int_0^{\pi} f(\lambda)\, m_i\, m_n\, \lambda\, l_o\, \delta d_{in}\, n_t\, C(\theta,\varphi)\, V \sin\theta\, d\theta\, d\varphi \tag{3.7}$$

To satisfy the conservation of momentum, the external virtual work must equal the internal virtual work i.e.

$$\delta W_{ext} = \delta W_{int} \tag{3.8}$$

Substituting Eqs. 3.1 and 3.7 into 3.8 yields:

$$\sigma_{in}\, \delta d_{in}\, v = n_t\, l_o\, V \int_0^{2\pi}\!\!\int_0^{\pi} f(\lambda)\, m_i\, m_n\, \lambda\, \delta d_{in}\, C(\theta,\varphi) \sin\theta\, d\theta\, d\varphi \tag{3.9}$$

It is noted that j = v / V, where j is the determinant of the deformation gradient , v is the deformed volume and V is the undeformed volume. Since only homogenous deformation gradients are considered Eq. 3.9 may be restated:

$$\left(\sigma_{in} - n_t\, l_o \frac{1}{j} \int_0^{2\pi}\!\!\int_0^{\pi} f(\lambda)\, m_i\, m_n\, \lambda\, C(\theta,\varphi) \sin\theta\, d\theta\, d\varphi\right) \delta d_{in} = 0 \tag{3.10}$$

In general the virtual deformation gradient δd_{in} is arbitrary; henceforth the Cauchy stress can be written:

$$\sigma_{in} = n_t\, l_o \frac{1}{j} \int_0^{2\pi}\!\!\int_0^{\pi} f(\lambda)\, m_i\, m_n\, \lambda\, C(\theta,\varphi) \sin\theta\, d\theta\, d\varphi \tag{3.11}$$

The polymer matrix also exhibits an additional resistance to volumetric change and in many cases is treated as incompressible. In this case the admissible deformations are considered isochoric such that virtual rate of deformation gradient $\delta d_{ii} = 0$. To apply this constraint, Eq. 3.8 must be modified as such:

$$\delta W_{ext} - \delta W_{int} + p\,(\delta_{in}\delta d_{in} - 0) = 0 \tag{3.12}$$

Where p is the undetermined Lagrange multiplier. Using 3.1, 3.8 and 3.12 gives:

$$\left(\sigma_{in} - n_t\, l_o \frac{1}{j} \int_0^{2\pi}\!\!\int_0^{\pi} f(\lambda)\, m_i\, m_n\, \lambda\, C(\theta,\varphi) \sin\theta\, d\theta\, d\varphi - p\, \delta_{in}\right) \delta d_{in} = 0 \tag{3.13}$$

Because of the Lagrange multiplier, the virtual rate of deformation gradient can again be considered arbitrary such that,

$$\sigma_{in} = n_t\, l_o \frac{1}{j} \int_0^{2\pi}\!\!\int_0^{\pi} f(\lambda)\, m_i\, m_n\, \lambda\, C(\theta,\varphi) \sin\theta\, d\theta\, d\varphi + p\, \delta_{in} \tag{3.14}$$

Eqs 3.11 and 3.14 are stated in terms of the variables (θ,ϕ) which represent the current orientation of the deformed fibers. The initial orientation of a given fiber may be represented by the spherical coordinates (Θ,Φ). As in Section 1, the deformed and undeformed coordinates are interchangeable and their transformations can be stated as such:

$$(\theta,\phi) = (\theta(\Theta,\Phi;t),\ \phi(\Theta,\Phi;t)) \tag{3.15 a}$$

$$J = \left|\frac{\partial(\theta,\phi)}{\partial(\Theta,\Phi)}\right| = \frac{\partial\theta}{\partial\Theta}\frac{\partial\phi}{\partial\Phi} - \frac{\partial\theta}{\partial\Phi}\frac{\partial\phi}{\partial\Theta} \tag{3.15 b}$$

$$d\theta\, d\phi = J\, d\Theta\, d\Phi \tag{3.15 c}$$

where J is jacobian. The deformed orientation m_i can be mapped to the undeformed coordinates by the following transformation:

$$m_i = \frac{1}{\lambda}\frac{\partial x_i}{\partial X_K} M_K \tag{3.16}$$

where M_K are the direction cosines for undeformed orientation.

$$\mathbf{M} = M_K\, \mathbf{e}_K = \sin\Theta \cos\Phi\ \mathbf{e}_1 + \sin\Theta \sin\Phi\, \mathbf{e}_2 + \cos\Theta\, \mathbf{e}_3 \tag{3.17}$$

Performing the transformation to undeformed coordinates on the integral 3.11 the following results:

$$\sigma_{in} = n_t\, l_o \frac{1}{j} \frac{\partial x_i}{\partial X_K} \frac{\partial x_n}{\partial X_L} \int_0^{2\pi}\!\!\int_0^{\pi} f(\lambda)\, M_K\, M_L \frac{1}{\lambda} C(\theta,\phi)\, J \sin\theta\, d\Theta\, d\Phi \tag{3.18}$$

Conservation of the number of fibers between the deformed and undeformed configuration requires that $C(\theta,\phi)\sin\theta\, d\theta\, d\phi = C(\Theta,\Phi)\sin\Theta\, d\Theta\, d\Phi$. Using (3.15 c) along with the assumption that the initial distribution of the chains is isotropic, i.e. $C(\Theta,\Phi) = 1/4\pi$, yields $C(\theta,\phi)\, J \sin\theta\, d\Theta\, d\Phi = (1/4\pi)\sin\Theta\, d\Theta\, d\Phi$. Hence, Eq. (3.18) becomes,

$$\sigma_{in} = n_t l_o \frac{1}{j} \frac{\partial x_i}{\partial X_K} \frac{\partial x_n}{\partial X_L} \int_0^{2\pi}\!\!\int_0^{\pi} f(\lambda)\, M_K M_L \frac{1}{\lambda} \frac{\sin\Theta}{4\pi}\, d\Theta\, d\Phi \tag{3.19}$$

The use of the deformed and undeformed orientations amounts to a Eulerian and Lagrangian description. The second Piola Kirchoff stress can easily be extracted from 3.19 giving:

$$S_{KL} = n_t l_o \int_0^{2\pi}\!\!\int_0^{\pi} f(\lambda)\, M_K M_L \frac{1}{\lambda} \frac{\sin\Theta}{4\pi}\, d\Theta\, d\Phi \tag{3.20}$$

Sometimes the force $f(\lambda)$ is the gradient of a free energy function such that,

$$f(\lambda) = \frac{\partial \Psi(\lambda)}{\partial \lambda} \tag{3.21}$$

Now $\lambda = \sqrt{M_K M_L C_{KL}}$ so that,

$$2\frac{\partial \lambda}{\partial C_{KL}} = \frac{M_K M_L}{\lambda} \tag{3.22}$$

where C_{KL} is the Green tensor. Substituting 3.21 and 3.22 shows that when $f(\lambda)$ is the gradient of a scalar function, the stress is the gradient of a scalar functional as follows,

$$S_{KL} = n_t l_o \int_0^{2\pi}\!\!\int_0^{\pi} \frac{\partial \Psi(\lambda)}{\partial \lambda}\, 2\frac{\partial \lambda}{\partial C_{KL}} \frac{\sin\Theta}{4\pi}\, d\Theta\, d\Phi$$

$$= n_t l_o 2 \frac{\partial}{\partial C_{KL}} \int_0^{2\pi}\!\!\int_0^{\pi} \Psi(\lambda) \frac{\sin\Theta}{4\pi} \sin\Theta\, d\Theta\, d\Phi = n\, l_o 2 \frac{\partial\langle\Psi\rangle}{\partial C_{KL}} \tag{3.23}$$

So, whether one obtains the stress from Eq. 3.20 or first obtains the free energy function $\langle\Psi\rangle$ and then uses (3.23) (as was done for the elasticity models), the results are entirely equivalent.

4. VISCOELASTICITY MODELS FOR RUBBER

4.1 Introduction

The large strain viscoelastic models of rubber used by solid mechanics analysts are purely phenomenological. More physically based models are examined which more directly incorporate the effects of intermolecular friction, and the transient nature of the forces and orientation of the polymer chains. Mechanisms which cause viscoelasticity in polymer liquids (i.e. polymer solutions and polymer melts) are similar to those in solid rubber. Hence, it will be instructive to present some of the concepts from polymer fluid dynamics. Rheologists have developed complete theories for the viscoelasticity of polymer solutions and polymer melts. These theories can provide a spectrum of relaxation times, the orientation distribution of the polymer chains and the constitutive law relating the stress to the time history of deformation. Many assumptions are made in these theories; therefore, they are only valid under very ideal conditions. For example the theory for polymer solutions assumes that the polymer chains are of sufficient molecular weight while very dilute such that the polymers chains do not interact. The reptation theory for polymer melts is only valid for monodisperse conditions etc. Nevertheless these theories are useful in relating certain underlying molecular mechanisms to macroscopic observations and can be modified phenomenological to reflect more realistic non-ideal conditions. The concepts used by rheologist for polymer fluids will be used here to develop viscoelasticity models for solid rubber.

The first theory developed here is primarily concerned with relatively short polymer chains in a highly crosslinked network. In this theory it is assumed that all the chains in the network are crosslinked such that there are no dangling or unattached chains which can affect the viscoelasticity of the rubber. This viscoelastic theory provides a time dependent 'backstress' which can be appended to the elastic stress given by the entanglement model developed in Section 2.

Another theory which incorporates effects from the uncrosslinked polymer chains is presented. The theory is an extension of the reptation model for polymer melts to solid rubber and is consistent with the entanglement model presented in Section 2. This model appears to give better correlation to available data from constant strain rate experiments .

Not very much attention has been paid to finite strain viscoelasticity of solid rubber in the literature. This is especially true for rubber where effects due to finite extensibility are apparent (i.e. upturn in stress verses strain curves). Phenomenological theories have been put forth by many authors. One reason that a comprehensive molecular theory has not been developed is that the problem is rather complex (the elasticity problem is hard enough!). In the following development, concepts from the rheology of polymer fluids are introduced. These concepts will clarify the origins of visoelasticity and motivate the viscoelastic model developed here.

4.2 Topics from Rheology

A typical uniaxial relaxation curve for a gum rubber (i.e. unfilled) is shown in Fig 1. The first theory attempts to describe the rubber as it goes from the glassy region to the rubbery region of behavior. As seen from Fig. 4.2.1 for a small step strain (≈5%) the stress goes from $1x10^9$ dynes/cm^2 (100 MPa) to $1x10^6$ dynes/cm^2 (0.1 MPa). At the very beginning of the glassy region for small strains, much of the deformation is due to the change in bond lengths in the polymer chain. Because these bonds are very strong, the material can be very stiff. The molecular chains do not find their equilibrium distribution immediately after deformation because friction from surrounding molecules inhibits their motion. For relaxation tests with strains higher than 5%, the bonds will break and or the chains atoms will flow immediately after deformation (Ward 1983). After some time has passed thermal motion of the chain atoms causes the polymer chains to reconfigure so that the high stress (100 MPa in Fig. 4.2.1) subsides (Ward,1983). This phenomenon occurs during the glass to rubber transition seen in Fig. 4.2.1. After substantial time has elapsed the polymer chains will find their equilibrium configuration which corresponds to maximum entropy. In order to model the viscoelastic (glass to rubber transition) the intermolecular friction is taken into account. This can be done in different ways depending on the nature of the polymer (i.e. rubber solid, polymer liquid, polymer melt).

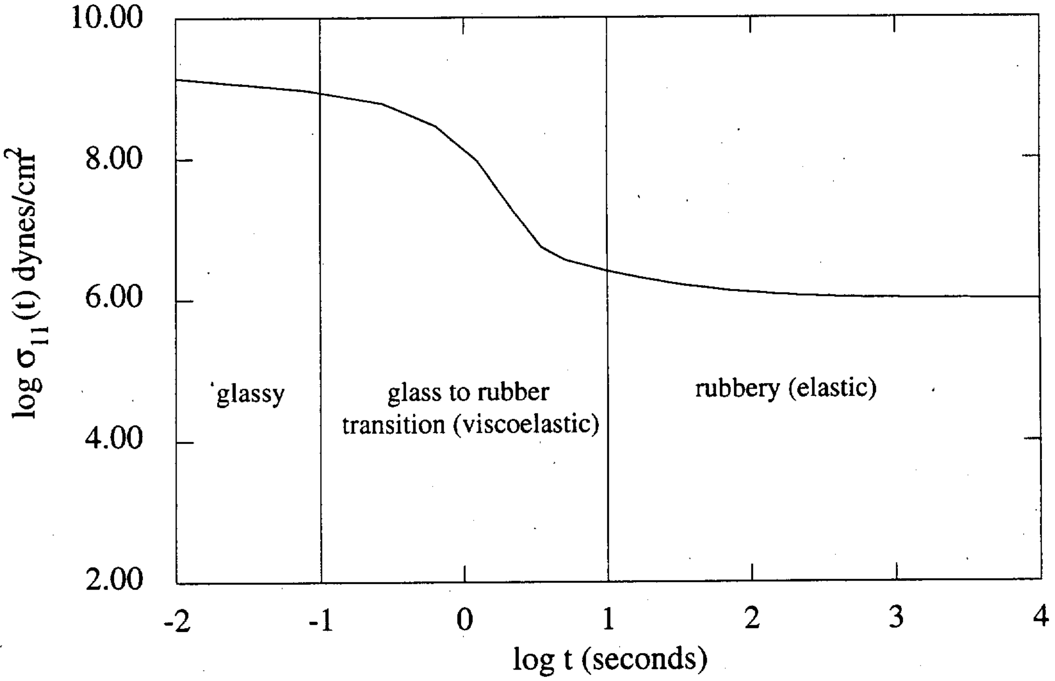

Fig. 4.2.1 Uniaxial relaxation curve for rubber after 5% step strain (taken from Ferry 1981).

Typical relaxation curves for a dilute polymer solution and a polymer melt in shear are shown in Fig. 4.2.2. Dilute polymer fluids are composed of solvent (e.g. decalin) and suspended polymer chains (e.g. isobutylene). A polymer melt is made up of uncrosslinked polymer chains and contains no solvent. The degree of polymerization can range from tens to thousands of monomer units per polymer chain. At short times both polymer fluids and rubber (Fig. 4.2.2) have similar types of behavior. The plateau behavior seen by the polymer melt is due to the entanglements encountered by polymer chains. The region where the stress decreases rapidly is called the terminal zone. As will be described further, rheologists use the Rouse theory to describe the behavior of the fluids at short times and reptation theory to describe the plateau and terminal behavior of the polymer melt.

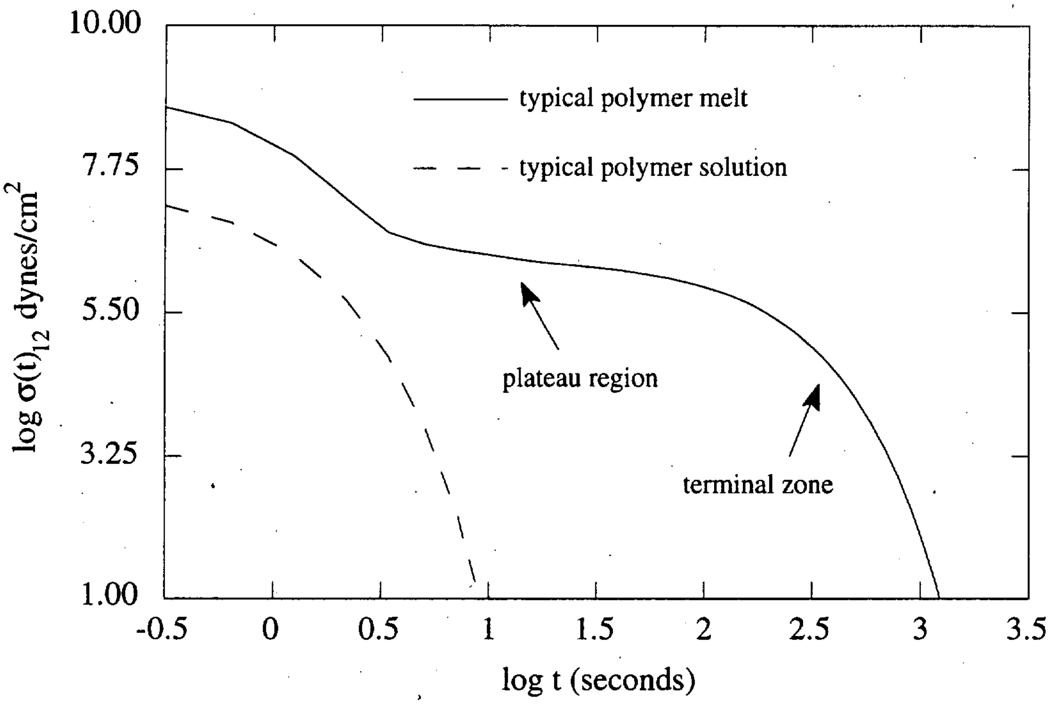

Fig. 4.2.2 Typical relaxation master curves for a dilute polymer solution and a polymer melt in shear.

4.2 a Polymer Fluids

Over the years rheologists have made substantial efforts in attempting to characterize the viscoelastic behavior of polymer solutions and melts. In fact the viscoelastic behavior of dilute polymer solutions is well understood. Under certain conditions the Rouse bead spring model can be used for this type of solution. For example, a long polymer chain (Fig. 4.2.3 a) can be modeled by a series of springs connected by beads (Fig. 4.2.3 b). Each spring is called a subchain and may consist of a hundred or so monomers. The number of beads and springs used to discretize the chain is usually determined heuristically. An equation of motion is derived for the bead chain molecule. Solving this equation yields the constitutive law for the polymer liquid.

The configurational distribution function $\psi(\mathbf{x}_1, \mathbf{x}_2, \ldots \mathbf{x}_i, \ldots \mathbf{x}_N)$ (or $\psi(\mathbf{x})$ for short) describes the likelihood that a given polymer chain (bead spring model that is) will be in some configuration $\mathbf{x}_1, \mathbf{x}_2, \ldots \mathbf{x}_i, \ldots \mathbf{x}_N$ where $\mathbf{x}_i$ is the position vector for the ith bead (See Fig. 4.2.3 b). The function $\psi(\mathbf{x})$ is normalized such that the integral of ψ over all orientations $\mathbf{x}_i$ is equals 1.

$$\int \psi(\mathbf{x}_1, \mathbf{x}_2, \ldots \mathbf{x}_N)\, d\mathbf{x}_1 d\mathbf{x}_2 \ldots d\mathbf{x}_N = 1 \qquad (4.2.1)$$

Since the solution is assumed to be very dilute, the polymer molecules are treated as though they do not interact and are only affected by the surrounding solvent. Consequently, the configurational distribution function for a given polymer molecule is independent of the other molecules. The configuration of a crosslinked polymer chain is not independent of surrounding chains and is hence more complicated to analyze.

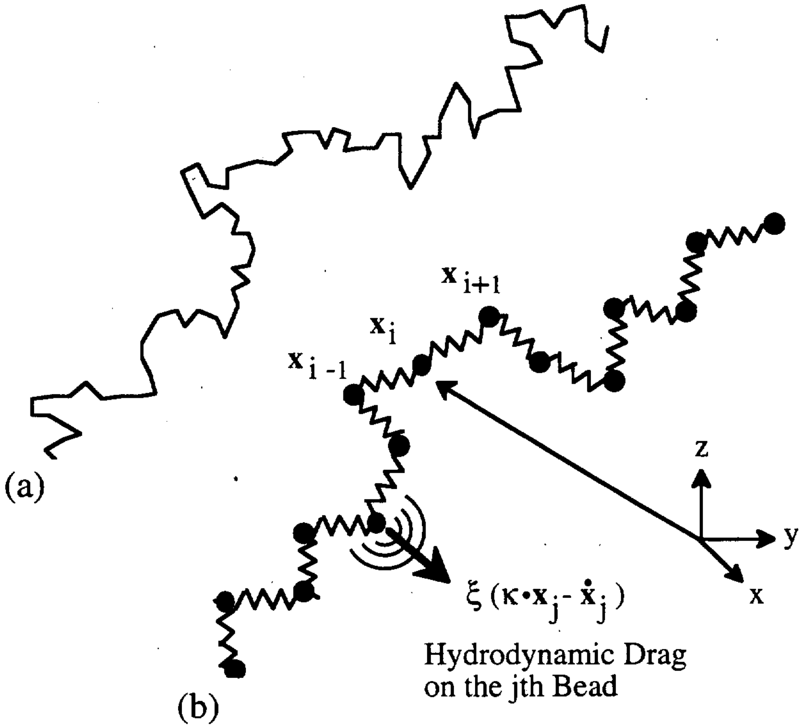

Fig. 4.2.3 (a) A polymer chain suspended in fluid. (b) The bead spring representation of the chain. Beads 1 to N are connected by springs.

Fluid flow produces viscous forces on the chain atoms. The hydrodynamic drag experienced by the subchain atoms is lumped at the beads. In fig. 4.2.3 (b), the i th bead is denoted by its position vector $\mathbf{x}_i$. If the fluid is subjected to a homogenous velocity gradient κ, the fluid velocity at $\mathbf{x}_j$ is defined by $\kappa \cdot \mathbf{x}_j$. Hence, the viscous force on the jth bead is $f^j_{drag} = \xi(\kappa \cdot \mathbf{x}_j - \dot{\mathbf{x}}_j)$ where ξ is the drag coefficient for the bead (usually considered a sphere).

Since the subchains are assumed to be sufficiently long, they are treated as Gaussian chains i.e. linear springs. Therefore, the force by the springs on the ith bead is

$$f^i_{spring} = 3\frac{kT}{b^2}(\mathbf{x}_{i+1} - \mathbf{x}_i) - 3\frac{kT}{b^2}(\mathbf{x}_i - \mathbf{x}_{i-1}) = 3\frac{kT}{b^2}(\mathbf{x}_{i+1} - 2\,\mathbf{x}_i + \mathbf{x}_{i-1})$$

Where k is Boltzmann's constant, T is the temperature, $b = \sqrt{N_s}\, l$ is the equilibrium length of a subchain, N_s is the number of monomer links in a subchain and l is the length of the monomer link.

The atoms which make up the subchains have a random motion known as Brownian motion due to thermal energy. The Brownian motion of the chain atoms is lumped at the beads so that the motion of the beads is considered random. The random motion of say the jth bead is not to be confused with $\dot{\mathbf{x}}_j$ which is the drift velocity (time averaged velocity) of the jth bead. Now the random motions of the beads is provided by so called Brownian motion forces. It is assumed that the Brownian force on the ith bead will be $f^i_{brownian} = -k_B T(\partial / \partial \mathbf{x}_i) \ln \psi(\mathbf{x})$ where k_B is Boltzmann's constant and T is temperature. Without going into detail, the force is entropic in nature such that the particles (beads in this case) tend to reduce the gradient of their distribution ψ; i.e. tend towards maximum entropy.

Neglecting inertia, the equation of motion of the ith bead is given by the summation of forces due to hydrodynamic drag, Brownian motion, and the springs connecting the (i - 1)th and the (i + 1)th bead (Bird et. al., 1987):

$$\underset{\text{Viscous force}}{\xi(\dot{\mathbf{x}}_i - \kappa\cdot \mathbf{x}_i)} \underset{\text{Brownian force}}{- kT \frac{\partial}{\partial \mathbf{x}_i} \ln \psi(\mathbf{x})} \underset{\text{Force due to connecting springs}}{+ 3 \frac{kT}{b^2} (\mathbf{x}_{i+1} - 2\,\mathbf{x}_i + \mathbf{x}_{i-1})} = 0 \,.$$

There are N such equations of motion; one for each bead. Now suppose that an impulsive flow $\kappa(t) = \kappa\ \delta(t)$, where $\delta(t)$ is the dirac delta function, is applied to a fluid in equilibrium. Examination of Eq. 4.2.2 shows that the viscous forces applied at the beads by the flow of the solvent would force the chain to deform affinely (Fig. 4.2.4) immediately after deformation is applied such that $\dot{\mathbf{x}}_i = \kappa\cdot \mathbf{x}_i$ and

$$\mathbf{x}_i(0^+) = \int_{-\infty}^{0^+} \kappa\ \delta(t)\cdot \mathbf{F}\cdot \mathbf{x}_i(0^-)\, dt = \int_{-\infty}^{0^+} \dot{\mathbf{F}}\cdot \mathbf{x}_i(0^-)\, dt = \mathbf{F}\cdot \mathbf{x}_i(0^-)$$

where **F** is the deformation gradient, $\mathbf{x}_i(0^-)$ is the position vector of the ith bead prior to the flow and $\mathbf{x}_i(0^+)$ is the position immediately after flow. This situation is illustrated in Fig 4.2.4 where the chain in equilibrium (Fig 4.2.4 a) is deformed affinely by a shear flow such that the subchains in the deformed chain (Fig 4.2.3 b) experience tension or compression depending on its orientation at instant of flow.

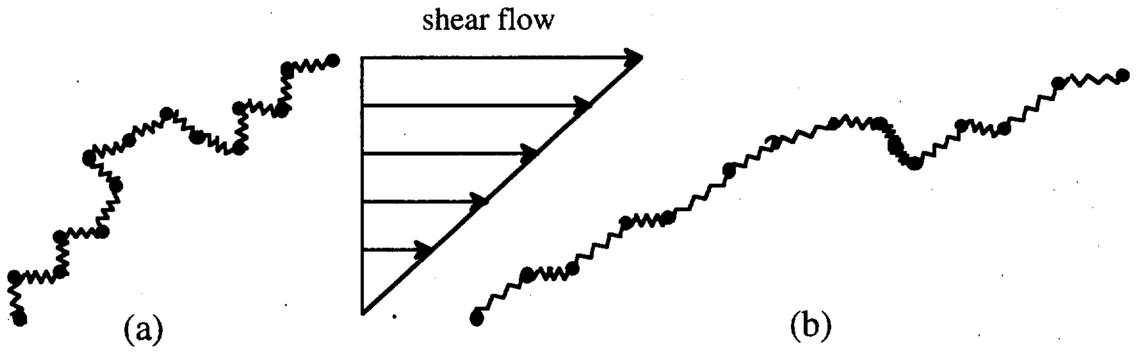

Fig. 4.2.4 (a) Bead-spring model of chain in equilibrium. (b) Chain after instantaneous shear flow is applied. Note tension and compression in subchains due to deformation.

After time, the tension and compression in the subchains will subside since the macroscopic flow has ceased and the chain will return to an equilibrium configuration. The relaxation process does not occur immediately because of the friction between the solvent and the beads. The evolution of this process is determined by the diffusion equation. The diffusion equation is derived by combining the N equations of motion given by Eq. 4.2.2 plus an additional equation. The additional equation is provided by taking the time derivative of Eq. 4.2.1. Since the orientation is a function of time i.e. $\mathbf{x}_i = \mathbf{x}_i(t)$, the time derivative of (4.2.1) gives

$$\frac{\partial \psi(\mathbf{x})}{\partial t} = \sum_{i=1}^{N} \frac{\partial}{\partial \mathbf{x}_i} \cdot (\dot{\mathbf{x}}_i \; \psi(\mathbf{x})) \qquad (4.2.3)$$

Solving for $\dot{\mathbf{x}}_i$ in Eq. 4.2.2 and substituting it into Eq. 4.2.3 gives the diffusion equation for evolution of the orientational distribution function $\psi(\mathbf{x})$ (Bird et. al., 1987)

$$\frac{\partial \psi}{\partial t} = \frac{1}{\xi} \sum_{i=1}^{N} \frac{\partial}{\partial \mathbf{x}_i} \cdot \left(kT \frac{\partial \psi}{\partial \mathbf{x}_j} - (\mathbf{x}_{i+1} - 2\mathbf{x}_i + \mathbf{x}_{i-1})\, \psi - \frac{1}{\mu}\, \kappa \cdot \mathbf{x}_i\, \psi\right) \qquad (4.2.4)$$

Due to its linearity, a separation of variables and a normal coordinate transformation applied to the diffusion equation yields a solution for the orientation distribution function $\psi(\mathbf{x}(t))$ (not shown here since the solution is rather complex). The orientation distribution function determines the likelihood that a given chain will take the configuration $\mathbf{x}_1, \mathbf{x}_2, \ldots \mathbf{x}_i, \ldots \mathbf{x}_N$. Furthermore, for each configuration $\mathbf{x}_1, \mathbf{x}_2, \ldots \mathbf{x}_i, \ldots \mathbf{x}_N$, the force in each subchain can be calculated. From this information, the average (i.e. over all possible configurations) force due to all polymer subchains passing though a given plane yields the contribution of stress due to the polymer molecules * . Adding the contribution of stress due to the solvent yields the following constitutive law:

$$\sigma_{ij}(t) = p\, \delta_{ij} + \eta_s\, d_{ij}(t) + \int_{-\infty}^{t} nkT \left(\sum_{m=1}^{N} \frac{1}{\lambda_m} e^{-(t-\tau)/\lambda_m} \right) B_{ij}(t,\tau)\, d\tau \qquad (4.2.5_1)$$

with the relaxation times λ_m given by

$$\lambda_m = \frac{\xi N_s l^2}{24\, kT \sin^2(m\pi/2N_s)} \qquad k = 1,2....N \;\; (N = \text{number of beads}) \qquad (4.2.5_2)$$

---

*Eq. 3.14 derived by the virtual work method can be used to provide the stress by performing a coordinate transformation from $\mathbf{x}_i$ to (θ_i, ϕ_i). Such a transformation converts the configuration distribution $\psi(\mathbf{x}_i)$ to the orientation distribution $C(\theta,\phi)$.

the Finger tensor $B_{ij}(t,\tau)$ is given by the relation

$$B_{ij}(t,\tau) = \frac{\partial x_i(t)}{\partial x_k(\tau)} \frac{\partial x_j(t)}{\partial x_k(\tau)} \qquad (4.2.5_3)$$

such that $x_i(t)$ is the current position and $x_k(\tau)$ is the position at the previous time τ, d_{ij} is the rate of deformation gradient, η_s is the viscosity of the fluid, n is the number of polymer molecules per unit volume, N_s is the number of monomers per subchain, and l is the length of each monomer link.

4.2 b Polymer Melts

The expression for stress (Eq. 4.2.5) has been shown to be successful in describing the behavior of dilute polymer solutions shown in Fig. 4.2.2. Because the fluid is assumed to be dilute, such that polymer chains do not interact, the friction applied to the beads is only due to the solvent. At very short times (See Fig. 4.2.2) the same bead spring model is also used for polymer melts. In this case the friction applied to the beads is due to the surrounding polymer chains and is treated by the same exact equations as described above for the solvent. The flow of surrounding polymer molecules around the beads of a bead spring chain seems to be more complicated than the flow of the solvent. Nevertheless, this is the simplified treatment made by rheologists in much of the literature (Bird et. al., 1987; Doi and Edwards, 1986; Ferry, 1981; etc.) (Bird, 1987 has incorporated an additional anisotropic friction coefficient called the link tension constant). To characterize the behavior of the melt at longer times additional mechanisms must be considered. The reptation theory developed by Doi and Edwards (1978) and to be described here is the accepted explanation for the plateau and terminal behavior of polymer melts and concentrated solutions. In a crosslinked rubber, the dynamics for the relaxation process at the early stages of incipient deformation (at very short times in Fig. 4.2.2) are basically the same as that for the uncrosslinked polymer melts.

According to Doi and Edwards (1978) "the major factor governing the motion of a polymer in a network is the effect of entanglements i.e., chains cannot pass though each other". The portrait of an entanglement network given (Fig. 4.2.5 a) is of a molecule (crosslinked or uncrosslinked) constrained by surrounding polymer chains (seen as dots in Fig. 4.2.5 a). The constraints of the network are idealized as a tube or cage surrounding the molecule (Fig. 4.2.5 b) . The center line, called the primitive chain, represents the average location of the molecule, since the molecule is constantly "wriggling" due to thermal fluctuations. The dots shown in Fig. 4.2.5 (a) and (b) actually represent the primitive chains of the surrounding molecules. The force in the chain is assumed to be along the primitive chain. Doi and Edwards give mathematical motivation for the tube and primitive chains , the concepts are merely illustrated here.

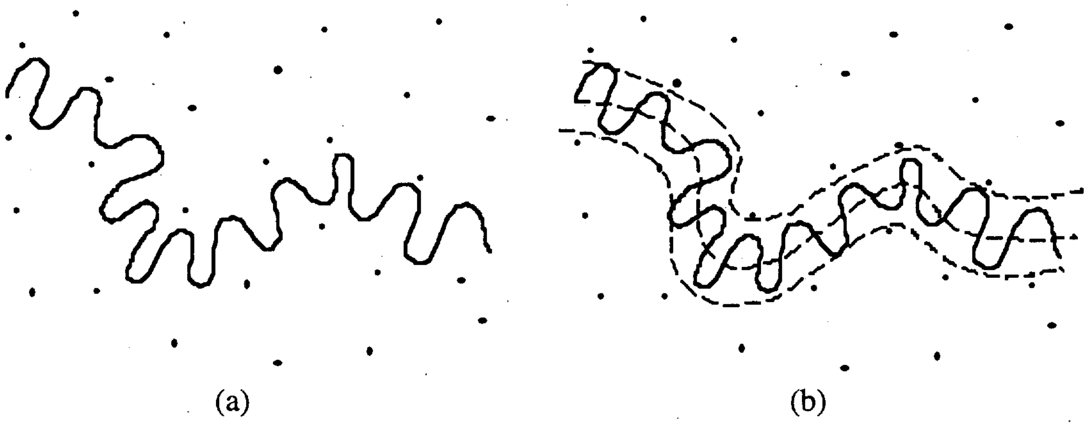

Fig. 4.2.5 (a) Schematic of a polymer chain in entanglement network where dots represent surrounding chains. (b) The idealized constraining tube and the primitive chain (centerline).

For the uncrosslinked melt, the tube confines the chain, otherwise the chain would be free to roam anywhere in the network and thereby violate the constraints of the surrounding chains. The process of confining the chain in such a tube reduces the configurational entropy and therefore requires a force to maintain the tube constraint even when the polymer melt is in equilibrium. This force is applied along the tube by the surrounding network (sort of a distributed force) and in the equilibrium state amounts only to a hydrostatic stress since the chains are randomly oriented. The tube is assumed to deform affinely while the chain inside is able to rearrange itself within and assume its most favorable position (i.e. relax, more about this later).

The tube model requires the calculation of a confinement force which is difficult. To simplify the model, Doi and Edwards further idealized the problem using the so called slip link model (Fig. 4.2.6 a) (see also chapter on elastic entanglement model). The slip links force the uncrosslinked polymer chain to maintain the confines of the tube. A fictitious force is applied to the ends of the chain which represents the effect of confinement. For example, if this force is not applied, the chain will escape from the slip links (i.e. escape from the tube) (Fig. 4.2.6 b).

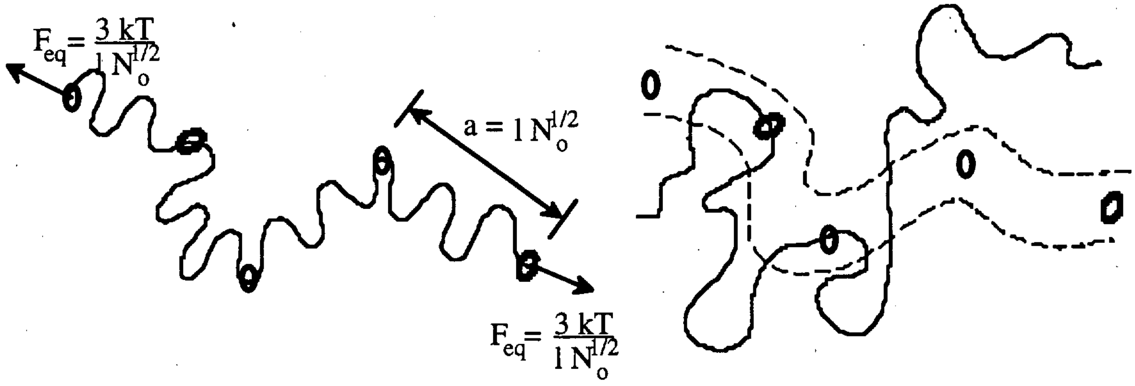
$F_{eq} = \frac{3\,kT}{l\,N_o^{1/2}}$
$a = l\,N_o^{1/2}$
$F_{eq} = \frac{3\,kT}{l\,N_o^{1/2}}$

(a) (b)

Fig. 4.2.6 (a) The slip link model of a confined chain with forces applied at ends. (b) The behavior of a chain if no force is applied at the end.

In the undeformed state, each slip link is assumed to be separated by some characteristic distance " a " (Fig. 4.2.6 a). Doi and Edwards (1978, 1986 etc.) considered this distance " a " a measure of confinement. Marrucci (1979) considered it the distance between entanglements. A Gaussian subchain with N_o monomers (or statistical links) each of length l spans each slip link such that $a = \sqrt{N_o}\, l$ is the mean square length of the chain and when undeformed (Fig. 4.2.6 a) the force is:

$$F_{eq} = \frac{3\,kT}{N_o\, l^2} L = \frac{3\,kT}{\sqrt{N_o}\, l} = \frac{3\,kT}{a} \tag{4.2.6}$$

As with the tube the slip links are assumed to deform affinely and the chain is able to slide freely through the slip links until it reaches its most favorable position.

The slip links play the same role as the entanglements (Fig. 2.2.1) shown in the presentation of the elasticity model. The entanglements were used by Marrucci and are simpler to conceive. It is not that important which conceptual device is used, they are both used to force the chain to deform with the surrounding network as opposed to a non-entanglement model where a chain between crosslinks is only affected by relative motion of the crosslinks. The main difference between the tube model and the slip link model is how the force in the chain is calculated. In the tube model, the entropy of a polymer chain bounded by a tube of a given configuration is calculated in a sophisticated manner. In the slip link model the equilibrium force is determined from the stretch of the subchain with N_o monomer links between adjacent sliplinks. This is what was done in the development of the elasticity model and is much simpler than the tube model.

Consider the chain in Fig 4.2.7 (a) and the detailed portion ABCD (Fig. 4.2.7 b) in its equilibrium state. In order to characterize its dynamic behavior the chain can be further subdivided giving a Rouse bead spring model of the chain (Fig. 4.2.8).

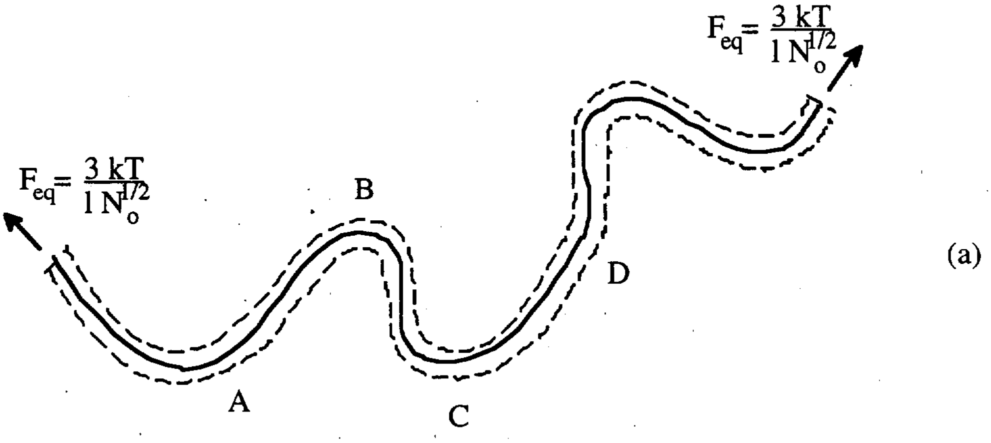
$F_{eq} = \frac{3\,kT}{l\,N_o^{1/2}}$
$F_{eq} = \frac{3\,kT}{l\,N_o^{1/2}}$
B
D
A
C
(a)

Fig. 4.2.7 (a) Long polymer chain in equilibrium The dotted lines are shown to illustrate the tube. and the solid line is the primitive chain.

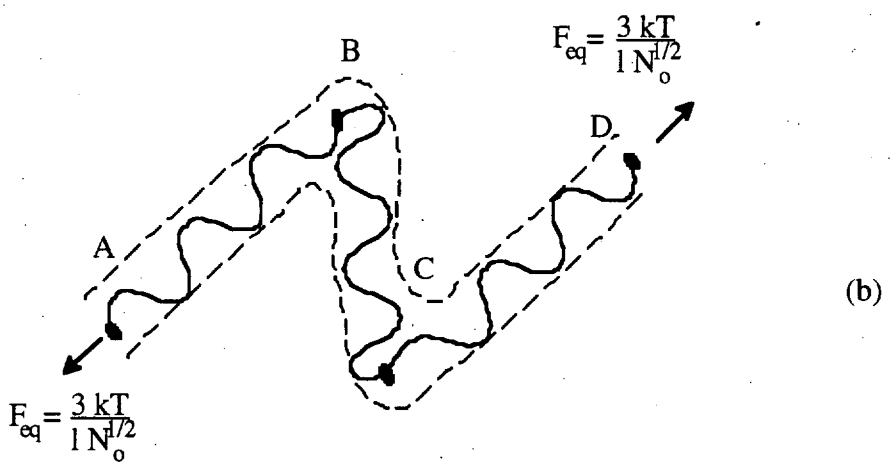
B
$F_{eq} = \frac{3\,kT}{l\,N_o^{1/2}}$
D
A
C
(b)
$F_{eq} = \frac{3\,kT}{l\,N_o^{1/2}}$

Fig. 4.2.7 (a) Long polymer chain in equilibrium The dotted lines are shown to illustrate the tube. and the solid line is the primitive chain. (b) Polymer section ABCD in. The force is calculated by the slip link method (with slip links at A,B,C and D).

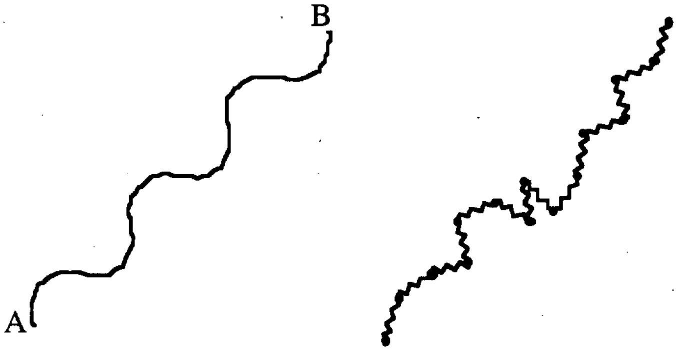

(a) (b)

Fig. 4.2.8 (a) The AB portion of the chain in Fig. 4.2.7 (b) A bead spring type representation of the AB portion. The entire chain of Fig. 4.2.7 (a) may be comprised of the Rouse bead chain models.

Don't be confused with the subchains used for the Rouse bead spring model and those used for the entanglement models. The subchains in the entanglement model represent excursions of the chain and tube (i.e. AB, BC, CD in Fig. 4.2.6) as it wanders through the entanglement network. Rouse subchains would be a further discretization of the chain; sort of subchains of a subchain in other words.

The following five steps describe the evolution of the dynamics of a chain during the relaxation process after the application of a single step strain. The relaxation curve in

Fig. 4.2.9 illustrates the chronology of the events during the relaxation process. As will be discussed, it is the first three steps "force equilibration" that also occur in crosslinked polymer chains. Doi and Edwards give only a qualitative description for the force equilibration process. In fact they only consider the disengagement process (e.g. Step 5 in Fig. 5.2.9) when deriving their constitutive law.

Step 1.

When a step strain is applied to a polymer melt or rubber in equilibrium , the viscous forces of the surrounding molecules transport every portion of the relaxed chain ABCD (Fig. 4.2.7) affinely into a new configuration A'B'C'D' (Fig. 4.2.10) as was the case for the polymer solution. The deformed chain is not in equilibrium. At this point the diffusion equation derived using the Rouse bead spring model (Fig. 4.2.3 and 4.2.8) would be the appropriate means for characterizing the relaxation of chain.

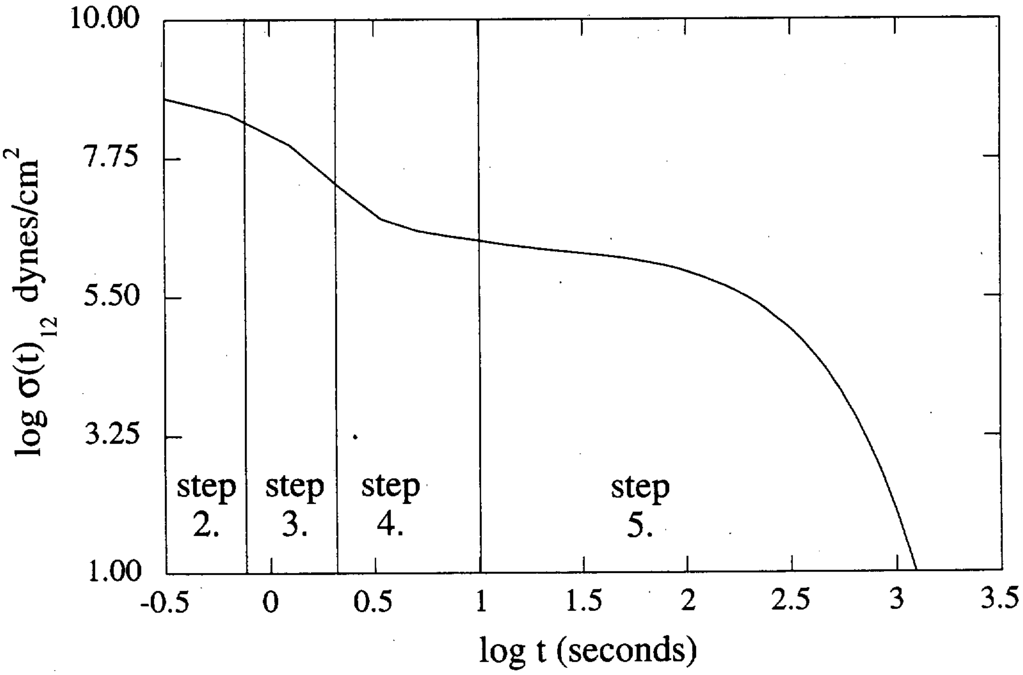

Fig. 4.2.9 Approximate sequence of events during relaxation process of a typical polymer melt. Step 1. is deformation. Step 2 and 3 is force equilibration. Step 4 is chain retraction and step 5 is the chain disengagement process.

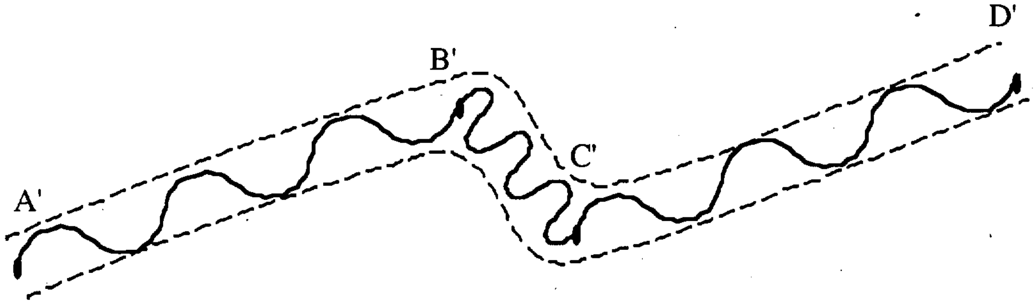

Fig. 4.2.10 The chain ABCD after affine deformation. Sections AB and CD have lengthened while BC has shortened.

Step 2.

According to Doi and Edwards (1986), the Rouse bead model (Fig. 4.2.3 and 4.2.8) could be used for times $t < \tau_e$ where τ_e* is the time where tube constraints become apparent. Unlike the Rouse chain in the fluid, the caged chain is not allowed to assume all configurations**. At this point the chain motion in the direction transverse to the tube has somewhat attenuated. This condition is shown schematically in Fig. 4.2.11. For example, in very simple terms, if section A'B' in Fig 4.2.10 was comprised of Rouse subchains, they would be highly extended since A'B' has yet to reconfigure. A short term reconfiguration is achieved by rotation of the subchains toward the direction of stretch .

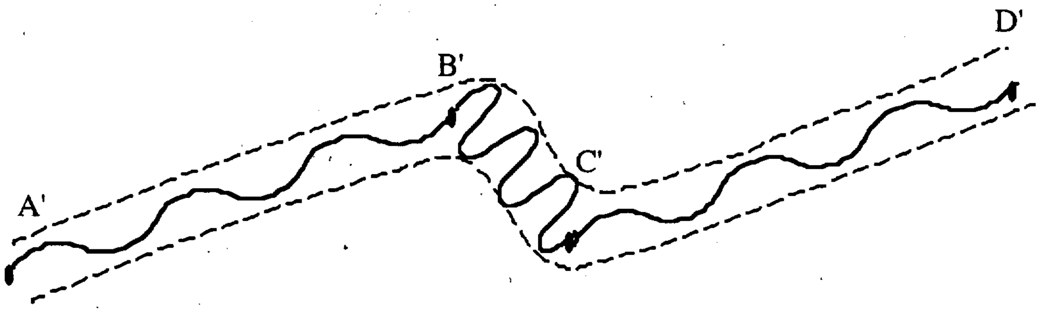

Fig. 4.2.11 Short term rearrangement of chain such that diffusion of the chain transverse to the tube has diminished.

This short term reconfiguration is shown schematically by the flat appearance of the chain segment A'B'. This amounts to a "local" relaxation process. The force in the primitive chain still varies along the length of the chain so that more relaxation is still to occur. A "one dimensional" diffusion process occurs in the next step to equilibrate the force.

---

* A rough calculation for this time is made by DeGennes (1971)

** This is why Eq. 4.2.5 is not valid for the whole relaxation process.

Step 3.

At this point the majority of the relaxation process is provided by diffusion along the length of the tube. During this process (for times $\tau_e > t > \tau_R$**) monomers from the compressed chain segment B'C' slide through the slip links in order to provide force equilibration along the chain. In actuality, the process of step 3 begins to be evident before the conclusion of step 2 especially near the points B' and C'. The equilibrated chain is shown schematically in Fig. 4.2.12. The force along the chain is constant and is calculated in identical fashion as that given in the development of the elasticity model (Section 2). Since the chain in Fig. 4.2.7 (a) is assumed to go through excursions in many different directions of three dimensional space, the stretch of the deformed contour length is given to be $\langle\lambda\rangle$ and the force for the Gaussian chain is calculated to be that shown in Fig. 4.2.12.

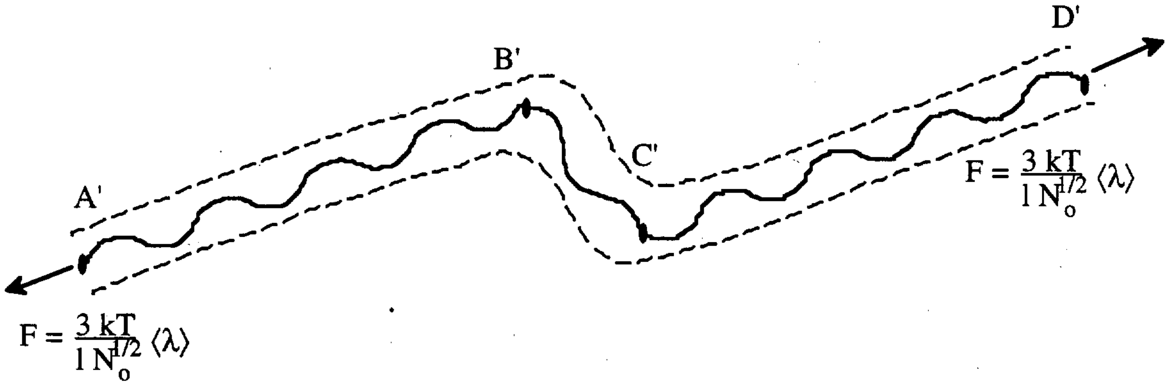
D'
B'
C'
A'
$F = \frac{3\,kT}{1\,N_o^{1/2}} \langle\lambda\rangle$
$F = \frac{3\,kT}{1\,N_o^{1/2}} \langle\lambda\rangle$

Fig. 4.2.12 Polymer chain after force equilibration along length.

Up to this point the behavior is much the same for the crosslinked and uncrosslinked polymer chains. Although the concepts given for the three steps shown are outlined by De

---

** τ_R is the longest Rouse relaxation time calculated by Eq. (4.2.5_2) at k = 1. It is shown by Doi and Edwards (1986) that the one dimensional diffusion process occuring along the length of the tube will have the same relaxation time as the three dimensional relaxation process given by Eq. (5.2.5_1)

Gennes (1971) and Doi and Edwards (1986), the details on how to implement these stages into a finite deformation constitutive model are not given nor how the transitions between the steps could be handled. These authors were more concerned with the subsequent chain retraction and disengagement process for the uncrosslinked chain since these are the mechanisms that provide the plateau and terminal regions of behavior in the relaxation curve (Fig. 4.2.2) for the polymer melt. Doi and Edwards (1986) consider only the disengagement process outlined in steps 5 when they construct their finite strain constitutive model for polymer melts.

Step 4.

If the polymer chain is not crosslinked the next process that occurs is called chain retraction. The deformed version of the entire chain shown in Fig 4.2.7 (a) is shown in Fig 4.2.13 after force equilibration (Step 3) has taken place.

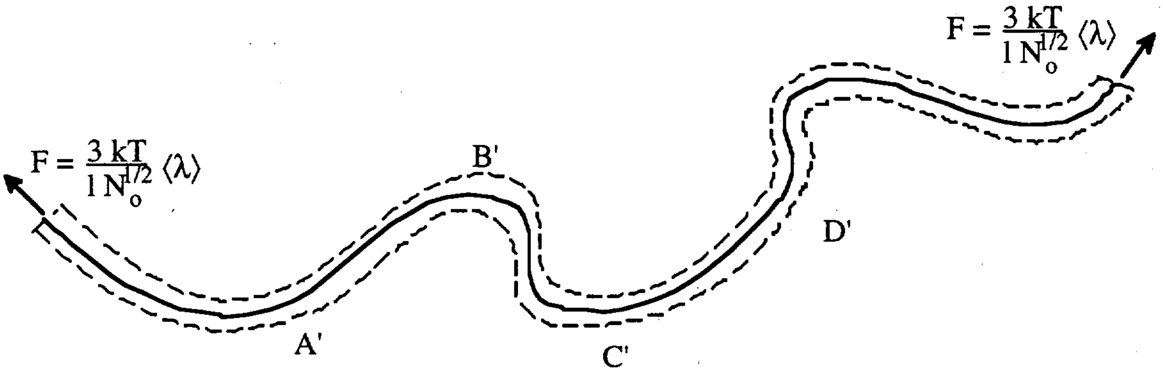
$F = \frac{3\,kT}{l\,N_o^{1/2}} \langle\lambda\rangle$
$F = \frac{3\,kT}{l\,N_o^{1/2}} \langle\lambda\rangle$
B'
D'
A'
C'

Fig. 4.2.13 The entire deformed chain after force equilibration

Chain retraction is the diffusion process such that the primitive chain returns to its equilibrium contour length. As the chain retracts, it slides along its length. In fact it is required that any motion of the chain must occur such that the chain remain in the tube except at the ends where it is free to take up new positions. This phenomenon is called reptation. The retracted chain is shown in Fig. 4.2.14. The force along the retracted chain is the equilibrium force since the chain has returned to its equilibrium contour length. The time that the chain has reached its equilibrium contour length marks the beginning of the plateau region in the stress relaxation curve (See Fig. 4.2.2 and 4.2.9)

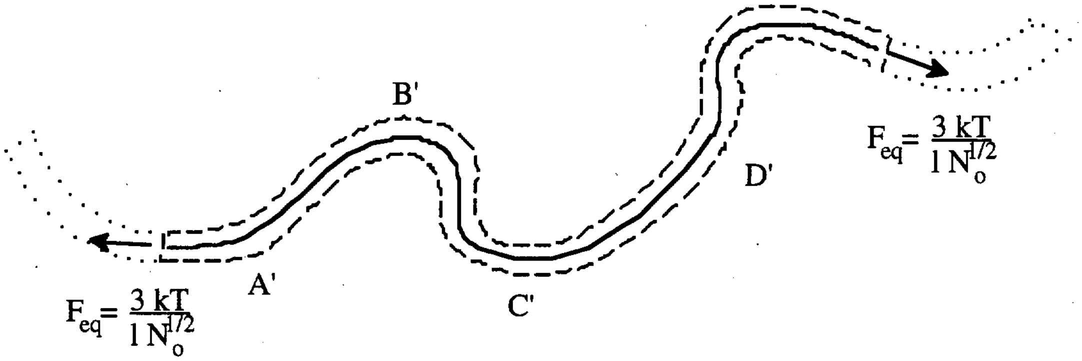
B'
D'
A'
C'
$F_{eq} = \frac{3kT}{l N_o^{1/2}}$
$F_{eq} = \frac{3kT}{l N_o^{1/2}}$

Fig. 4.2.14 The deformed chain after chain retraction. The chain retracts such that it slides along its contour (i.e. reptates). The fine dotted line represents the obsolete portion of tube.

Step 5

Despite the resumption of the equilibrium force of all the chains in the network, the stress tensor is not isotropic. The chain sections are still highly oriented due to the deformation, hence the anisotropy. At this point the diffusion process occurs such that the chain slides back and forth along its length (reptation) becomes recognizable. With each excursion at the chain ends, the chain forms new sections of tube as it winds it way through the surrounding network (Fig. 4.2.15 a, b, c). Clearly this mechanism is present throughout the first four steps, but since the process occurs slowly, it is negligible at the early times. Because of the random motion of the chain ends, the average orientation of all the new chain portions is isotropic; therefore, the remaining portion of the original tube is the sole contribution to the anisotropy and the sole contribution to the anisotropy of the stress tensor. In Fig. 4.2.15 (a), the chain slides to the left forming a new portion of tube and leaving a vacant portion (shown by fine dotted line). In Fig 4.2.15 (b) and (c) the chain slides two successive increments to the right. The length of the increments and their direction is random. The shaded portion of the tube (4.2.15 a, b, c) indicates the original tube before the chain began to escape. For all the polymer chains, only the length of chain that resides in the original tube contributes to the stress tensor since the orientation of its segments remain anisotropic. Eventually the length of original tube vanishes and the stress becomes isotropic and the polymer melt is in equilibrium. This process is call chain disengagement and is the mechanism that governs the behavior in the terminal zone of the stress relaxation curve.

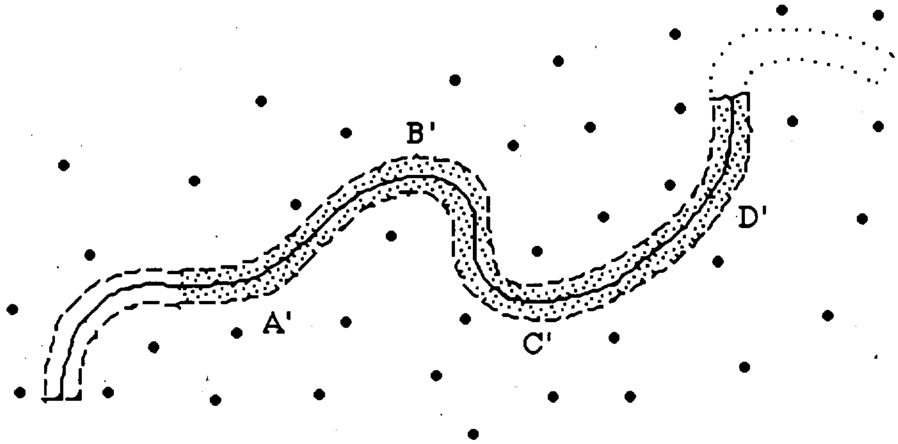

(a)

Fig. 4.2.15 (a) Polymer chain after an incremental motion towards the left. The lightly dotted line represents the portion of tube vacated after the incremental motion. The shaded portion represents the length of chain occupying the original portion of tube.

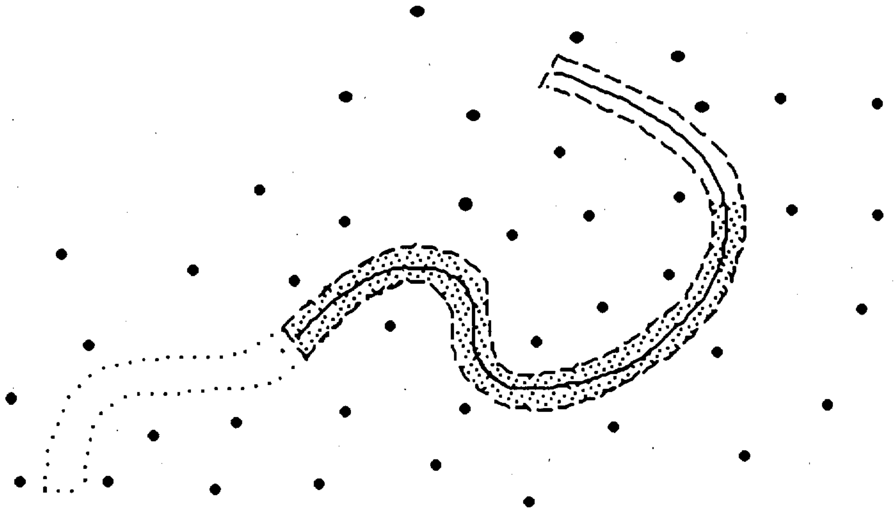

(b)

Fig. 4.2.15 (b) Polymer chain after an incremental motion towards the right. Notice how the new tube sections only appear at the end of the chain such that the chain slides along its length. The lightly dotted line represents the portion of the tube vacated after the incremental motion.

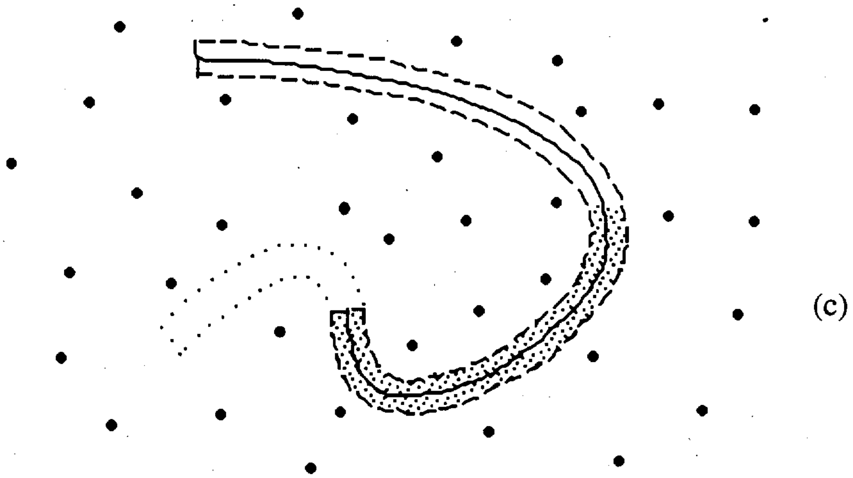

Fig. 4.2.15 (a) Polymer chain after another incremental motion to the right. At this point the a large portion of the original tube (shaded region) has diminished.

The above steps 1-5 outlined the relaxation process occurring during a single step strain. It is easy to derive the equation for the stress during this relaxation process considering only the effects of disengagement. If each polymer chain is assumed to have n_s subchains prior to the step strain, each will have $n_s / \langle\lambda\rangle$ subchains after chain retraction (Step 4) occurs due to shrinking of the polymer chain inside the stretched tube. Furthermore, the force in the chain upon retraction is merely the equilibrium force $3kT/\sqrt{N_o l}$ (cf. Eq. 4.2.6). Replacing n_t with $n\,n_s / \langle\lambda\rangle$ (n is the total number of polymer chains), l_o with the original subchain length $\sqrt{N_o}\,l$ (cf. Fig. 4.2.6), and $f(\lambda)$ with $3kT/\sqrt{N_o l}$ in Eq. 3.19 yields the equation for the stress upon chain retraction but before disengagement,

$$\sigma_{in} = \frac{n\,n_s}{\langle\lambda\rangle}\sqrt{N_o}\,l\,\frac{\partial x_i}{\partial X_K}\,\frac{\partial x_n}{\partial X_L}\int_0^{2\pi}\!\!\int_0^{\pi}\frac{3kT}{\sqrt{N_o}\,l}\,M_K\,M_L\,\frac{1}{\lambda}\,\frac{\sin\Theta}{4\pi}\,d\Theta\,d\Phi + p\,\delta_{in} \qquad (4.2.7)$$

During the disengagement process the ends of the chain form new tubes which on the average are isotropic; therefore, it is only necessary to include the amount of chain length remaining in the original tube when calculating the stress tensor. The quantity $\mu(t)$ (4.2.8) represents the fraction of chain remaining in the original tube, on average, at time t after loading and is calculated statistically by Doi and Edwards (1978) for the step strain to be,

$$\mu(t) = \sum_{p;\,odd}^{\infty} \frac{8}{\pi^2 \tau_d} e^{-(p^2 t/\tau_d)} \text{ where } \tau_d = \frac{\xi\, n_s^3 (N_o l)^2}{\pi^2 kT} \qquad (4.2.8)$$

where ξ is the coefficient of friction between the chain and the tube. The function $\mu(t)$ represents the relaxation function and is appended to Eq. 4.2.7 to give the stress as a function of time during the disengagement process;

$$\sigma(t)_{in} = \mu(t) \frac{G_d}{\langle\lambda\rangle} \frac{\partial x_i}{\partial X_K} \frac{\partial x_n}{\partial X_L} \int_0^{2\pi}\!\!\int_0^{\pi} M_K M_L \frac{1}{\lambda} \frac{\sin\Theta}{4\pi} d\Theta\, d\Phi + p\,\delta_{in} \qquad (4.2.9)$$

where $G_d = 3\ kT\ nn_s$. Normally the quantities for τ_d in (4.2.8) are not known and τ_d is chosen from experimental results. Again (4.2.9) represents the stress due to a single step strain after the retraction process has occurred. The constitutive law for arbitrary flow histories at rates sufficiently low that effects only due to disengagement are noticeable is given by Doi and Edwards (1978) to be*,

$$\sigma(t)_{in} = G_d \int_{-\infty}^{t} \mu(t-\tau) \frac{\partial x(t)_i}{\partial x(\tau)_k} \frac{\partial x(t)_n}{\partial x(\tau)_l} \int_0^{2\pi}\!\!\int_0^{\pi} \frac{m_k m_l}{\lambda(t,\tau)^2} \frac{\sin\theta}{4\pi} d\theta\, d\phi\, d\tau + p\,\delta_{in} \qquad (4.2.10)$$

where $\dfrac{\partial x(t)_i}{\partial x(\tau)_k} = F_{ik}(t,\tau)$ is the relative deformation gradient and $\lambda(t,\tau)$ is the relative stretch such that $\lambda(t,\tau)^2 = m_k F_{ik}(t,\tau) F_{il}(t,\tau) m_l$. As it turns out, when a step strain is applied, Eq. 4.2.10 is slightly different than 4.2.9 due to the so called independent alignment assumption used to derive (4.2.10). This discrepancy is small at moderate strains but becomes considerable at large strains. Equation 4.2.7 and 4.2.10 is considered in Sections 4.8 and 4.9. An approximate form for Eq. 4.2.10 was given by Currie (1982) and is shown in Eq. 4.9.1.

---

[*] A constitutive law for arbitrary flow histories that includes chain retraction along with chain disengagement has yet to be developed. An equation which describes the stress during relaxation upon a step strain and includes retraction and disengagement is available (Doi and Edwards, 1986).

4.3 Proposed Force Equilibration Viscoelasticity Model

The first three mechanisms of viscoelasticity described above for the polymer melt are the same for the polymer solid and are the basis for the viscoelasticity model described here. Since all the chains are assumed to be crosslinked, no chain retraction (step 4) and chain disengagement (step 5) can occur. It remains to describe the force in the chain during its non-equilibrium stages. A complete kinetic theory could be developed to achieve the analysis, but this is deemed too difficult. The approach used here to describe the non-equilibrium force in the chain is empirical. A suitable approximation is postulated. It is unclear what effects finite extensiblity of chains have on the viscoelastic behavior of rubber. Finite extensibility has already been incorporated in the equilibrium, elastic model given in Section. 2. Development of the viscoelastic model will be in the context of infinitely extensible chains. The model can be easily generalized to the finite extensible case; at least for the equilibrium stress given by Eq. 2.4.6.

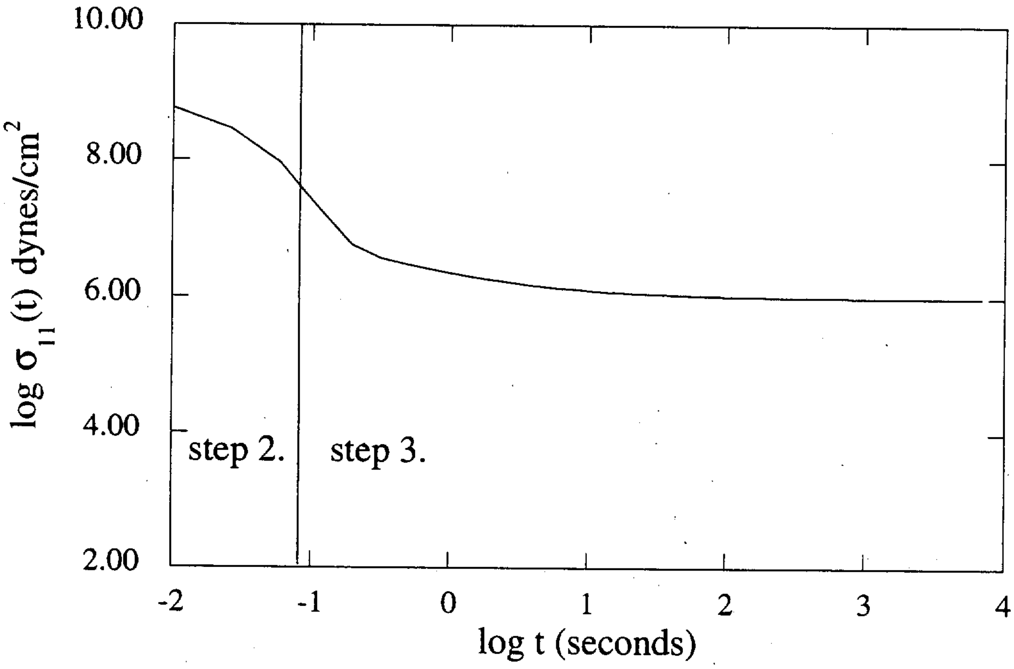

Fig. 4.3.1 Approximate sequence of events during relaxation process of a typical solid rubber. During step 1. the rubber is deformed and step 2. and 3. together comprise the chain force equilibration process.

It is useful to review the processes of relaxation considered (See Fig. 4.3.1).

(Step 1.) When the step strain is applied, friction from surrounding chains transports every point (not just the endpoints) of the chain affinely into the non-equilibrium configuration (Fig. 4.3.2 a) At this point forces in the chain may be very high. In fact, bonds between adjacent monomer links in the chain may stretched producing a glassy response.

(Step 2.) The first stage of relaxation is mainly influenced by chain diffusion occurring transverse to the tube (Fig. 4.3.2 b) In this stage, portions of the chain reconcile their non-equilibrium configuration locally (i.e. short term reconfiguration). This occurs only for a short time since the constraints of the tube disallows large scale motion in the transverse direction.

(Step 3.) Since the tube is not straight and zigzags its way through the network, portions of the chain may be in tension while others in compression. This second stage of relaxation is mainly due to diffusion along the length of the tube until the force equilibration achieved (Fig. 4.3.2 c).

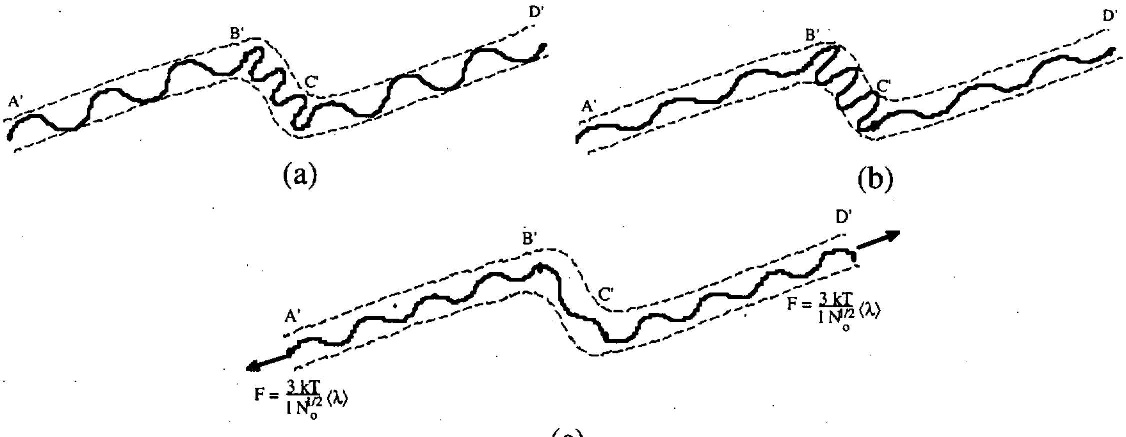
A'
B'
C'
D'
(a)
A'
B'
C'
D'
(b)
A'
B'
C'
D'
F = $\frac{3kT}{l N_o^{1/2}}(\lambda)$
F = $\frac{3kT}{l N_o^{1/2}}(\lambda)$
(c)

Fig. 4.3.2 (a) Affine motion of entire chain. (b) Relaxation of chain transverse to tube. (c) Relaxation along length of tube.

A Rouse bead chain model could be used to model step one and two although it could never capture the glassy response. After step one and two the orientational distribution function given by the solution to (4.2.4) would no longer be valid due to tube constraints. A one dimensional diffusion equation could be used for step three. Instead it is merely recognized that the forces in the chain while in the non-equilibrium state (Figs. 4.3.2 a and b) are greater than that of the relaxed chain. Furthermore, after sufficient time the chain will relax once force equilibration along the chain has been reached. The following expression is used in an attempt to describe the transient force in the chain:

$$f(t) = f_e(t) + f_v(t) = \frac{3\,kT}{\sqrt{N_o}\,l}\langle\lambda(t)\rangle + \int_{-\infty}^{t} G(t-\tau)\frac{d\lambda(\tau)}{d\tau}d\tau \qquad (4.3.1\text{ a})$$

$$\text{where } f_e(t) = \frac{3\,kT}{\sqrt{N_o}\,l}\langle\lambda(t)\rangle \quad \text{and} \quad f_v(t) = \int_{-\infty}^{t} G(t-\tau)\frac{d\lambda(\tau)}{d\tau}d\tau$$

The elastic portion of the force $f_e(t)$ represents the equilibrium value of the force for a Gaussian chain after force equilibration has been reached (the Langevin chain could also be used). The viscoelastic portion of the force $f_v(t)$ reflects the additional amount of force in the chain before equilibrium has been attained. The kernel $G(t - \tau)$ is some experimentally determined function. It would most likely be a Prony series,

$$G(t-\tau) = \sum_{i}^{N} c_i e^{-(t-\tau)/\tau_i}$$

or power law:

$$G(t-\tau) = \frac{E}{1+\left(\frac{t-\tau}{t_o}\right)^n} \qquad (4.3.1\text{ b})$$

When deformation has ceased, it is intended that $f_v(t) \to 0$ and $f(t) \to f_e(t)$ after sufficient time has passed. The form of $f_v(t)$ attempts to take into consideration the affine motion of the tube and the force fluctuations along the chain during the deformation process. The relaxed chain is shown in Fig 4.3.3 (a). As deformation is applied, the tube and surrounding network deform affinely carrying the chain into non-equilibrium configurations. Each individual section of the tube (e.g. A'B' in Fig 4.3.3 b) stretches differently depending on its orientation (θ,ϕ). Consequently, the non-equilibrium force in each section of chain is influenced by the rate of stretch of the tube $\dot{\lambda}(t)$. For example, sections of chain in tubes which experience high stretch rates $\dot{\lambda}(t)$ will experience high forces since the tube applies friction to the chain. .

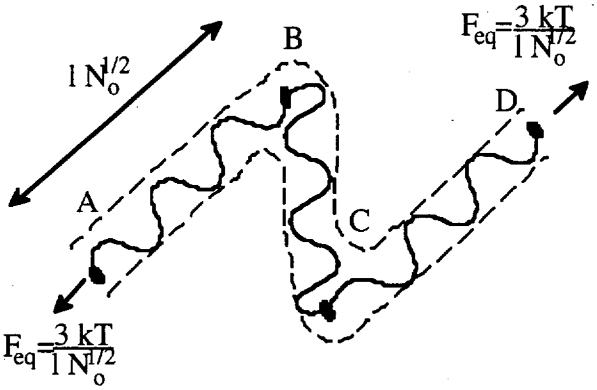
$1\,N_o^{1/2}$
B
$F_{eq}=\frac{3\,kT}{1\,N_o^{1/2}}$
D
A
C
$F_{eq}=\frac{3\,kT}{1\,N_o^{1/2}}$

Fig. 4.3.3 (a) Chain in equilibrium.

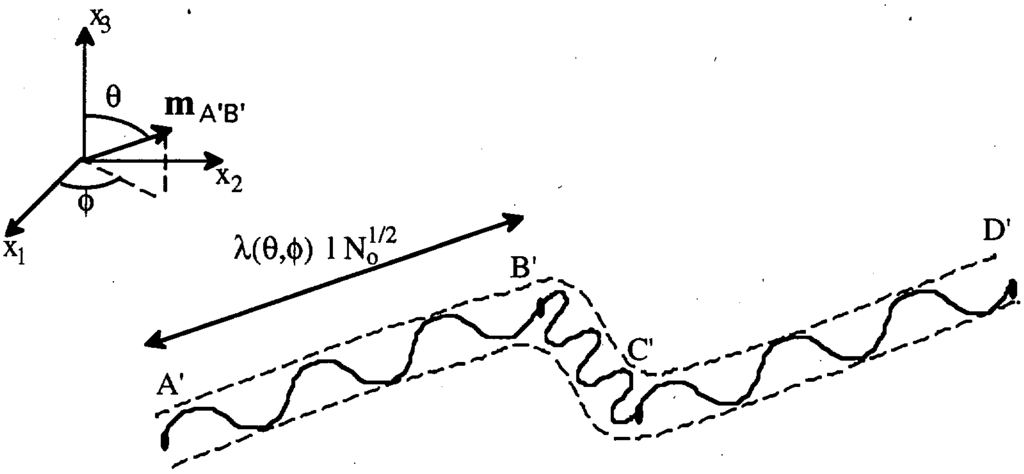

Fig. 4.3.3 (b) Chain after deformation. Tube sections stretch according to their orientation (θ,ϕ). The unit vector of $\mathbf{m}_{A'B'}$ represents the orientation of A'B'. Section A'B' has been stretched while B'C' has been compressed.

The easiest way to illustrate the model is to use a mechanical analogy. The non-equilibrium force f_v is equivalent to a spring and damper element. The undeformed chain shown in Fig. 4.3.3 (a) is shown as an assembly of these spring damper elements in Fig. 4.3.4 (a). After deformation the points ABCD transform affinely and the non-equilibrium force can be calculated. For example the force $(f_v)_{A'B'}$ (Fig. 4.3.4 b) in the deformed segment can be calculated exactly by the following hereditary integral,

$$f_v(t)_{A'B'} = \int_{-\infty}^{t} k l_o \, e^{-(t-\tau)/t_o} \frac{d\lambda(\tau)}{d\tau} \, d\tau \qquad (4.3.2)$$

where k is the spring constant, t_o is a relaxation time, and l_o is the undeformed length (See Fig 4.3.4 a). Clearly the force in the spring damper system diminishes over time once the deformation has ceased.

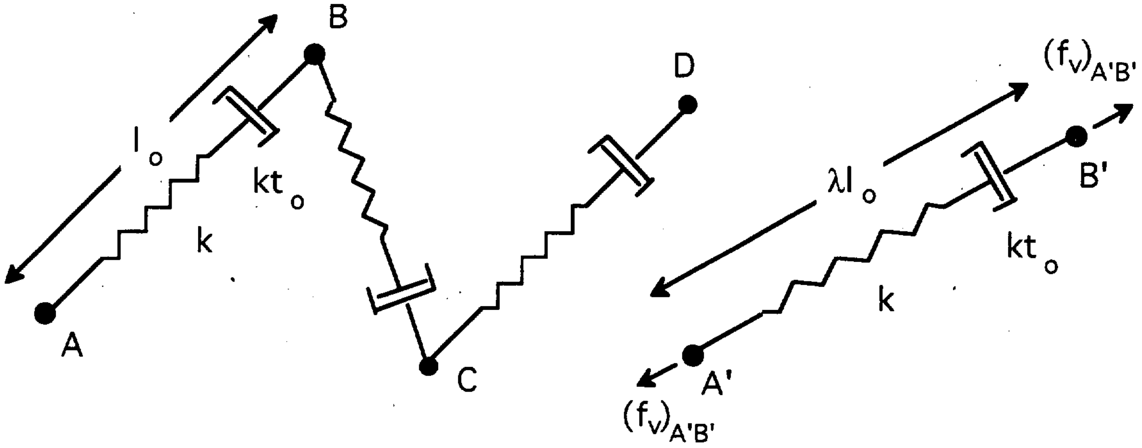

(a) (b)

Fig 4.3.4 (a) The undeformed assembly of spring dampers elements. The spring constant is k and the damping coefficient is kt_o where t_o is some relaxation time. (b) The segment AB after deformation. Segment AB length lo is stretched by a factor of λ.

The force in the chain (Eq. 4.3.1) along with Eqs. 3.19 or 3.20 are used to find the stress tensor. The total number of subchains $n_t = n\, n_s$, where n is the number of polymer chains and n_s is the number of subchains per polymer chain. Associating l_o with $\sqrt{N_o}\, l$ (the undeformed subchain length) and using Eq. 4.3.1 for the force in the chain in Eq. 3.20 gives the following equation for the second Piola Kirchoff stress,

$$S_{KL}(t) = n n_s \sqrt{N_o}\, l \int_0^{2\pi}\!\!\int_0^{\pi} \left(\frac{3kT}{\sqrt{N_o}\, l} \langle\lambda\rangle + \int_{-\infty}^{t} G(t-\tau) \frac{d\lambda(\Theta,\Phi,\tau)}{d\tau} \, d\tau \right) \times$$

$$\frac{M_K M_L}{\lambda(\Theta,\Phi)} \frac{\sin\Theta}{4\pi} \, d\Theta \, d\Phi + p\, F^{-1}_{Kn} F^{-1}_{Ln} \qquad (4.3.3)$$

The stress can be divided into the elastic and viscoelastic contributions:

$$S^{e}_{KL}(t) = 3\,G\,\langle\lambda\rangle \int_{0}^{2\pi}\!\!\int_{0}^{\pi} \frac{M_K\,M_L}{\lambda(\Theta,\Phi)}\,\frac{\sin\Theta}{4\pi}\,d\Theta\,d\Phi + p\,F^{-1}_{Kn}\,F^{-1}_{Ln} \qquad (4.3.4)$$

$$S^{v}_{KL}(t) = \int_{0}^{2\pi}\!\!\int_{0}^{\pi} \left(\int_{-\infty}^{t} G(t-\tau)\frac{d\lambda(\Theta,\Phi,\tau)}{d\tau}\,d\tau \right) \frac{M_K\,M_L}{\lambda(\Theta,\Phi)}\,\frac{\sin\Theta}{4\pi}\,d\Theta\,d\Phi \qquad (4.3.5)$$

where $G = nn_s$ in Eq. 4.3.4 and $nn_s\sqrt{N_o\,l}$ from Eq. 4.3.3 is subsumed into the kernel function $G(t-\tau)$ in Eq. 4.3.5. The elastic portion $S^{e}_{KL}(t)$ is the Piola Kirchoff stress equivalent to Eq. (2.2.20 a) considering infinitely extensible chains. It remains to analyze the viscoelastic backstress.

4.4 Thermodynamic Considerations

For a Prony series kernel, it is shown in Appendix C that the viscoelastic backstress is actually the gradient of the following scalar potential functional:

$$\Psi^{V} = \frac{1}{2}\int_{0}^{2\pi}\!\!\int_{0}^{\pi} \sum_{i}^{N} \left(\int_{-\infty}^{t} c_i\, e^{-(t-\tau)/\tau_i}\frac{d\lambda(\Theta,\Phi,\tau)}{d\tau}\,d\tau \right)^{2} \frac{\sin\Theta}{4\pi}\,d\Theta\,d\Phi \qquad (4.4.1)$$

such that

$$S^{v}_{KL}(t) = \frac{\partial\Psi^{V}}{\partial E_{KL}} \qquad (4.4.2)$$

where E_{KL} is the Greens strain tensor. If a power law kernel is used the summation in Eq. 4.4.1 is replaced by a Fourier transform integral over the frequency domain. Because of Eq. (4.4.2), Ψ^{v} is the free energy functional and the constitutive law is termed hyperviscoelastic. The rate change of the free energy Ψ^{v} is

$$\dot{\Psi}^{v}(E_{KL},t) = \frac{\partial\Psi^{v}}{\partial E_{KL}}\,\dot{E}_{KL} + \frac{\partial\Psi^{v}}{\partial t} \qquad (4.4.3)$$

and the rate of dissipation (Christensen, 1982) is defined by

$$\Lambda = -\frac{\partial \Psi^{v}}{\partial t} \qquad (4.4.4)$$

It is shown in Appendix C that rate of dissipation of energy is always nonnegative i.e. $\Lambda \geq 0$. Consequently the constitutive law satisfies the Clausius Duhem inequality (Eringen, 1967) for isothermal processes:

$$\Lambda = S_{KL}\dot{E}_{KL} - \dot{\Psi}^{v} \geq 0 \qquad (4.5.5)$$

Since the stress is the gradient of a scalar, a suitable approximation for Ψ^{v} will yield a symmetric tangent stiffness matrix for finite element analysis.

4.5 Approximation of the Viscoelastic Backstress

Equation 4.3.5 cannot be solved analytically. Several attempts were made to get the best approximation. Two approximations are developed here. Both approximations rely on the approximation for the stretch λ (shown plotted in Figs. 2.4.2-3)

$$\lambda(\Theta,\Phi) \approx \sqrt{I_1/3} + \frac{1}{2}\left(\frac{I_1}{3}\right)^{-1/2}(\lambda^{2}(\Theta,\Phi) - \frac{I_1}{3}) + \frac{1}{8}\left(\frac{I_1}{3}\right)^{-3/2}(\lambda^{2}(\Theta,\Phi) - \frac{I_1}{3})^{2} \qquad (4.5.1)$$

where $\lambda^{2}(\Theta,\Phi) = M_K\, C_{KL}\, M_L$, the integral identities Eq. 1.16-1.19 and other similar approximation techniques.

The first approximation is made directly on Eq. 4.3.5 and is shown in Eq. 4.5.2

$$S^{v}_{ij}(t) \approx \frac{I_1^{-1/2}}{30}\left[(14 - 9\frac{I_2}{I_1^{2}})\,\delta_{ij}\delta_{kl} - \frac{9}{I_1}\delta_{ij}C_{kl} - \frac{18}{I_1}\delta_{kl}C_{ij} + 6\,\delta_{ik}\delta_{jl}\right]\int_{-\infty}^{t} G(t-\tau)\frac{d}{d\tau}(I_1^{-1/2}\, C_{kl})\, d\tau \qquad (4.5.2)$$

Eq. 4.5.2 is fully derived in Appendix D. The advantage of this approximation is that it gave the best results compared to exact numerical solution of Eq. 4.3.5 using the least amount of terms. Approximations made directly on Eq. 4.3.5 are not guaranteed to give visco-hyperelastic forms (See Section 4.4). It turns out that Eq. (4.5.2) is not viscohyperelastic and the resulting tangent stiffness matrix is not symmetric. Consequently, symmetry is sacrificed for accuracy.

The second method approximated the free energy functional Eq. 4.4.1 and is shown for the case of a single exponential kernel in Eq. 4.5.3

$$\Psi^{v} \approx \frac{3c}{20}\left(\int_{-\infty}^{t} e(t - \tau)/t_o \frac{d}{d\tau}(I_1(\tau))^{1/2}\, d\tau\right)^{2} +$$

$$\frac{c}{20}\int_{-\infty}^{t}\int_{-\infty}^{t} e^{(2t - \tau - \eta)/t_o} \frac{d}{d\tau}\left(I_1(\tau)^{-1/2} C_{kl}(\tau)\right) \frac{d}{d\eta}\left(I_1(\eta)^{-1/2} C_{kl}(\eta)\right) d\tau\, d\eta \qquad (4.5.3)$$

Eq. 4.5.3 is derived in Appendix D. The stress is the gradient of the free energy function (4.5.3) with respect to the Green strain and is shown for the case of a general Prony series of a power law kernel in Eq. 4.5.4

$$S_{ij}^{v}(t) \approx \frac{1}{10\, I_1^{1/2}}\left[3\, \delta_{ij}\delta_{kl} - \frac{1}{I_1}\delta_{ij}C_{kl} + (\delta_{il}\delta_{jk} + \delta_{ik}\delta_{jl})\right]\int_{-\infty}^{t} G(t - \tau)\, \frac{d}{d\tau}(I_1^{-1/2}\, C_{kl})\, d\tau \qquad (4.5.4)$$

The advantage of this approximation is that it satisfies the Clausius Duhem inequality, and yields a symmetric stiffness matrix. It will be shown that this method is not as accurate as the first method. Using an additional term for the approximation of λ (Eq. 4.5.1) will give a more accurate approximation for the stress, but would include eighth order tensors in the expression and would be too unwieldy.

To determine the efficacy of the approximations, a single exponential kernel (Eq. 4.5.5) was used (relaxation time $t_o = 0.75$ minutes and $c = 1$ MPa) and both methods were compared to the numerical solution of Eq. 4.3.5.

$$G(t) = c\, e^{-t/t_o} = 1\, e^{-4/3\, t} \qquad (4.5.5)$$

The numerical solution of Eq. 4.3.5 was provided by a Gauss point integration similar to the one made for the elasticity equations in Section 1 and Appendix A. An additional numerical solution to the hereditary integral included in Eq. 4.3.5 is found using a recursion algorithm at every Gauss point. As with the numerical solution made in Appendix A the spherical domain is mapped to a rectangular domain and then discretized. Unlike before, the adaptive algorithm was not used since the strain history was required at the Gauss points. Typically 20 panels with 6x6 Gauss points were found to be more than adequate to perform the integration. The uniaxial stretch history shown in Fig. 4.5.1 (a) was used to evaluate the two approximations against the exact numerical solution with the results shown in Fig. 4.5.1 (b). The first method corresponding to Eq. 4.5.2 is called the direct approximation while the second method (Eq. 4.5.4) is called the symmetric approximation. It is seen that the symmetric approximation at $\lambda = 4$ is off by almost 15% while the direct is off by 8%.

The direct method is also compared to the numerical integration for a ramp loading in shear (Fig. 4.5.2 a). The results for the shear stress are shown in Fig. 4.5.2 (b) and the results for first and second normal stress are shown in Fig. 4.5.2 (c). The direct method gave good approximations for the both the shear stress and the normal stresses up to shear a shear of 2. The direct method was used to generate all the results given in Section 4.6.

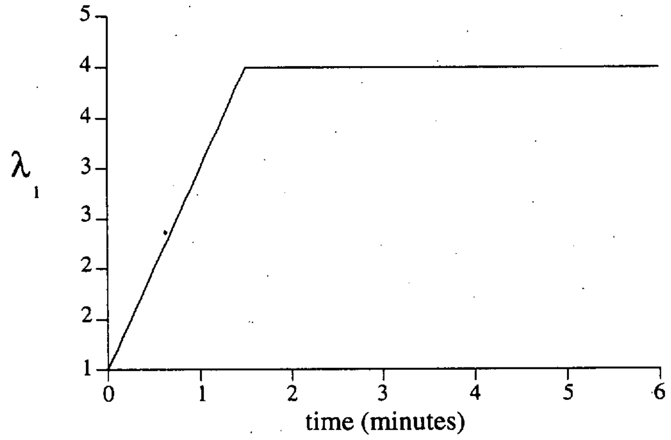

Fig. 4.5.1 (a) Axial stretch history used for evaluation of approximations

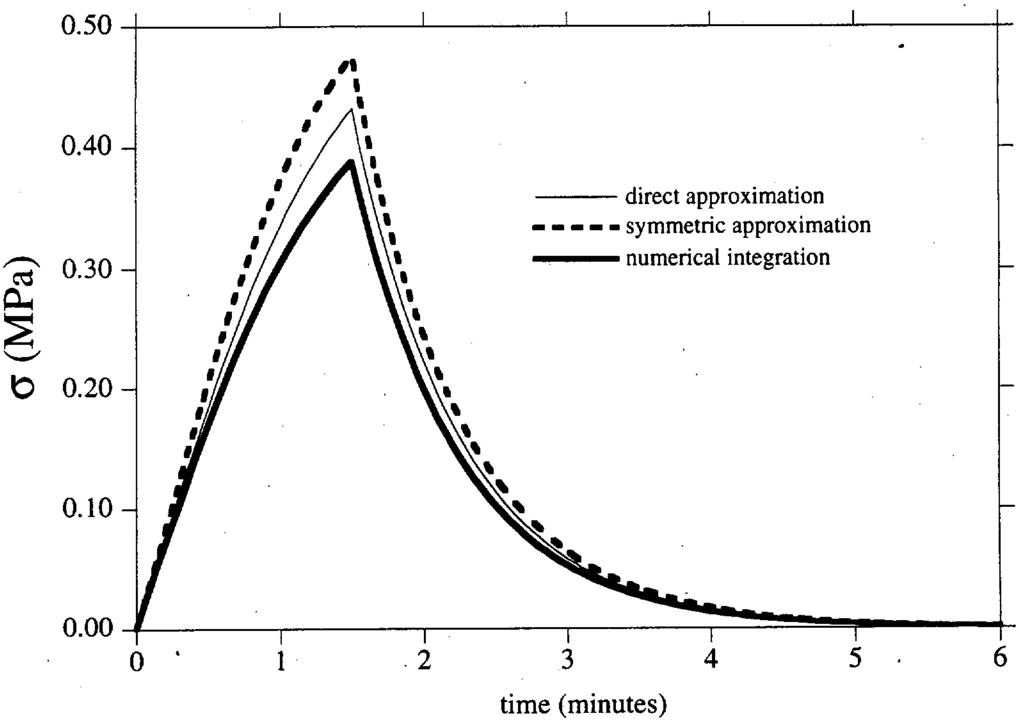

Fig. 4.5.1 (b) Comparison of approximation methods to numerical integration of Eq. 4.3.5 for axial loading shown in Fig. 1.

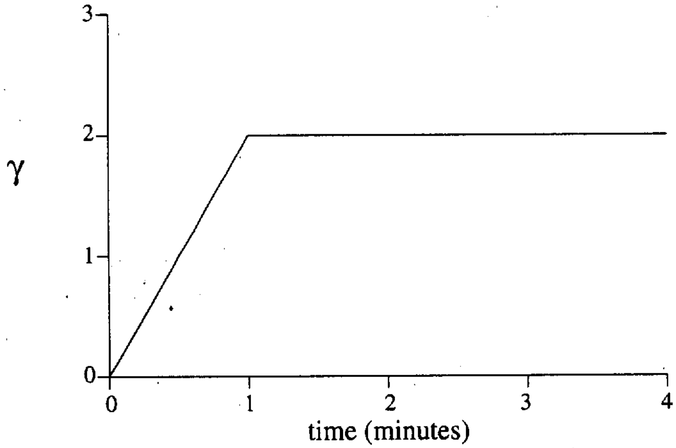

Fig. 4.5.2 (a) History function for shear loading

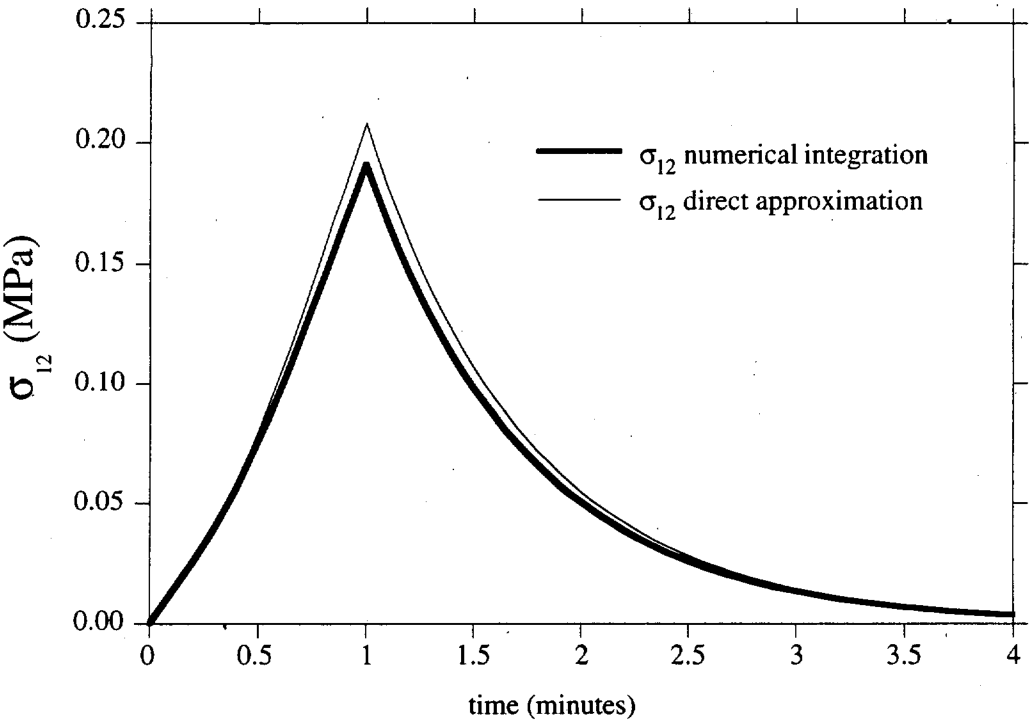

Fig. 4.5.2 (b) Comparison of approximation shear stress to numerical integration of Eq. 4.3.5 for shear loading shown in Fig. 4.5.3 (a)

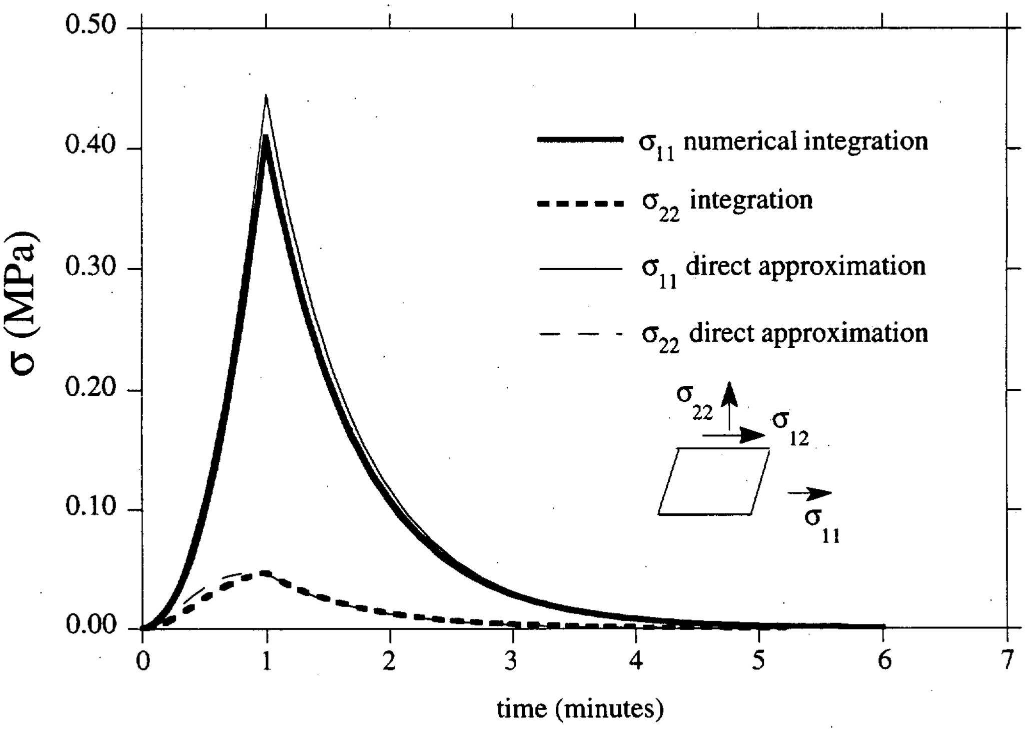

Fig. 4.5.2 (c) Comparison of approximate normal stress to numerical integration of Eq. 4.3.5 for shear loading shown in Fig. 4.3.3.

4.6 Comparison of Force Equilibration Viscoelastic Model to Experimental Results

A literature search was made to find published finite strain viscoelastic data for unfilled crosslinked rubber. Some of the data found is listed in the following articles: T.L Smith (1962,1969); Bloch, Chang and Tschoegle (1978,1978); McGuirt and Lianis (1969, 1979); Goldberg and Lianis (1970); Yuan and Lianis (1972); Scholtens and Leblans (1986); L.J. Zapas et. al. (1965, 1966). More published data is available; most of it was published by the authors given in the previous list. Most of the data is for uniaxial relaxation and stretching at a constant stretch rate. Goldberg and Lianis (1970) and Yuan and Lianis (1972) are the only articles found with data relating to shear deformation. Zapas (1966) and McGuirt and Lianis (1970) include some biaxial relaxation data.

In the following, unpublished data by Dafalias and data by Bloch, Chang and Tschoegle (1978) is used to evaluate the force equilibration model. It must be mentioned that the force equilibration model was based on the assumption that the majority of the chains in the network are crosslinked. It is realized that most rubber would probably not meet this stipulation. Nevertheless, in developing the model it was hoped that the ideal conditions would prevail and that additional viscoelasticity due to other effects could still be captured successfully.

The force equilibration viscoelastic model is used to simulate unpublished shear relaxation and cyclic shear data from Dafalias. The chemical properties of the rubber were not made available by the proprietor. The model is the sum of elastic and viscoelastic contributions to the stress.

$$\sigma_{ij} = \sigma^{e}_{ij} + \sigma^{v}_{ij} + p\,\delta_{ij} \qquad (4.6.1)$$

where the elastic portion of stress is defined is:

$$\sigma^{e}_{ij} = \frac{3\,G\,\frac{\sqrt{3}}{10}\left(3I_1^{1/2} + \frac{I_2}{I_1^{3/2}}\right)}{1 - \left(\frac{1}{\sqrt{N_o}}\,\frac{\sqrt{3}}{10}\left(3I_1^{1/2} + \frac{I_2}{I_1^{3/2}}\right)\right)^3}\left(\frac{\sqrt{3}}{2}\left(I_1^{-1/2} - \frac{3}{5}\,\frac{I_2}{I_1^{5/2}}\right)B_{ij} - \frac{2\sqrt{3}}{5}\,I_1^{-3/2}\,B^2_{ij}\right) \qquad (4.6.2)$$

and the viscoelastic second Piola Kirchoff stress is:

$$S^v_{ij} = \frac{I_1^{-1/2}}{30}\left[\left(14 - 9\frac{I_2}{I_1^2}\right)\delta_{ij}\delta_{kl} - \frac{9}{I_1}\delta_{ij}C_{kl} - \frac{18}{I_1}\delta_{kl}C_{ij} + 6\,\delta_{ik}\delta_{jl}\right]\int_{-\infty}^{t} G(t-\tau)\,\frac{d}{d\tau}(I_1^{-1/2}\,C_{kl})\,d\tau \tag{4.6.3}$$

The viscoelastic Cauchy stress is found by the transformation $\sigma^v_{ij} = F_{iK}\,S^v_{KL}\,F_{jL}$ where F_{iK} is deformation gradient. In order to model data, values for the rubbery modulus G and the number of links between entanglements must be chosen. Furthermore, a relaxation function G(t) must be chosen. Data from the shear relaxation test provided by Dafalias is shown in Fig. 4.6.1. A step shear strain $\gamma = 1.1$ was applied to a thin walled cylindrical sample over the period of 5 seconds after which relaxation occurred. The following constitutive parameters were used to model the experimental relaxation curve:

$G = .627$ (MPa)
$N_o = 3.8$
$G(t) = 28.1\,e^{-t/4} + 0.135\,e^{-t/5\times10^3} + 0.135e^{-t/4\times10^4}$ (MPa) where time is in seconds

The data is also shown using a log-log plot in Fig. 4.6.2. Examination of Fig. 4.6.2 shows that the stress in the sample has yet to relax. Results from a cyclic shear experiment $|\gamma|_{max} = 2$ along with the simulated results using the above parameters are shown in Fig. 4.6.3. The rate of shear was $\dot{\gamma} = 0.01335\ s^{-1}$ such that it took 150 sec. for the shear strain to go from 0 to 2. It is seen that the experimental data is not symmetric about the undeformed configuration due to some experimental error. Nevertheless, the simulation appears to give good results. The model is capable of capturing the thinning of the loop near the undeformed configuration. The amount of upturn in the curves at such low strains seems rather unusual.

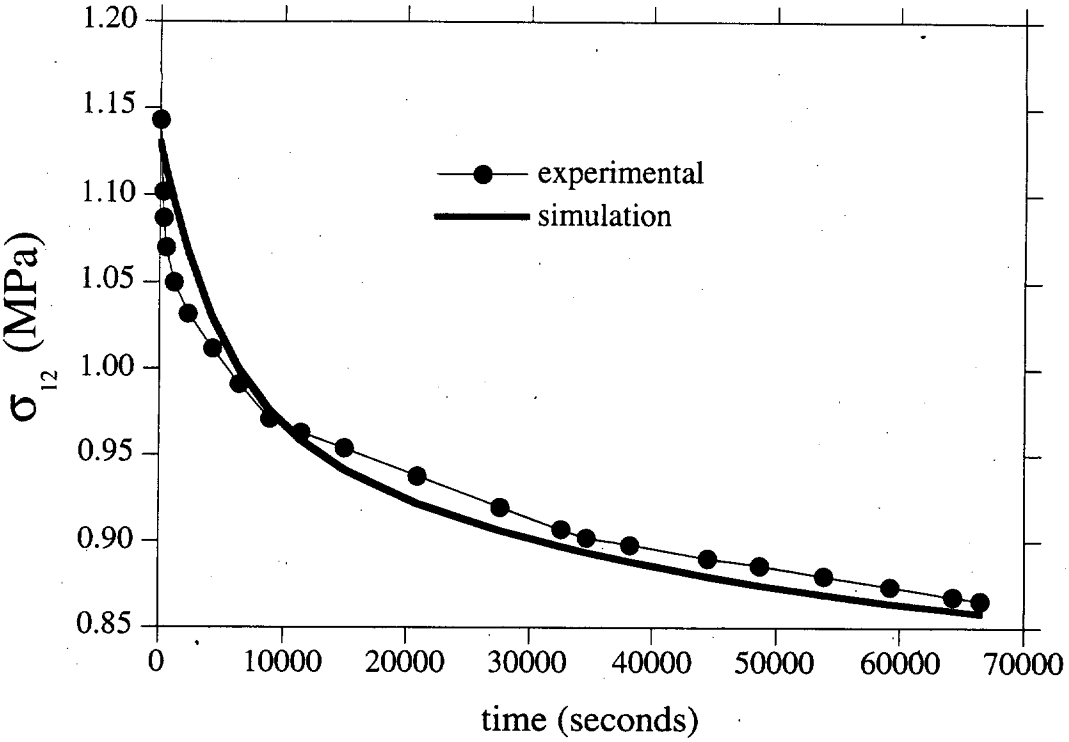

Fig. 4.6.1 Experimental relaxation data along with simulation. A shear of $\gamma = 1.1$ was applied to a cylindrical sample and allowed to relax. (data from Dafalias unpublished)

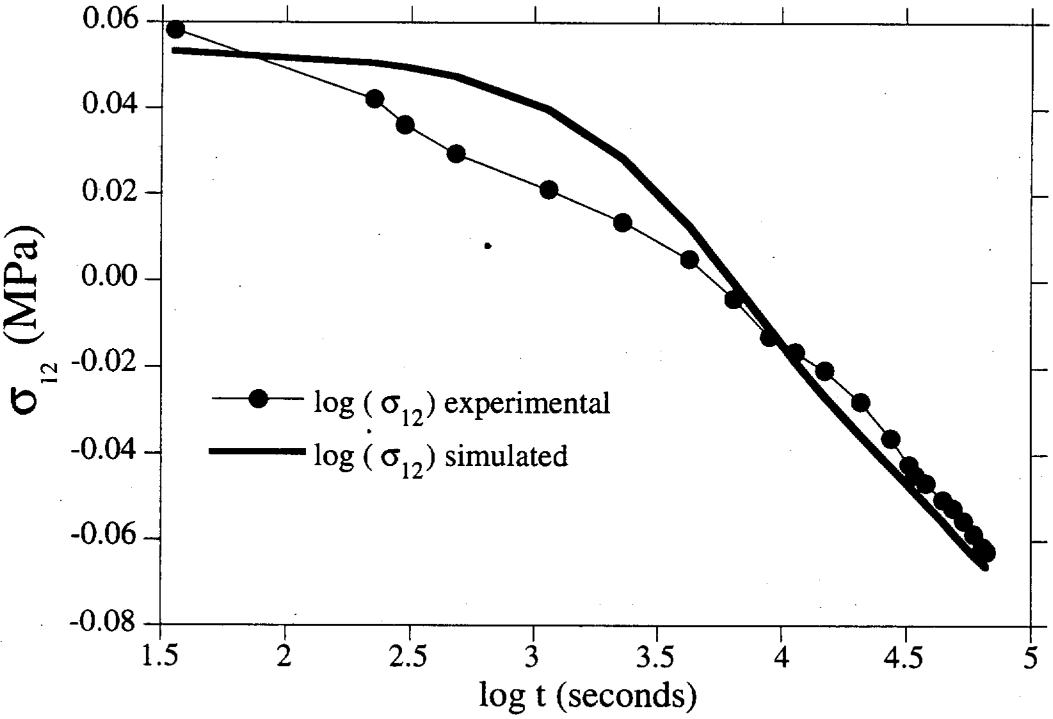

Fig. 4.6.2 Relaxation data and simulation for step shear $\gamma = 1.1$ plotted in log-log format. Notice that the stress over the time period considered has yet to fully relax.

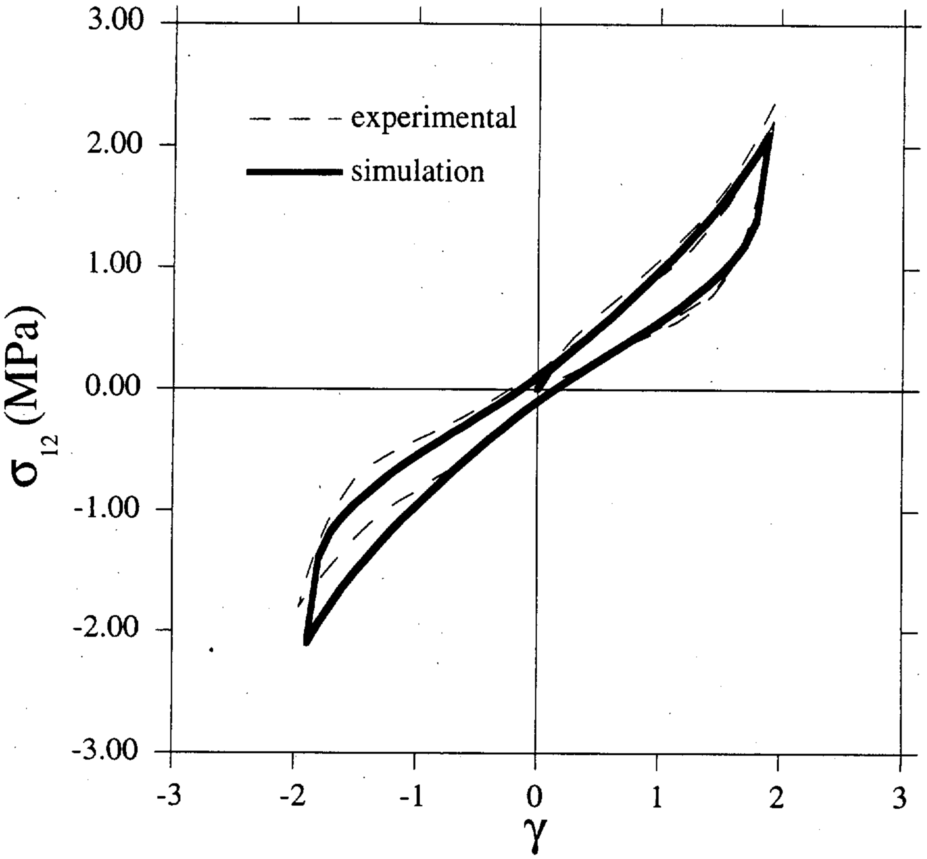

Fig. 4.6.3 Cyclic shear strain for strain rate $\dot{\gamma} = 0.01335$.

A particularly low value of N_0 ($N_0 = 3.8$) was used to capture the upturn. One must remember that in strict terms N_0 does not really represent the number of monomers between entanglements, but instead represents the number of statistical links due to steric hinderances between bonds of adjacent monomers. Nevertheless, N_0 is ridiculously low. This is probably due to strain induced crystallization occurring. It is hard to determine this precisely since the chemical composition of the elastomer was not divulged.

Finite strain uniaxial data from Bloch, Chang and Tschoegle (1978) is shown in Figs. 4.6.4 - 4.6.7. The experiments were performed on SBR rubber samples. This rubber is typically used for automobile tires due to its toughness and is probably the elastomer most often studied. In Fig. 4.6.4, data for uniaxial stretching at three different stretch rates is shown. The stress 'f' in Fig. 4.6.4 is the force per undeformed area. The material parameters and relaxation function used to model the data are the following:

$G = 2.73$ (MPa)

$N_o = 50$

$$G(t) = \frac{150}{1 + (t / 1\text{x}10^{-5})^{0.4}} \text{ (MPa) where } t_o = 1\text{x}10^{-5} \text{ minutes}$$

The samples were stretched at a constant rate such that $\lambda(t) = 1 + r\,t$ with $r = 0.011$ min.$^{-1}$, 0.442 min.$^{-1}$, and 4.42 min.$^{-1}$. The data was fit as best as possible using the proposed viscoelastic model. The method seems to be ineffective in capturing the large amount of curvature apparent in the experimental data. The failure of the method is not due to the choice of parameters of the model, but is an inherent trait of the model. Different kernels for the viscous stress could not reproduce the amount of negative curvature observed in the data.

The Cauchy stress for the same data is plotted in Fig. 4.6.5. The difference in curvature is particularly apparent in this plot. Whereas the simulated results are concave up and then proceed as straight lines, the experimental results are just straight lines. In fact, for much of the other data surveyed the Cauchy stress plots are concave down up to a stretch of about two before proceeding in a straight line.

It is assumed that at $r = 0.0011$, the experimental data in Fig. 4.6.4 and 4.6.5 is mostly elastic (at $r = 0.0011$, it takes 21 hours to stretch the sample to $\lambda = 2.4$) The stress at $r = 0.0011$ is subtracted from the stress at $r = 4.42$ and 0.442 and plotted in Fig. 4.6.6 (e.g. $\sigma^v = \sigma_{r = 4.42} - \sigma_{r = 0.0011}$). The stress σ^v in Fig. 4.6.6 is basically the viscoelastic Cauchy backstress (i.e. stress/deformed area). The backstress for the proposed model is concave up while the experimental backstress appears concave down.

Another useful perspective is provided by the Mooney stress plots shown in Fig. 4.6.7. The behavior at $\lambda = 1$ is usually disregarded due to experimental error and small strain effects. Examination of the experimental data in Fig. 4.6.7 reveals that the viscous portion of the stress (i.e. the difference between the r=4.42 and r=0.0011 curve) is more profound at the small strains and that the experimental curves for the different rates

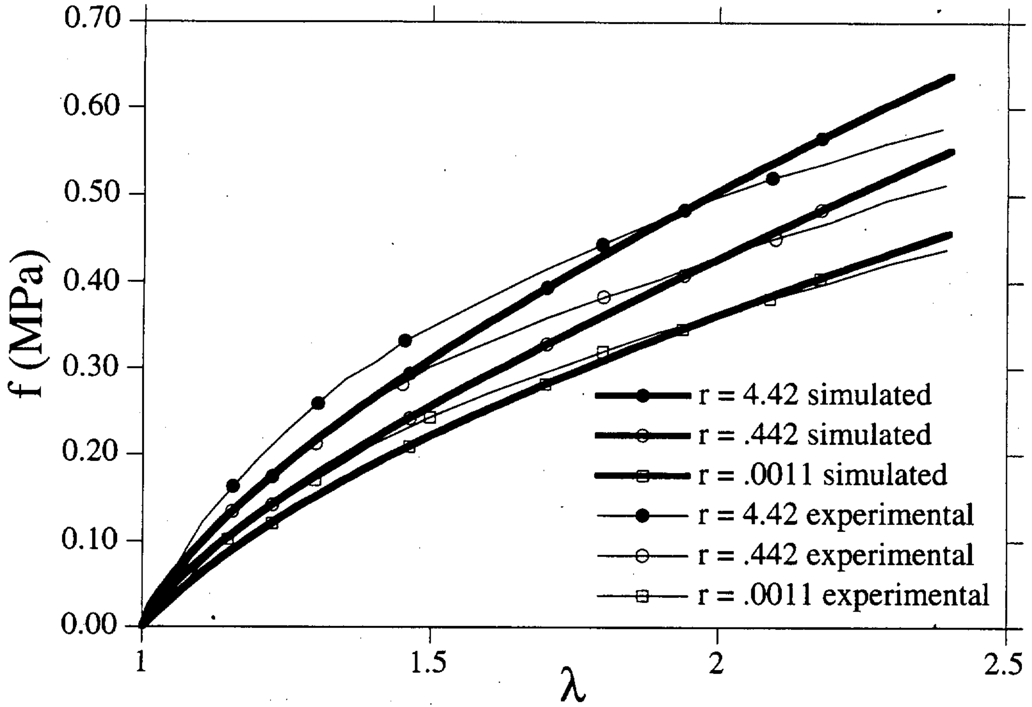

Fig. 4.6.4 Force per undeformed area for three different uniaxial stretch rates. Experimental data taken from Bloch, Chang and Tshoegle (1978)

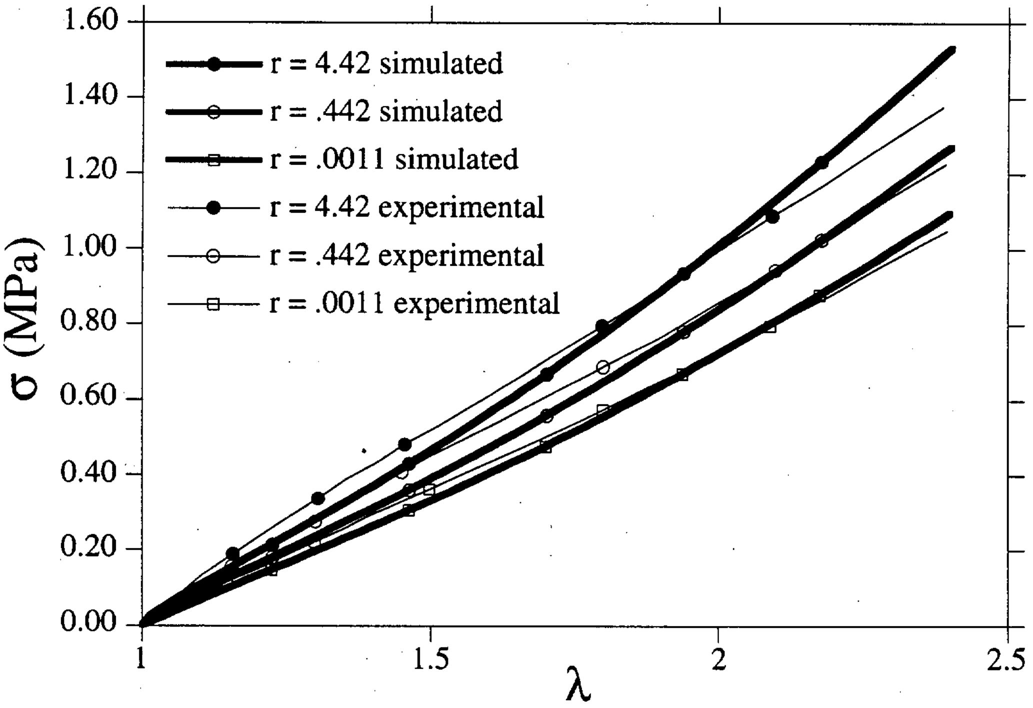

Fig. 4.6.5 Cauchy stress for three different uniaxial stretch rates Notice the concave upward nature of the simulations compared to the experimental data. (data from Bloch et. al. 1978)

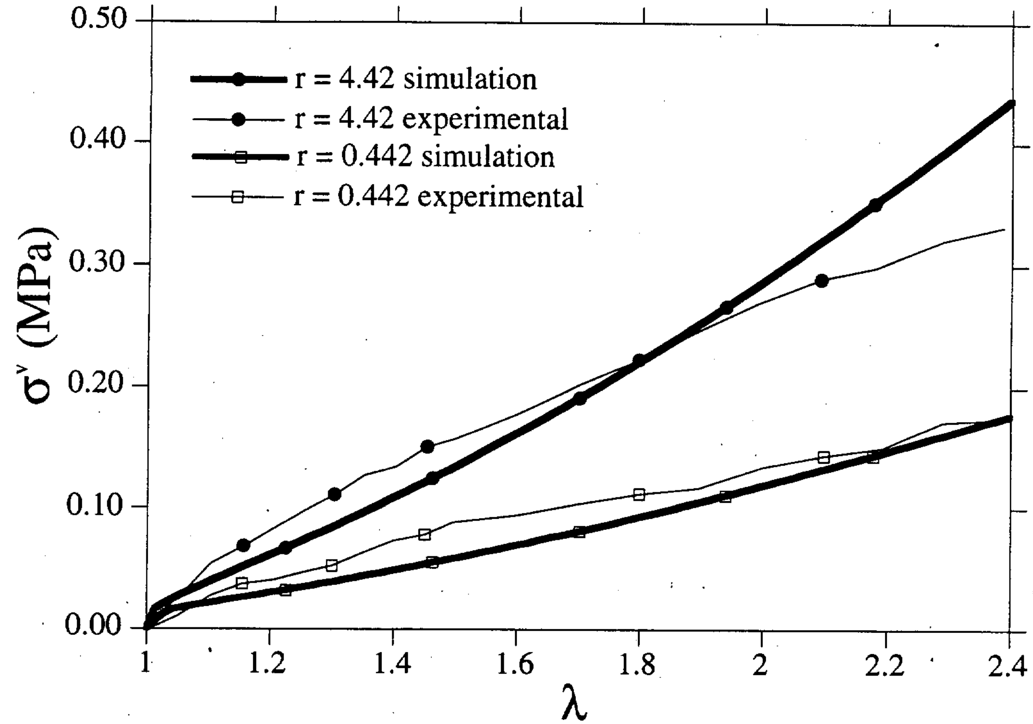

Fig. 4.6.6 Viscoelastic 'backstress' for r = 4.42 and r = 0.442. Stress is plotted as force per deformed area (i.e. Cauchy) (data from Bloch et. al. 1978)

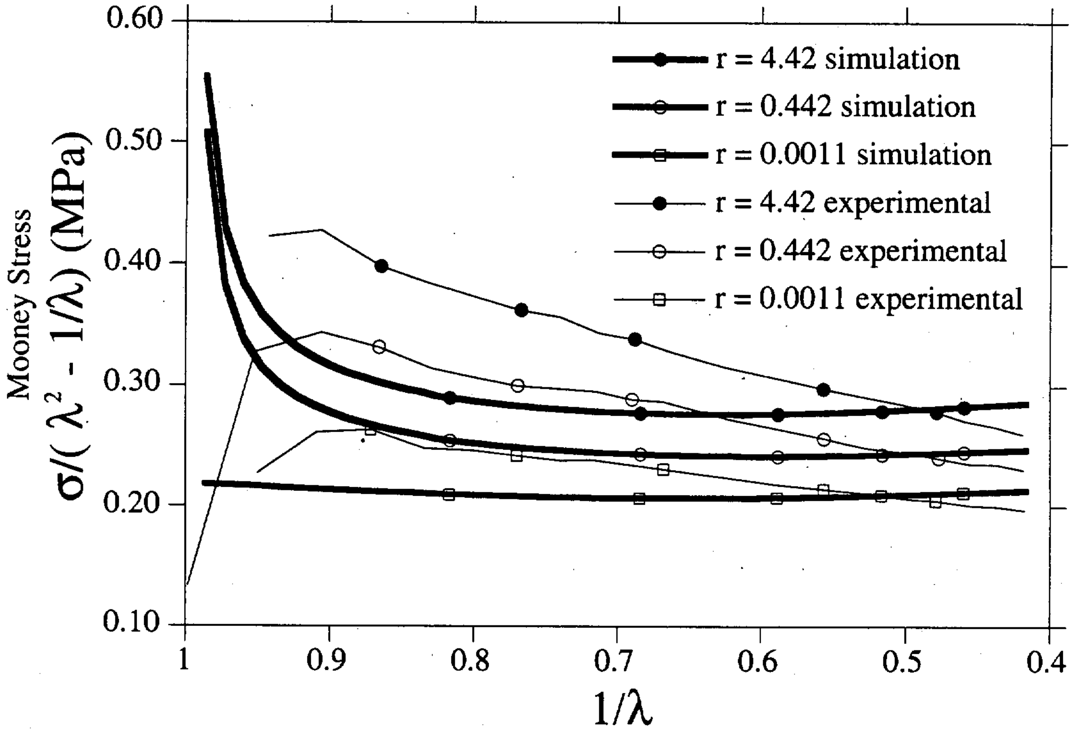

Fig. 4.6.7 Mooney Rivlin plot. (data from Bloch et. al. 1978)

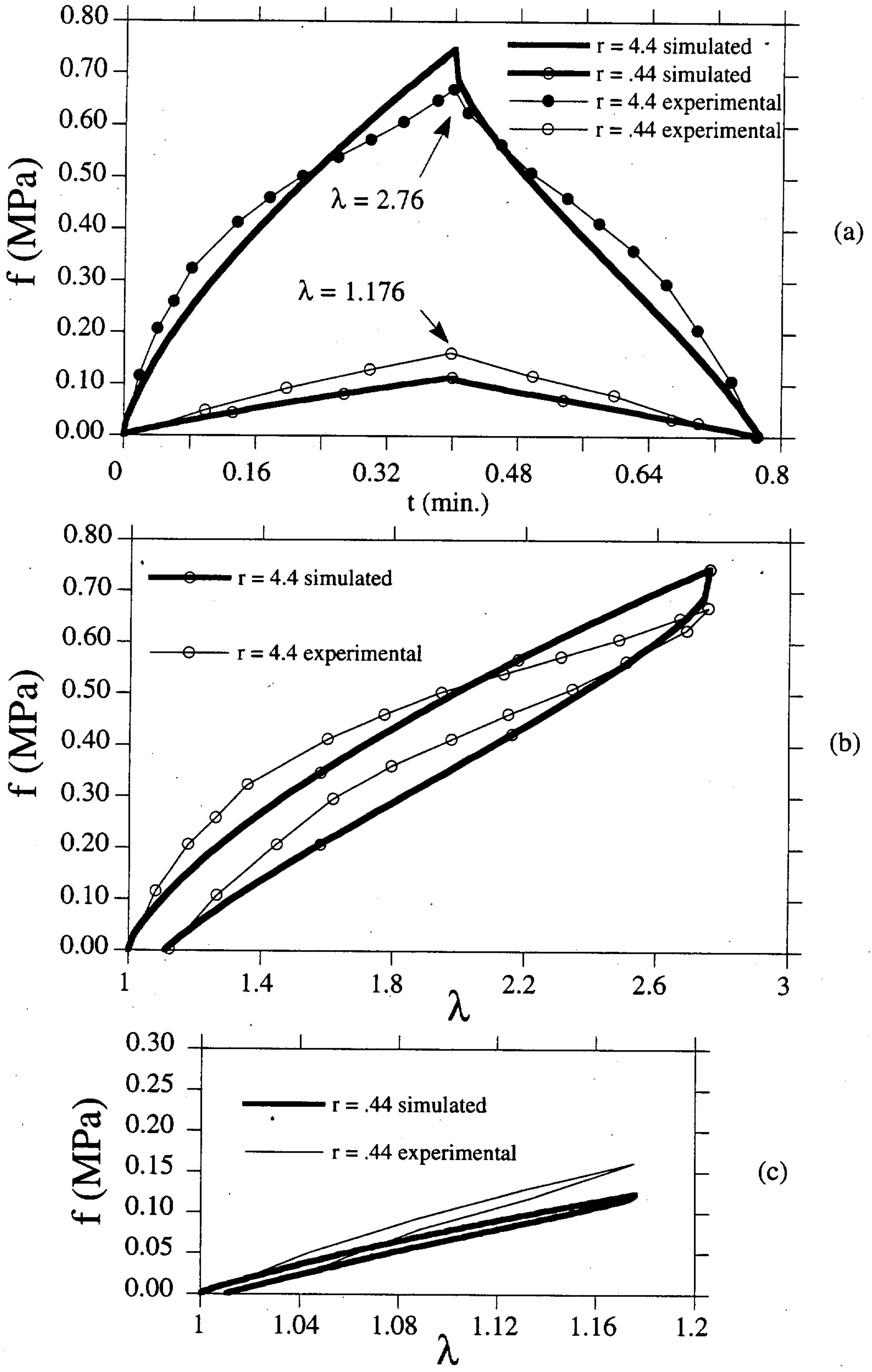

Fig. 4.6.8 Cyclic axial stretching at constant rate ± r. (data from Bloch et. al. 1978) (a) Plotted on time scale. (b) and (c) plotted by stretch.

appear to converge as the stretch increases. Apart from the behavior near $\lambda = 1$, the curves for the proposed model are parallel. It is seen that the Mooney plots reveal a discrepancy in the elastic stress. This has been noted by Gottlieb et. al. (1983) for the elastic entanglement model used, but this discrepancy is not serious when the data is plotted using the Cauchy stress and force/undeformed area. This discrepancy becomes even less apparent when finite strain effects become apparent as was seen Section 2.

Additional data from Bloch et. al. (1978) with simulations for axial cyclic loading are shown in Figs. 4.6.8 (a), (b) and (c). Again the stress f used in plotting is the force per undeformed area. These plots naturally reflect the same discrepancies as seen in Fig. 4.6.5. Evaluation of Figs. 4.6.5 - 4.6.8 show that the model clearly has the wrong strain dependence. Possible causes behind the models inability to simulate the experimental data are discussed in the following sections.

4.7 Evaluation of Results

The proposed model appeared to give good quantitative and qualitative results for the shear relaxation and cyclic shear tests. Actually the cyclic shear data appears to be different than that seen from tests perform on filled rubber bearings (Kelly 1990). In Kelly's tests, the loops do not thin near the reference configuration. It is hard to say whether the loops of an unfilled rubber always experience such a large amount of thinning. It is recognized from Fig. 4.6.8 that the loops in cyclic axial loading thin slightly at the reference configuration. Surprisingly, no other finite strain cyclic shear results were found in the literature. Some date for monotonic constant rate shear was published by Yuan and Lianis (1972). Their test were not performed at sufficiently different rates and hence did not reflect significant viscoelastic behavior. Results for shear relaxation were published by McGuirt and Lianis (1970). The models ability to simulate the cyclic shear is inconclusive, particularly in view of results from axial stretch tests.

It is instructive to consider additional published constant axial stretch rate data Experimental results given by Smith (1962) and Scholtens and Leblans (1986) are shown in Figs. 4.7.1 and 4.7.2. Both figures plot the Cauchy stress verses stretch for different stretch rates*. Whereas the Cauchy stress plots of Tschoegle's (Fig. 4.6.5) test results are nearly straight lines, Figs. 4.7.1 and 4.7.2 show a significant amount of negative curvature at initial stretching. McGuirt and Lianis (1970) published data for uniaxial stretching at a constant rate (2 curves at about the same rate) and the results appeared similar to that of Bloch et. al. (1978). It is hard to generalize the results seen in the published data, since there are many variables involved (i.e. molecular composition, molecular weight, amount and method of crosslinking, temperature, etc). It does appear that the positive curvature produced by the force equilibration model (Fig. 4.7.5) is not normal.

The constitutive model is clearly incapable of capturing the qualitative nature of the rubber in constant stretch rate loading. There are many possible reasons behind the inadequacy of the model. The deficiency of the model is most probably due to the fact that much of the viscoelasticity occurring during a constant strain rate test is due to imperfections in the network. At the outset it was mentioned that these effects are not considered in this model. It was assumed that the network was perfect. Near perfect networks can be synthesized (Mark and Erman, 1988), but are probably more elastic (i.e. less viscous) than the rubber used in the experiments considered here. Network imperfections take the form of dangling chains and sol fraction. Dangling chains are chains which are not crosslinked at both ends and sol fraction are chains which are not crosslinked at all. Both these types of chains would experience the effects of chain retraction and chain disengagement described in section 4.2. During relaxation, the effects of chain retraction and disengagement mainly occur after force equilibration.

---

* The EPDM rubber in Fig. 5.7.2 was known not to be highly crosslinked whereas the SBR in Fig. 5.7.3 was at -34° C. (there is not a lot of published data)

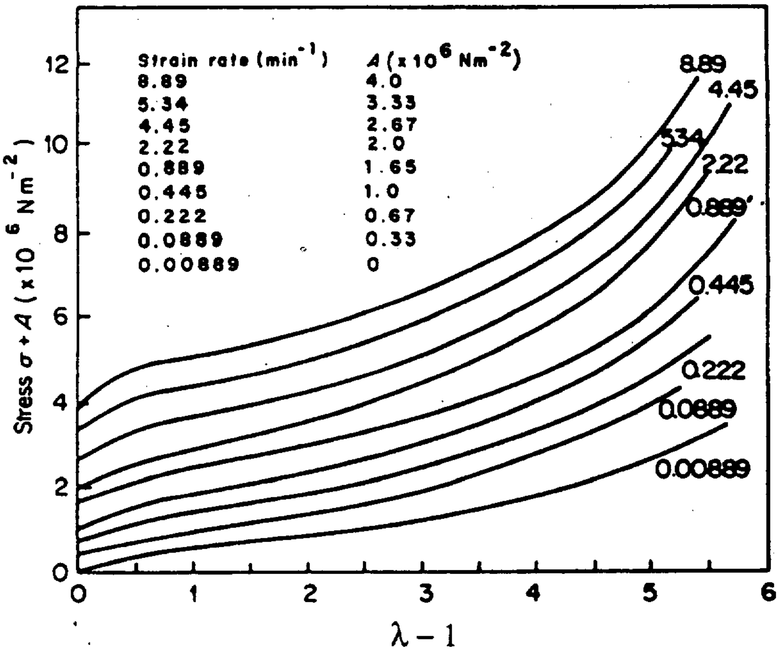

Fig. 4.7.1 Cauchy stress for constant axial stretch rate experiments on SBR vulcanized rubber. Stetch rates range from 0.00889 - 8.889 min $^{-1}$.The stress ordinates are displaced A to enable distinction of curves (1 MPa = 1 N/m^2) Data taken from Smith (1962).

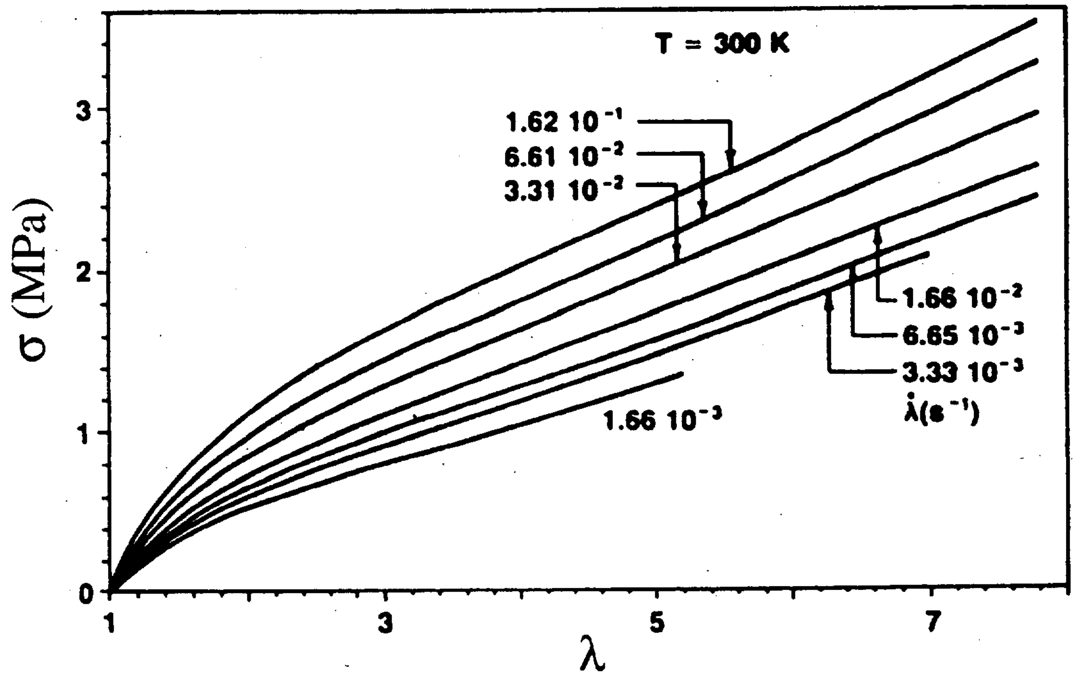

Fig. 4.7.2 Cauchy stress for constant axial stretch rate experiments on EPDM vulcanized rubber for different stretch rates (data taken from Scholtens and Leblans, 1986).

These network imperfections cause the relaxation which occurs after long times. Their are some small strain viscoelastic theories for solid rubber which include the effects of the dangling chains and unattached chains (Gaylord et. al., 1986; Curro et. al., 1985; Curro and Pincus, 1983). Because they are small strain theories, they only consider the relaxation times and not the strain dependence given by the reptation theory. The relaxation times used here to model the experimental data are higher than realistically expected for force equilibration to occur. The relaxation time for force equilibration to occur will be slightly less than the longest Rouse relaxation time (Doi and Edwards, 1986). The longest Rouse relaxation time can be calculated by Eq. $4.2.5_2$ with $k = 1$ (i.e. the longest relaxation time) if the values of the necessary parameters are known. These values are usually not known, but typical magnitudes range from 10^{-2} to 10^{1} seconds (Ferry, 1981) depending mainly on the molecular weight of the rubber (i.e. higher molecular weight rubbers have higher relaxation times). These times are lower than that used to model the results here. To simulate the relaxation curve given by Dafalias (Fig. 4.6.1) relaxation times of 4, $2\text{x}10^3$ and $4\text{x}10^4$ seconds were used. The relaxation function used to simulate the axial stretch data is shown in Fig. 4.7.3. It shows relaxation occurring well beyond the normal Rouse relaxation times. For many solid rubbers, relaxation occurs at times much higher than that given by the Rouse relaxation time. The high relaxation times seen in the data can probably be attributed to the unattached chains. For polymer melts, investigators such as Doi, Edwards, Bird, Graessely, Wagner and others do not emphasize the force equilibration process and concentrate on the chain retraction and disengagement process. Of course these affects are much more profound in polymer melts.

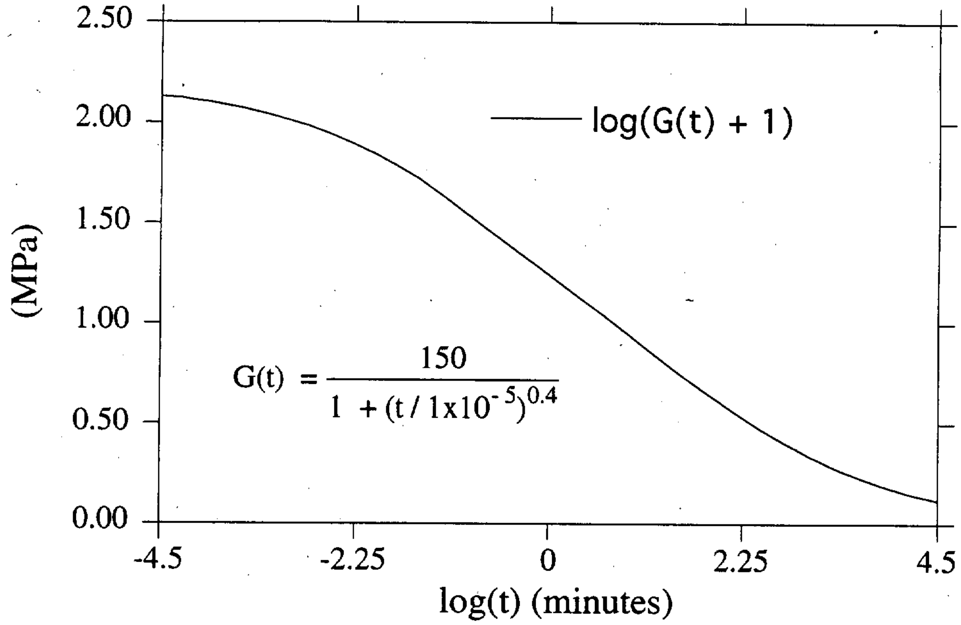

Fig. 4.7.3 Relaxation function used to model uniaxial constant stretch rate data in Section 4.6.

Again, the model was predicated on the idea of a perfect network. It was assumed that the majority of the network was crosslinked and effects due to imperfections would not be very apparent. It was hoped that by applying high relaxation times, despite the theoretical conflicts, effects due to non-ideal conditions could still be captured. The effects were not captured and the inadequacy of the model is manifested in the strain dependence it predicts.

4.8 Two Network Theory

The strain dependence for the chain disengagement process is different than that of force equilibration. The so called "fixed network" theory of polymer melts given by Doi and Edwards (1978 and 1986) and outlined in Section 4.2 assumes that the tube and the friction it applies are the only factors which influence the behavior of an unattached polymer chain. The tube is deformed affinely by the macroscopic deformation and new tube sections are formed randomly. The "fixedity" of the network implies that relaxation of the surrounding network does not affect the kinematics of the tube or the growth of new tube sections. One could imagine a more complex model where relaxation of the surrounding network would cause the tube to straighten or inhibit the growth of new tubes. A crosslinked chain would also be influenced by the tube but would not reptate. The fixed network theory assumes that chains and tubes are treated independently from the surrounding network. A network which includes both crosslinked and unattached chains is seen in Fig. 4.8.1. Since the "fixed network" theory assumes that the chains behave independently, the stress due to crosslinked chains " σ_c " and the stress due to unattached chains " σ_u " could merely be superimposed i.e.

$$\sigma = \sigma_c + \sigma_u \tag{4.8.1}$$

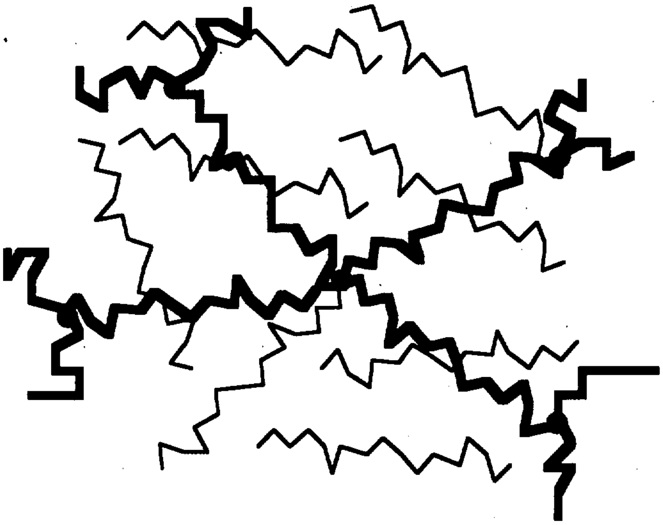

Fig. 4.8.1 A network of crosslinked and unattached chains. The crosslinked chains are shown in bold. Some of the unattached chains are crosslinked at one end while some are not crosslinked at all.

All the elasticity effects would be attributed to the crosslinked chains. The stress " σ_u " would be strictly viscous and would not contribute to the equilibrium stress. The "two network" model would be both a solid and a fluid. The crosslinked network will always retain its "memory" of the undeformed reference configuration while the fluid phase will become isotropic after flow has ceased due to the disengagement process.

The qualitative effects of unattached chains are assessed in the following for a constant axial stretch rate deformation. The constitutive equation which considers the effects due to the disengagement process is shown in Eq. 4.2.10. Unfortunately there is no equation which incorporates effects due to the retraction process for arbitrary deformation gradient histories. Furthermore, Eq. 4.2.10 was derived for unattached chains and does not consider dangling chains. For this case, we will treat dangling chains the same as the unattached chains although they do behave differently (Curro and Pincus, 1983). For uniaxial deformation Eq. 4.2.7 can be integrated analytically (Doi and Edwards, 1978 Part 4.) such that the equation describing the Cauchy stress is,

$$\sigma_1 = G_d \int_{-\infty}^{t} \mu(t-\tau)\left(\frac{3}{2}\,\frac{\lambda_1^3(t,\tau)}{1-\lambda_1^3(t,\tau)}\left(1-\frac{\tan^{-1}\sqrt{\lambda_1^3(t,\tau)-1}}{\sqrt{\lambda_1^3(t,\tau)-1}}\right)-\frac{1}{2}\right)d\tau \qquad (4.8.2)$$

where $\lambda_1(t,\tau) = \frac{\lambda_1(t)}{\lambda_1(\tau)}$ is the relative stretch, $\mu(t)$ is given by (4.2.8) and $G_d = 3\ kT\ nn_s$ as defined in Section 4.2. Values for τ_d in 4.2.8 can range from 10^2 to 10^5 seconds depending on molecular weight of the polymer chains. Just considering the effects of chain disengagement and ignoring retraction and force equilibration, Eq. 4.6.2 was used for σ_c and Eq. 4.8.2 was used for σ_u to fit the data given by Bloch et. al. (1978). The following parameters were chosen:

for σ_c (same as used previously):

$G_e = 2.73$ (MPa)

$N_o = 50$

for σ_u:

$G_d = 0.41$ (MPa)

$\tau_d = 10$ minutes

In Fig. 4.8.2 the results for the 3 different rates r = 0.0011 min.$^{-1}$, 0.442 min.$^{-1}$, and 4.42 min.$^{-1}$ are shown. Again, the viscoelastic portion of stress (σ_u for this case) is small for r = 0.0011. The viscoelastic backstress $\sigma^v = \sigma_u$ for r = .442 and 4.42 is shown in Fig. 4.8.3.

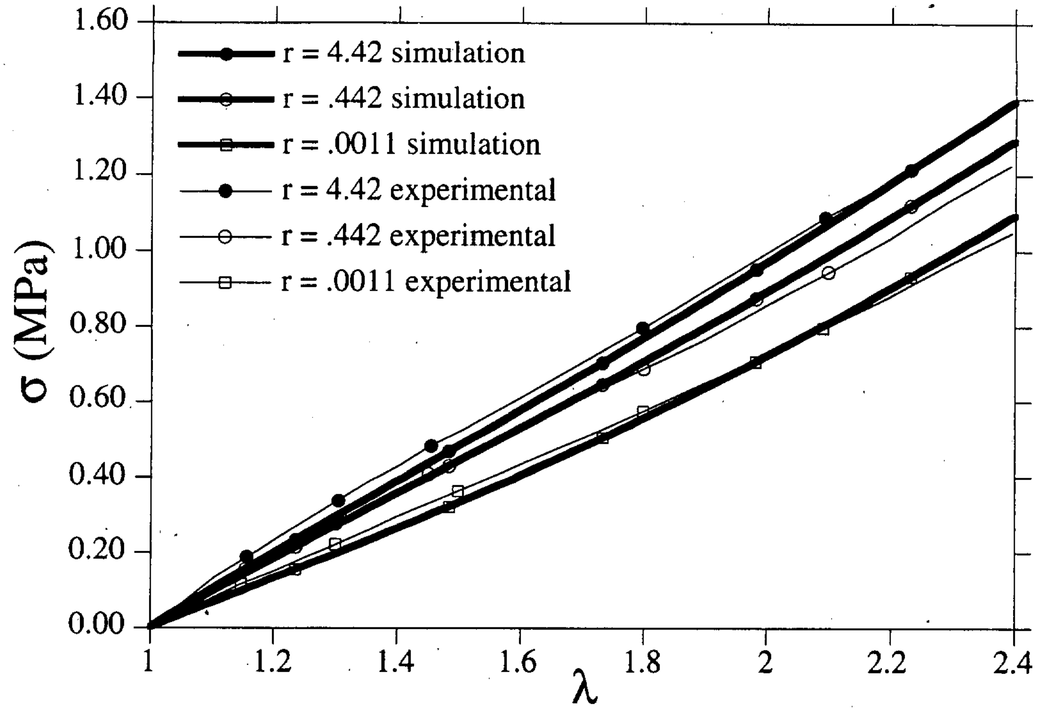

Fig. 4.8.2 Cauchy stress for three different uniaxial stretch rates. Chain disengagement model provided simulated results. (data from Bloch et. al. 1978)

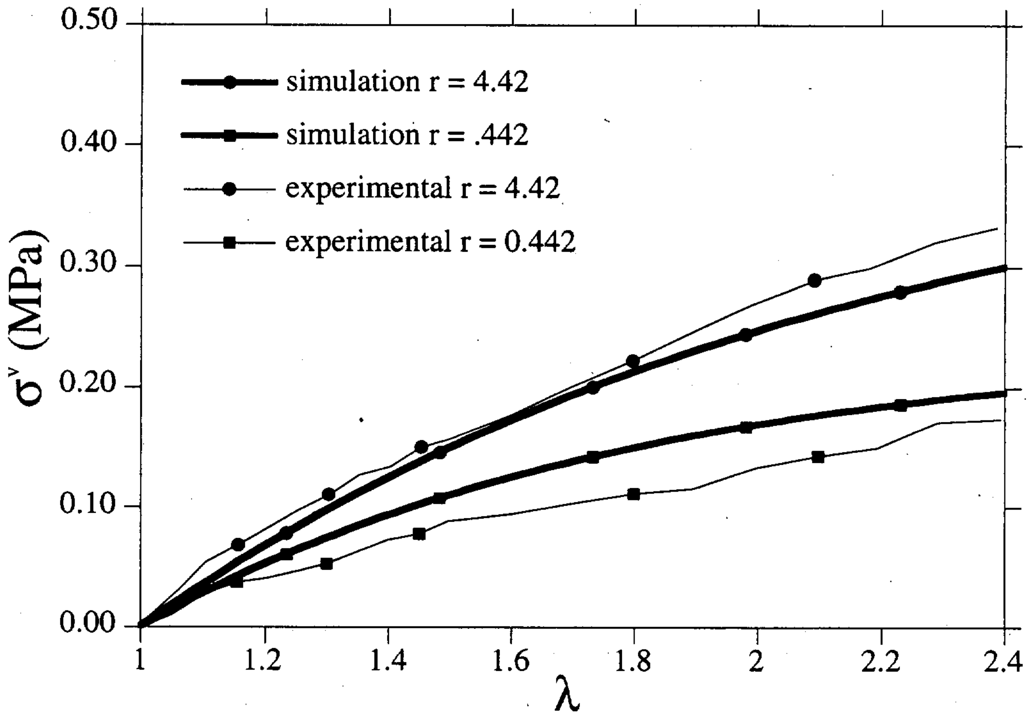

Fig. 4.8.3 Viscoelastic 'backstress' for r = 4.42 and r = 0.442. Chain disengagement model was used for simulated results (data from Bloch et. al. 1978).

Comparison of Figs. 4.6.5-6 (force equilibration) to Figs. 4.8.2-3 (chain disengagement) show a marked difference in strain dependence. The results using chain disengagement appear to be qualitatively better than that using force equilibration. Examination of Fig. 4.8.3 shows that the relaxation function doesn't give the proper time dependence for the different rates. This inadequacy has also been reported in applications of the reptation model to polymer melts. One reason for the discrepancy is that the derivation of the Eq. 4.2.7 was based on the assumption of monodisperse polymer chains (i.e. all the chains are the same length). There are modified versions of Eq. 4.2.7 which consider polydispersity. Wagner (1992) claims that effects due to chain retraction need to be considered especially when polydispersity is included. Again, there is no molecular constitutive model which incorporates chain retraction for arbitrary (homogeneous) deformation histories * . It is expected that incorporating effects due to force equilibration for both the crosslinked and uncrosslinked chains plus chain retraction for the uncrosslinked chains could give good quantitative results.

4.9 Proposed Phenomenological Model

The two network model provided reasonably good qualitative results for the constant axial stretch rate behavior. As mentioned, the time dependence could not be predicted by the kernel given by Eq. 4.2.8. The effect of monodisperse polymer chains was considered to be one reason the time dependence was not captured. Another reason is due to the fact that Eq. 4.2.8 and 4.2.10 are not valid for the dangling chains. A solid rubber will have many dangling chains due to incomplete curing (Mark and Erman, 1988). It is expected that a different kernel function would yield better results. A power law kernel such as that given by Eq. 4.3.1 (b) would be a suitable form. An approximate form for Eq. 4.2.10 was given by Currie (1982),

---

* It seems that an assumption of the chain force and rate of retraction could be made and put into Eq. 3.3.2 would provide a suitable approximation.

$$\sigma_{ij}(t) = G_d \int_{-\infty}^{t} \frac{5\,\mu(t-\tau)}{I_1^t + 2(I_2^t + 13/4)^{1/2} - 1} \left(\bar{C}_{ij}^{-1} - (I_2^t + 13/4)^{-1/2}\,\bar{C}_{ij}\right) d\tau \qquad (4.9.1)$$

where $\bar{C}_{ii}^{-1} = \frac{\partial x_k(t)}{\partial x_i(\tau)} \frac{\partial x_k(t)}{\partial x_j(\tau)}$ is the relative Cauchy Green tensor, the invariants are $I_1^t = \bar{C}_{ii}^{-1}$ and $I_2^t = \bar{C}_{ii}$, the kernel function is given by (4.2.8) and $G_d = 3$ kT nn_s as defined in Section 4.2. Substitution of the power law kernel into Eq. 4.9.1 should yield good results, Because (4.9.1) is in terms of the Cauchy stress and the relative strain tensors, it is not as amenable to finite element formulations as a methods given in terms of the second Piola Kirchoff stress and the Cauchy Green tensor. Although Eq. 4.9.1 could be put in terms of the second Piola Kirchoff stress and Cauchy Green tensor, the conversion would be complicated. The following equation for the Kirchoff stress is proposed as an approximation,

$$S(t)_{KL} = \int_{-\infty}^{t} \mu(t-\tau) \frac{G_d}{\langle\lambda(\tau)\rangle} \frac{\partial}{\partial\tau}\left(\int_0^{2\pi}\!\!\int_0^{\pi} M_K\, M_L \frac{1}{\lambda(\tau)} \frac{\sin\Theta}{4\pi}\, d\Theta\, d\Phi \right) d\tau + p\, F_{Kj}^{-1} F_{Lj}^{-1} \qquad (4.9.2)$$

Although Eq. 4.9.2 is an empiricism, for a single step strain it is the Kirchoff stress equivalent to Eq. 4.2.9* . The quantity $\langle\lambda\rangle$ and the integral over the orientation space in Eq. 4.9.2 are approximated by Eq. D.8 and D.10 from Appendix D and substituted into Eq. 4.9.2 giving,

$$S(t)_{KL} = \int_{-\infty}^{t} \frac{\mu(t-\tau)\, G_d}{(3\, I_1^{1/2} - I_2/I_1^{3/2})} \frac{d}{d\tau}\left(\left(\frac{5}{2} I_1^{-1/2} - \frac{3}{5} \frac{I_2}{I_1^{5/2}} \right) \delta_{KL} + I_1^{-3/2}\, C_{KL} \right) d\tau + p\, F_{Kj}^{-1} F_{Lj}^{-1} \qquad (4.9.3)$$

Eq. 4.9.3 is used in place of σ_u given by the two network theory as the stress of the unattached chains. In order to match the constant axial stretch rate data given by Bloch et. al. (1978), the following material parameters were used with Eq. 4.6.2 and 4.9.3, for σ_c :

---

* Eq. 4.2.9 is considered to be the more rigorous solution for a single step strain compared to Eq. 4.2.10 and especially Eq. 4.9.1.

$G_e = 2.5$ (MPa)
$N_o = 50$

for σ_u i.e. Eq. 4.9.3

$$G(t) = \mu(t)\, G_d = \frac{13}{1 + (t/1\text{x}10^{-8})}$$

Results using 4.6.2 and 4.9.3 with the above parameters are compared to the experimental data in Figs. 4.9.1, 4.9.2 and 4.9.3. Because of the kernel used to fit the data, the r = 0.0011 min^{-1} curves in Figs. 4.9.1-2 contain a small amount of the viscoelastic stress. Coincidentally, this produced a better fit at the slow rate after slightly reducing G_e from 2.73 (MPa) used in Sects. 2.6 and 2.8 to 2.5 (MPa). The viscoelastic backstress shown in Fig. 4.9.3 is still the difference between the r = 4.42 and the r = 0.0011 curve and r = 0.442 curve and the r = 0.0011 curve. Because some viscoelastic stress was seen at r = 0.0011, Fig. 4.9.3 is not exactly the viscoelastic backstress; but it is close. Eq. 4.9.3 appears to provide good fits of the experimental data.

4.10 Conclusions

It is concluded that the contribution of force equilibration alone is not sufficient in describing the viscoelastic behavior of many rubbers. Effects due to network imperfections must be considered. The rationale and possibly the methods used to develop the force equilibration viscoelastic model are not wrong, per se. It is wrong to attribute too much of the irreversible portion of the stress to the force equilibration process. This is done by using relaxation functions G(t) and relaxation times that exaggerate the effects of force equilibration. Realistic relaxation times for the force equilibration process would be on par with the Rouse relaxation times given by Eq. (4.2.5$_2$). Overemphasis of the force equilibration yields the wrong strain dependency as seen by constant strain rate experiments. It would be interesting to see if the method proposed here was applicable to high strain rate experiments. For such a case, the method could still be applied to imperfect networks since unattached chains still experience force equilibration. Nevertheless, a more physically based prediction of the nonequilibrium force than that given by Eq. 4.3.1 would be useful (the statistical mechanics are available for such an approach).

The "two network model" appeared to give acceptable qualitative results. A model that combined the effects of force equilibration, chain retraction and chain disengement should be considered. Such a model would be able to capture effects (i.e. time and strain dependence) due to high and low strain rate loading.

It was expected that the mechanistic (or molecular) models considered here could better serve to motivate more phenomenological models than to quantitatively model experimental results. The empirical constitutive law presented in Sect. 4.9 was based on the disengagement of unattached chains and provided good qualitative and quantitative results to the experimental data.

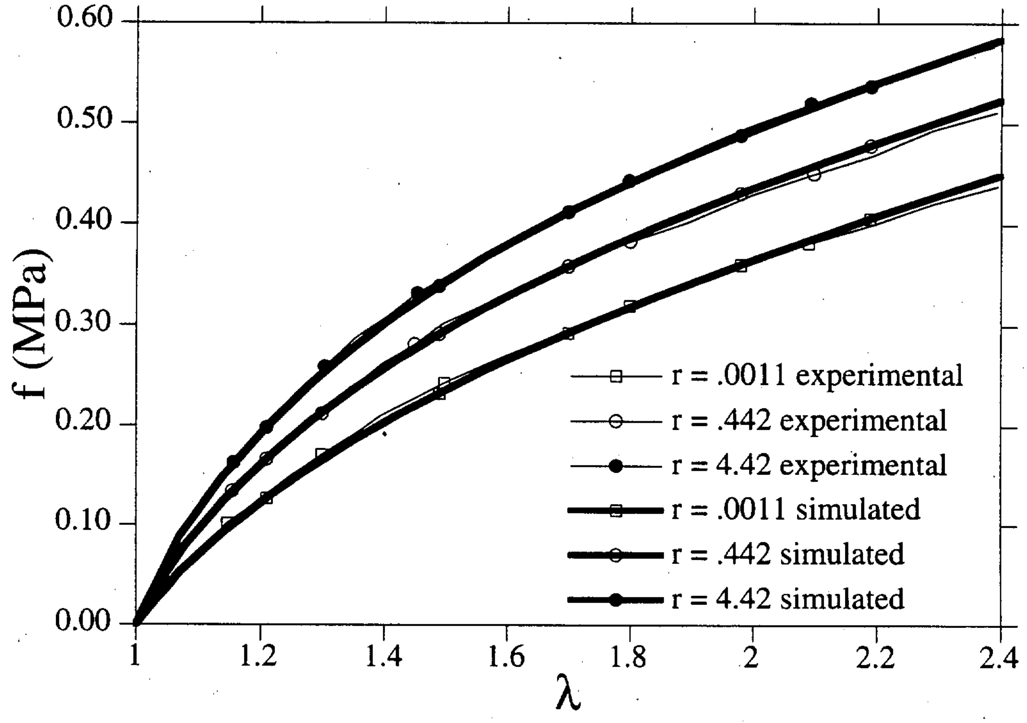

Fig. 4.9.1 Force per undeformed area for three different uniaxial stretch rates. The empirical chain disengagement model was used for simulated results. (data from Bloch et. al. 1978)

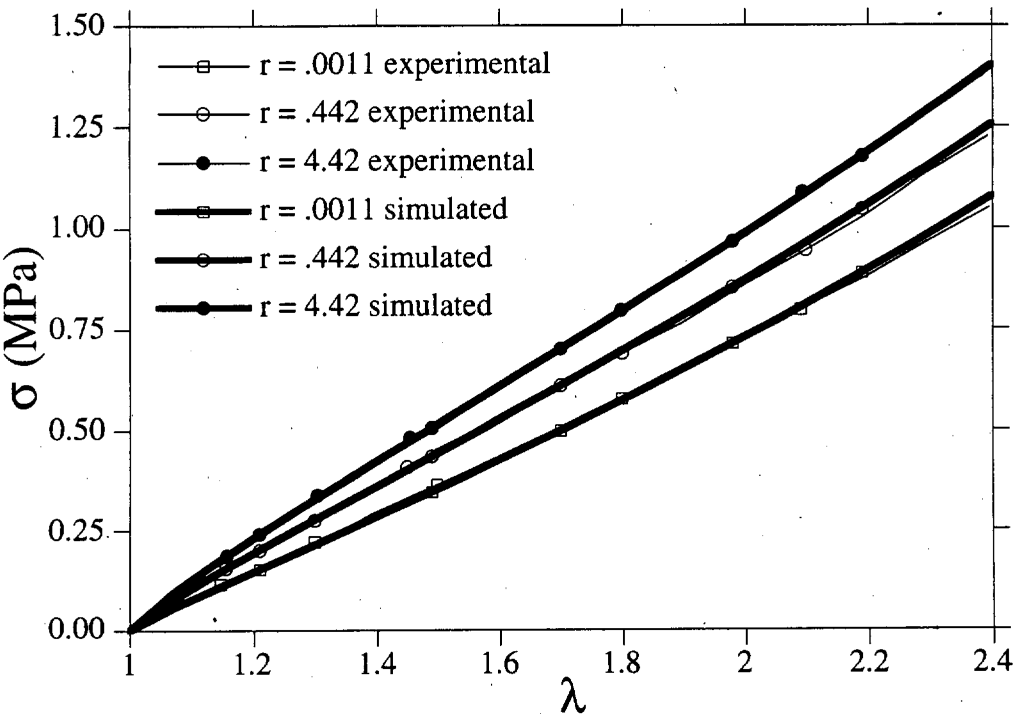

Fig. 4.8.3 Viscoelastic Cauchy stress for r = 4.42 and r = 0.442. The empirical chain disengagement model was used for simulated results (data from Bloch et. al. 1978).

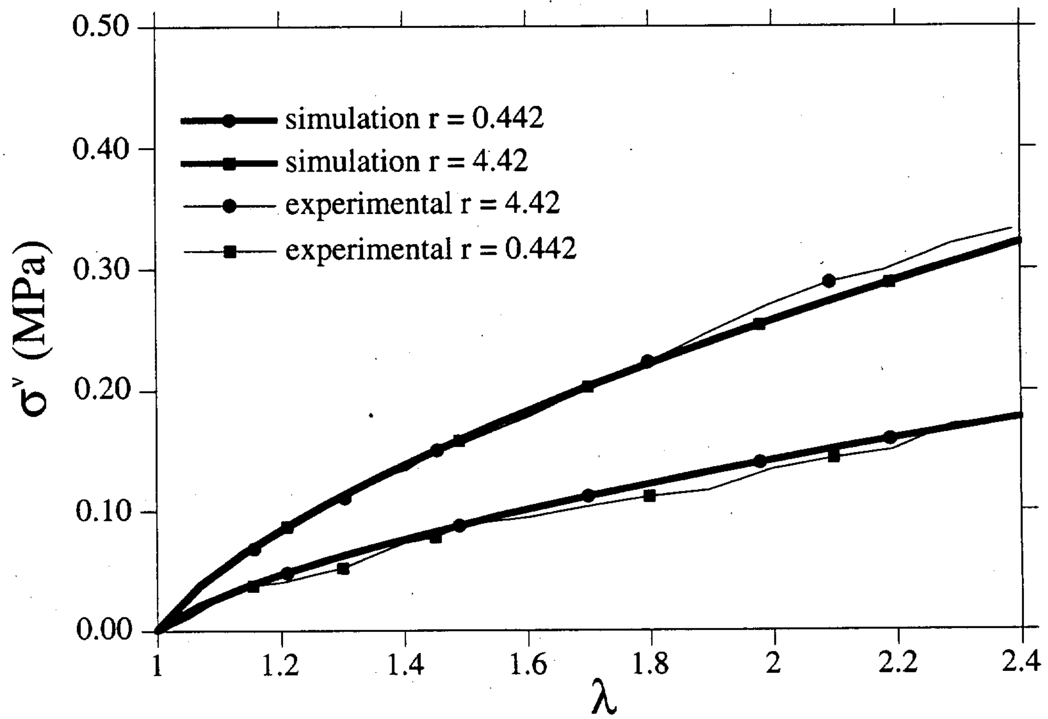

Fig. 4.9.3 Viscoelastic 'backstress' for r = 4.42 and r = 0.442. The empirical chain disengagement model was used for simulated results (data from Bloch et. al. 1978).

5. FINITE ELEMENT IMPLEMENTATION

A plane strain finite element program was developed to implement the proposed elastic-viscoelastic models. The program used a total Lagrangian formulation and a Newton Raphson algorithm to solve the governing (geometric and material) nonlinear equations. The algorithm provided for consistent tangent stiffness moduli through exact linearization of the recursion approximation of the hereditary integral such that second order convergence was achieved. A quasi-incompressible formulation was used such that a suitable expression was chosen for the volumetric free energy as a penalty function. The method exhibits incompressible behavior in the limit as the penalty parameter tends to infinity. The details specific to this program are discussed in the following.

The rubber has so far been considered incompressible. The development of the rubber elasticity model here only considered the entropic portion S of the free energy Ψ and neglected the contribution of the internal energy E where

$$d\Psi = dE - T\,dS \tag{5.1}$$

and T is the temperature. It is known that rubber is somewhat compressible and does exhibit changes in internal energy due to deformation. Most of the internal energy changes are due to dilation* . Usually this internal energy contribution is treated empirically and there are many postulated forms. Since, a sophisticated treatment of this topic is beyond the scope of this work, the introduction of compressibility made here will only be in the form of a penalty function to facilitate finite element analysis. In this case, the material is treated to be very nearly incompressible. Considering only the elastic case for a moment, the following form for the equilibrium free energy is used:

$$\Psi(F) = W^{vol}(J) + W^{entropic}(F) \tag{5.2}$$

---

* Although at small strains this is often not the case (Treloar, 1958) . Some investigator have reported the necessity of including distortional contributions to the internal energy (Peng et. al., 1972, 1975)

were $W^{entropic}(F)$ is the entropic portion of the free energy given by Eq. 2.2.17 and $W^{vol}(J)$ is the portion of the free energy which depends on the volume ratio J and maintains the near incompressibility constraint. Sometimes analysts make the entropic portion of the free energy invariant to dilation by substituting the deviatoric deformation gradient F_{dev} * for F such that $W^{entropic} = W^{entropic}(F_{dev})$, but this leads to an unnecessarily complicated formulation. The following was used because of its simplicity,

$$W^{vol}(J) = \frac{1}{2}\kappa (J - 1)^2 - c\, J \tag{5.3}$$

The constant c is chosen to provide stress free conditions in the undeformed state. The constant κ is the penalty parameter chosen to provide near incompressibility. Many other forms are available but it was found that results are rather insensitive to the form when the deformation field is nearly isochoric. Using 5.2 and 5.3 to calculate the elastic portion of stress gives,

$$\sigma_{ij}^{elastic} = \frac{2}{J} F_{iK}\left(\frac{\partial}{\partial C_{KL}}\left(W^{entropic} + W^{vol} \right)\right) F_{jK} = \sigma_{ij}^{entropic} + (\kappa (J-1) - c)\,\delta_{ij} \tag{5.4}$$

where is $\sigma_{ij}^{entropic}$ is given by Eq. 2.4.5 or 2.4.6 divide by the volume ratio J as such,

$$\sigma_{ij}^{entropic} = \frac{1}{J} G \sqrt{N_o}\, L^{-1}\!\left(\frac{\langle\lambda\rangle}{\sqrt{N_o}}\right)\left(\frac{\sqrt{3}}{2}\left(I_1^{-1/2} - \frac{3}{5}\frac{I_2}{I_1^{5/2}}\right) B_{ij} - \frac{\sqrt{3}}{5} I_1^{-3/2} B_{ij}^2 \right) \tag{5.5}$$

For the undeformed state, it can be shown by replacing $F_{iK} = \delta_{iK}$ into Eq. 5.5 gives,

$$\sigma_{ij}^{entropic} = \frac{1}{2}\,\frac{G}{1 - (N_o)^{-3/2}}\,\delta_{ij} \tag{5.6}$$

If the rubber is in equilibrium in the undeformed state then $\sigma_{ij}^{elastic} = 0$ so that substitution of J = 1 and 5.6 into 5.4 provides the value of c:

---

*$F_{dev} = J^{-1/3} F$ where F is the deformation gradient and $J = \det | F |$

$$c = \frac{1}{2} \frac{G}{1 - (N_o)^{-3/2}} \quad . \tag{5.7}$$

Including the contribution of the viscous portion of the stress is made as usual,

$$\sigma_{ij} = \sigma_{ij}^{\text{elastic}} + \sigma_{ij}^{\text{viscous}} \tag{5.8}$$

where $\sigma_{ij}^{\text{elastic}}$ is given by Eq. 5.4 and $\sigma_{ij}^{\text{viscous}}$ is given by the transformation:

$$\sigma_{ij}^{\text{viscous}} = \frac{1}{J} F_{iK}\, S_{KL}^{v}\, F_{jL} \tag{5.9}$$

and S_{KL}^{v} is given by Eq. 4.5.2 (or 4.5.4). At equilibrium in the undeformed state $\sigma_{ij}^{\text{viscous}} = 0$ so that no special consideration need be made for $\sigma_{ij}^{\text{viscous}}$. Furthermore, the penalty number κ will maintain near incompressible conditions for the elastic and viscoelastic cases.

The penalty method can be implemented with a mixed formulation using a separate pressure and displacement field. But, exploiting the element equivalence as outlined by Malkus and Hughes (1978) for finite strain formulations, a single displacement field with reduced and selective integration is used. For the 2D plane strain finite element program developed here, 4 node bilinear finite elements were used. The stress given by the penalty function is sampled at the center Gauss point (Fig. 5.1) while the remainder of the stress given by Eq. 5.8 and 5.4 is sampled at the 2x2 Gauss points.

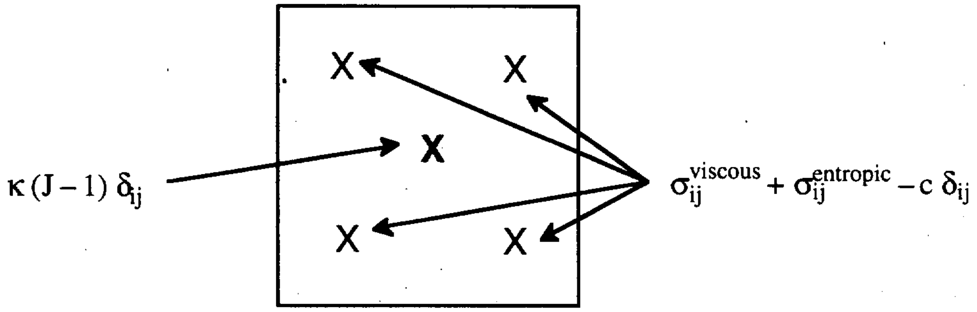
$\kappa (J-1)\, \delta_{ij}$
X
X
X
X
X
$\sigma_{ij}^{\text{viscous}} + \sigma_{ij}^{\text{entropic}} - c\, \delta_{ij}$

Fig. 5.1 Four node bilinear element with selective and reduced integration. Constraint is applied by sampling penalty function at center Gauss point.

In order to achieve second order convergence, the tangent moduli L_{ijkl} given by:

$$L_{ijkl} = \frac{\partial S_{ij}}{\partial C_{kl}} \qquad (5.10)$$

must be computed from an exact linearization of the constitutive law. The process is trivial for the elastic portion of the stress but requires numerical integration of the hereditary integral for the viscoelastic stress. A procedure similar to that given by Herrmann and Peterson, (1968) is used. Considering only a single exponential kernel with relaxation time t_o, the viscoelastic stress given by Eq. 4.5.2 or 4.5.2 is of the following form:

$$S^{v}_{ij}(t) = f_{ijop}(C_{mn}) \int_{-\infty}^{t} c\, e^{-(t-\tau)/t_o} \frac{d}{d\tau}(I_1^{-1/2}\, C_{op})\, d\tau \qquad (5.11)$$

Taking the gradient of $S^{v}_{ij}(t)$ and using the chain rule gives,

$$L^{v}_{ijkl} = \frac{\partial}{\partial C_{kl}}\left(f_{ijop}(C_{mn}) \int_{-\infty}^{t} c\, e^{-(t-\tau)/t_o} \frac{d}{d\tau}(I_1^{-1/2}\, C_{op})\, d\tau \right) \qquad (5.12_1)$$

$$= \left(\frac{\partial}{\partial C_{kl}} f_{ijop}(C_{mn})\right) \int_{-\infty}^{t} c\, e^{-(t-\tau)/t_o} \frac{d}{d\tau}(I_1^{1/2}\, C_{op})\, d\tau + f_{ijop}(C_{mn}) \frac{\partial}{\partial C_{kl}} \int_{-\infty}^{t} c\, e^{-(t-\tau)/t_o} \frac{d}{d\tau}(I_1^{-1/2}\, C_{op})\, d\tau \qquad (5.12_2)$$

where L^{v}_{ijkl} are the tangent moduli for the viscoelastic stress. The gradient of the first part of the rhs of Eq. 5.12_2 is straight forward. The gradient of the second part requires numerical integration of the hereditary integral. The following recursion relation is used to get the value of the integral at time t from time t - Δt:

$$\int_{-\infty}^{t} c\, e^{-(t-\tau)/t_o} \frac{d}{d\tau}(I_1^{-1/2}(\tau)\, C_{op}(\tau))\, d\tau \approx t_o \left(\frac{1 - e^{-\Delta t/t_o}}{\Delta t}\right)\left(I_1^{1/2}(t)\, C_{op}(t) - I_1^{1/2}(t\text{-}\Delta t)\, C_{op}(t\text{-}\Delta t) \right)$$

$$+ e^{-\Delta t/t_o} \int_{-\infty}^{t-\Delta t} c\, e^{-(t-\Delta t-\tau)/t_o} \frac{d}{d\tau}(I_1^{-1/2}(\tau)\, C_{op}(\tau))\, d\tau \qquad (5.13)$$

Consequently the gradient of the hereditary integral is approximated as follows,

$$\frac{\partial}{\partial C_{kl}(t)} \int_{-\infty}^{t} c\, e^{-(t-\tau)/t_o} \frac{d}{d\tau}(I_1^{-1/2}(\tau)\, C_{op}(\tau))\, d\tau \approx t_o \left(\frac{1 - e^{-\Delta t/t_o}}{\Delta t} \right) \frac{\partial}{\partial C_{kl}(t)} \left(I_1^{-1/2}(t)\, C_{op}(t) \right)$$

$$= t_o \left(\frac{1 - e^{-\Delta t/t_o}}{\Delta t} \right) \left(-\frac{1}{2} I_1^{-3/2}(t)\, \delta_{kl}\, C_{op}(t) + I_1^{-1/2}(t)\, \delta_{ko} \delta_{lp} \right) \qquad (5.14)$$

As mentioned in Sect. 4.5, if the constitutive law is given by Eq. 4.5.2, the tangent moduli L^{v}_{ijkl} are not symmetric. If the constitutive law is given by Eq. 4.5.4, the tangent moduli L^{v}_{ijkl} are symmetric. The symmetric tangent moduli are computationally much more efficient.

As an example, the solution is given for the boundary value problem corresponding to the rubber block fixed on both ends and sheared (Fig. 5.2 and 5.3). The constitutive equation for the elastic stress was given by Eq. 5.5. The unsymmetric form of Eq. 4.5.2 was used for the viscoelastic stress. The material parameters are given by,

elastic rubbery modulus	$G_e = 0.32$ MPa
number of links between entanglements	$N_o = 75$
relaxation time	$t_o = 0.25$ seconds
relaxation function	$G_v(t) = 2\, e^{-(t/0.25)}$
penalty parameter	$\kappa = 1000$

The undeformed block is shown by dotted line in Fig. 5.2 (a) and is of unit dimensions (meters). The mesh consisted of 100 4 node bilinear elements . A cyclic shear strain history (Fig 5.2 (b)) in the form of a triangular pulse is applied to the block. The maximum shear strain applied is $\gamma = 1$. The deformed bearing at $\gamma = 1$ is shown in Fig. 5.2 and the average shear stress (V = average τ_{xy}) is shown in Fig. 5.3. Forty steps were used to complete a cycle of loading such that it took 10 steps from ($t = 0, \gamma = 0$) to ($t = 30$, $\gamma = 1$). The Euclidean norm of the out of balance force vector was used as the convergence criterion. Second order convergence was achieved as evident by the values for the error norm in Table. 1 for a few of the initial steps. The penalty parameter $\kappa =$

1000 was effective in maintaining the near incompressibility constraint . Most of the values of the volume ratio were within ± 1×10^{-6} of unity except for a few elements in the corners where $0.997 < J < 1.003$ (J being the volume ratio).

Table 1.
Values of the Euclidean norm of the residual

Step number	Error
1 (γ=0 to 0.1)	6.25430E-01
	2.93721E-01
	6.41837E-03
	3.84168E-03
	1.80959E-04
	3.08567E-06
2	7.33610E-01
	2.89386E-01
	5.86986E-03
	3.40927E-03
	1.66387E-04
	2.78671E-06
.	.
.	.
.	.
8	2.65322E+00
	1.24420E-01
	2.00771E-03
	3.03412E-04
	5.96701E-05
9	2.91919E+00
	9.88782E-02
	1.92582E-03
	3.12610E-04
	5.79649E-05
10 (γ=0.9 to 1)	3.14567E+00
	7.92877E-02
	1.84041E-03
	3.16853E-04
	5.67332E-05

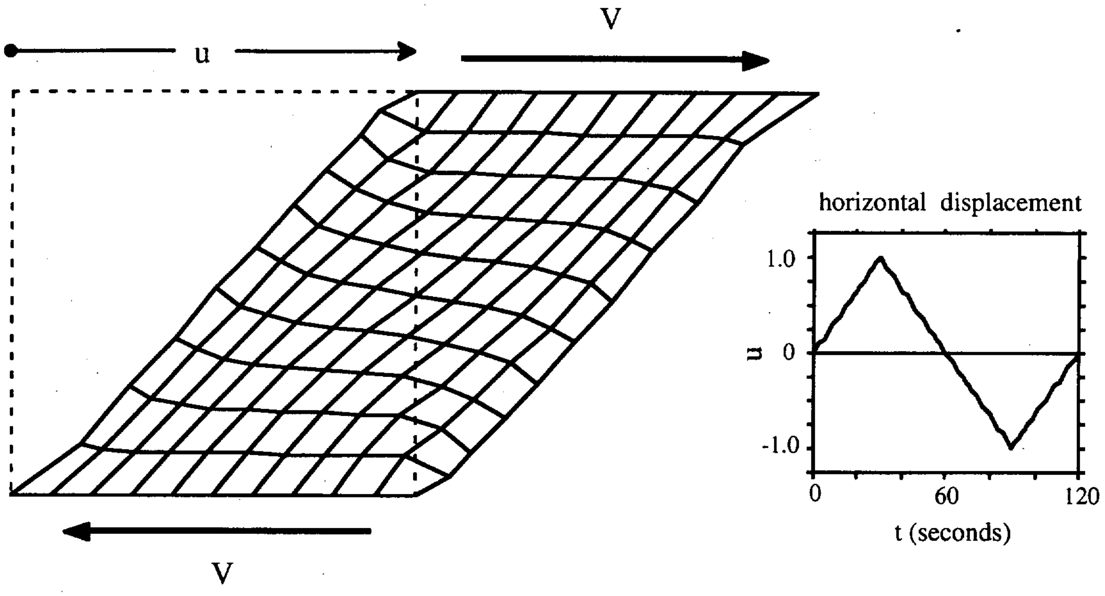
V
u
V
horizontal displacement
1.0
0
-1.0
u
0
60
120
t (seconds)

(a) (b)

Fig. 5.2 (a) Undeformed unit (1m x 1m x 1m) block show in dotted line along with deformed block and mesh. (b) Displacement history function applied to block.

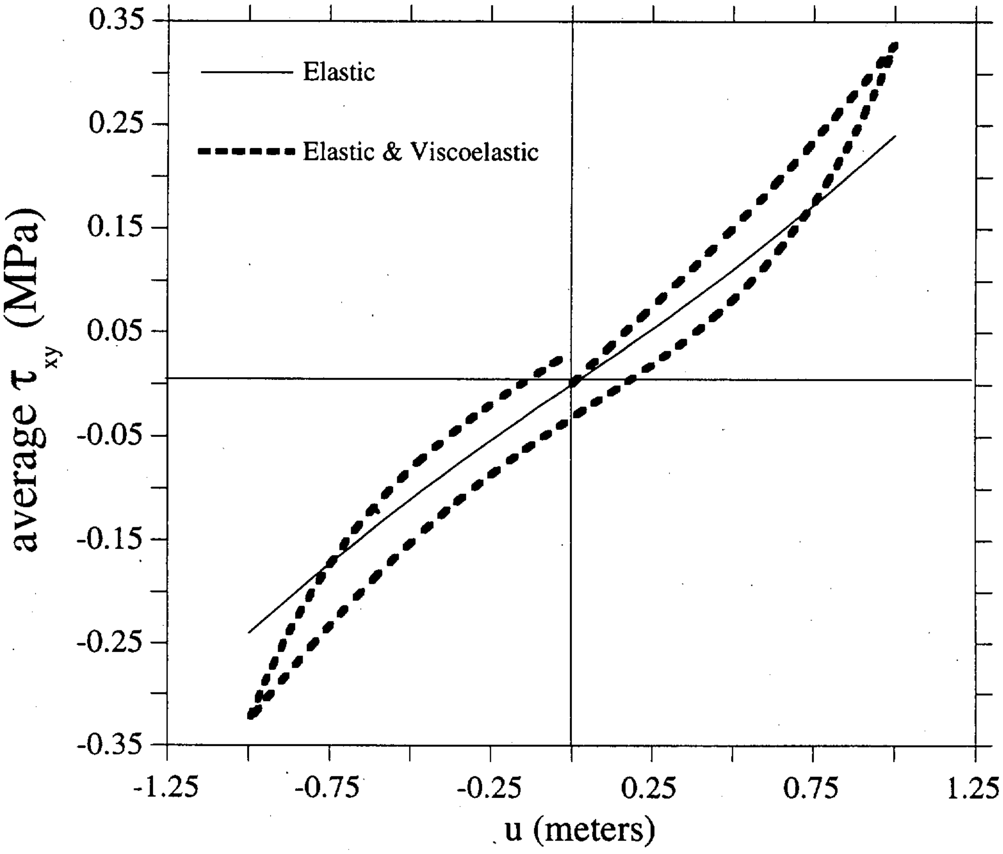

Fig. 5.3 Average shear stress τ_{xy} verses horizontal displacement u for bearing in Fig. 5.2

CONCLUSIONS AND RECOMMENDATIONS

Different physically based constitutive models were examined in this study and different degrees of success were achieved in qualitatively and quantitatively matching experimental results. At the very least, valuable experience is gained when it is shown that the assumptions predicating a given model do not provide a realistic representation of the physical system. It seems that a comprehensive regime of tests on commonly used rubber solids under highly controlled conditions could be very useful in elucidating the generalized behavior of the material (assuming there is a generalized behavior).

The scheme used to approximate the orientation space integrals in terms of strain and strain invariants gave good results compared to the exact numerical integration solution of the integrals. Application of the scheme to the elasticity models gave very good approximations up to relatively high strains; especially for the entanglement model. To a lesser degree, application of the scheme to the force equilibration viscoelasticity model also gave good results.

As was seen in Section 1, the classical theory when fitted for uniaxial data could not fit the equibiaxial data. The proposed entanglement model provided much better fits to the experimental data, but as was shown in Section 4.6 shows some discrepancy when plotted using a Mooney plot. Other theories such as hoop and tube models can provide better Mooney plots (Higgs et. al., 1990), since these models are more sophisticated than the entanglement model used here. Nevertheless, these models don't consider finite extensible chains. It seems plausible that these models could be modified for finite extensibility, furthermore the hoop and tube models are based on the familiar average stretch quantity $\langle\lambda\rangle$ which can be well approximated.

The force equilibration model clearly shows the wrong strain dependence compared to experimental data for the constant axial stretch rate deformation. It would be instructive to see if the force equilibration model could predict high strain rate test results, since it seems that hardening would occur as opposed to the characteristic softening (i.e., slight concave down appearance of curves in Fig. 4.6.5, 4.7.1 and 4.7.2) behavior seen at the slow rates. One explanation of the softening could be that chains are broken during the loading process. Another explanation is that many unattached chains may exist within the rubber matrix. The latter explanation is the basis of the so called two network model considered here.

The two network model appeared to give good qualitative results compared to the uniaxial constant stretch rate experiments. In this model the unattached chains disengage from the tube of constraints as explained in the Doi and Edwards reptation theory. A general model that considers effects due to force equilibration, chain retraction, and chain disengagement of unattached and dangling chains could be useful. The two network model motivated the empirical model which provided very good fits to the experimental data.

REFERENCES

Arridge, R. G. C. (1985). "An Introduction to Polymer Mechanics," Taylor and Francis.

Arruda, E. M. and Boyce, M. (1993). "A Three-dimensional Constitutive Model for the Large Stretch Behavior of Rubber Elastic Materials," *J. Mech. Phys. Solids*, **41**, 2, pp. 389 - 412.

Ball, R. C., Doi, M., Edwards. S. F. and Warner, M. (1989) *Polymer*, **22**, p. 1010.

Bathe, K. J. (1982). "Finite Element Procedures in Engineering Analysis," Prentice-Hall.

Ben-Zvi, R. (1990). "A Simple Implementation of a 3D Thermo-viscoelastic Model in a Finite Element Program," *Computers and Structures*, **34**, 6, pp. 881 - 883.

Bernstein, B., Kearsley, E. A. and Zapas, L. J. (1963). "A Study of Stress Relaxation with Finite Strain," *Transactions of the Society of Rheology*, **7**, pp. 391 - 410.

Bird, R. B., Armstrong, R. C. and Hassager, O. (1987). "Dynamics of Polymer Liquids Volume 1. Fluid Mechanics," John Wiley and Sons.

Bird, R. B., Curtiss, C. F., Armstrong, R. C. and Hassager, O. (1987). "Dynamics of Polymer Liquids Volume 2. Kinetic Theory," John Wiley and Sons.

Bloch, R.F. and Chang, W.V. and Tschoegl, N.W. (1978)., "The Behavior of Rubberlike Materials in Moderately Large Deformations," *Journal of Rheology* , **22**, 1, pp. 1-31.

Bloch, R.F. and Chang, W.V. and Tschoegl, N.W. (1978)., "Strain Independent Nonlinearity in Peroxide Cured Styrene Butadiene Rubber" *Journal of Rheology* , **22**, 1, pp. 32-51.

Bloch, R.F. and Chang, W.V. and Tschoegl, N.W., (1976)., "On the theory of the viscoelastic behavior of soft polymers in moderately large deformations," *Journal of Rheology* , **15**, 1, pp. 368-377.

Bogert, P. A. J. van den. (1991). "Computational Modelling of Rubberlike Materials," Ph. D. Dissertation, Department of Civil Engineering, Delft University of Technology.

Brereton, M. G. and Klein, P. G. (1988). "Analysis of the Rubber Elasticity of Polyethylene Networks Based on the Slip Link Model of S. F. Edwards *et. al.*, " *Polymer*, **29**, pp. 970 - 974.

Chompff, A. J. and Duiser, J. A. (1966). "Viscoelasticity of Networks Consisting of Crosslinked of Entangled Macromolecules. I. Normal Models and Mechanical Spectra," *The Journal of Chemical Physics*, **45**, 5, pp. 1505 - 1514.

Christensen, R. M. (1980). "A Nonlinear Theory of Viscoelasticity for Application to Elastomers," *Journal of Applied Mechanics*, **47**, pp. 763 - 768.

Christensen, R. M. (1982). "Theory of Viscoelasticity An Introduction," Academic Press.

Christensen, R. M. (1988). "A Two Material Constant, Nonlinear Elastic Stress Constitutive Equation Including the Effect of Compressibility," *Mechanics of Materials*, **7**, pp. 155 - 162.

Churchill, Ruel V. (1972). "Operational Mathematics," McGraw - Hill.

Coleman, Bernard D. and Noll, Walter (1961). "Foundations of Linear Viscoelasticity," *Reviews of Modern Physics*, **33**, 2, pp. 239 - 248.

Currie, P. K. (1982). "Constitutive Equations for Polymer Melts Predicted by the Doi - Edwards and Curtiss Bird Kinetic Theory Models," *Journal of Non-Newtonian Fluid Mechanics*, **11**, pp. 53 - 68.

Curro, John G. and Pearson, Dale S. and Helfand, Eugene (1985). "Viscoelasticity of Randomly Cross-Linked Polymer Networks. Relaxation of Dangling Chains," *Macromolecules*, **18**, pp. 1157 - 1162.

Curro, John G. and Pincus, Philip (1983). "A Theroetical Basis for Viscoelastic Relaxation of Elastomers in the Long-Time Limit," *Macromolecules*, **16**, pp. 559 - 562.

Dafalias, Y. F. (1991). "Constitutive Model for Large Viscoelastic Deformations of Elastomeric Materials," *Mechanics Research Communications*, **18**, pp. 61 - 66.

deGennes, P. G. (1971). *J. Chem. Phys.*, **55**, p. 572

Doi, Masao and Edwards, S. F. (1978) "Dynamics of Concentrated Polymer Systems Part 1. - Brownian Motion in the Equilibrium State," *Journal Faraday Transactions II: Chemical Physics*, **74**, pp. 1789 - 1801.

Doi, Masao and Edwards, S. F. (1978) "Dynamics of Concentrated Polymer Systems Part 2. - Molecular Motion under Flow," *Journal Faraday Transactions II: Chemical Physics*, **74**, pp. 1802 - 1817.

Doi, Masao and Edwards, S. F. (1978) "Dynamics of Concentrated Polymer Systems Part 3. - The Constitutive Equation," *Journal Faraday Transactions II: Chemical Physics*, **74**, pp. 1818 - 1832.

Doi, Masao and Edwards, S. F. (1978) "Dynamics of Concentrated Polymer Systems Part 4. - Rheological Properties," *Journal Faraday Transactions II: Chemical Physics*, **75** pp. 38 - 54.

Doi, Masao, and Edwards, S. F. (1986). "The Theory of Polymer Dynamics," Oxford University Press.

Edwards, S. F. (1977). "The Theory of Rubber Elasticity," *The British Polymer Journal*, pp. 140 - 143.

Eringen, A. C. (1967). "Mechanics of Continua," John Wiley & Sons.

Feng, William W. and Hung, T. (1992). "Extension and Torsion of Hyperviscoelastic Cylinders," *International J. Non-Linear Mechanics*, **27**, 3, pp. 329 - 335.

Ferry, John D. (1980). "Viscoelastic Properties of Polymers ," John D. Ferry. 3d ed.John Wiley and Sons.

Ferry, John D. (1991). "Some reflections on the early development of polymer dynamics: viscoelasticity, dielectric dispersion, and self diffusion," *Macromolecules*, **24**, 19, pp. 5237 - 5245.

Flory, P. J. (1943). *J. Chem. Physics*, **11**, p. 512.

Flory, P. J. (1961). "Thermodynamic Relations for High Elastic Materials," *Transactions Faraday Society*, **57**, pp. 829 - 838.

Flory, P. J. (1977). "Theory of Elasticity of Polymer Networks. The Effect of Local Constraint on Junctions," *The Journal of Chemical Physics,* **66,** pp. 5720 - 5729.

Gaylord, R. and Weiss, G. and Dimarzio, E. (1986). "Nonequilibrium Mechanical Response of a Cross-Linked Network," *Macromolecules* , **19**, pp. 927 - 929.

Goldberg, W. and Lianis, G. (1970)., "Stress Relaxation in Combined Torsion Tension," *Journal of Applied Mechanics, Trans. ASME*, **37**, 1, pp. 53-60.

Gottlieb, Moshe and Gaylord, R. (1983). "Experimental Tests of Entanglement Models of Rubber Elasticity: 1. Uniaxial Extension-Compression," *Polymer*, **24**, pp. 1644 - 1646.

Graessley, W. W. (1982). *Adv. Polym. Sci.*, **46**, p. 67.

Herrmann, L. R. (1965). "On a General Theory of Viscoelasticity," *Journal of the Franklin Institute*, **280**, 3, pp. 244 - 255.

Herrmann, L. R. and Peterson, F. E. (1968). "A Numerical Procedure for Viscoelastic Stress Analysis," Proceedings 7th Meeting of ICRPG Mechanical Behavior Working Group, Orlando, FL.

Higgs, P. G. and Gaylord, R. J. (1990). "Slip - links, Hoops, and Tubes: Tests of Entanglement Models of Rubber Elasticity," *Polymer*, **31**, pp. 70 - 73.

Hughes, Thomas J. R. (1980). "Finite Rotation Effects in Numerical Integration of Rate Constitutive Equations Arising in Large-Deformation Analysis," *Inter. J. Numerical Meth. Engng.*, **15**, pp. 1862 - 1867.

Hughes, Thomas J. R. (1987). "The Finite Element Method," Prentice-Hall

James, A. G., Green, A. and Simpson, G. M. (1975). *Journal of Applied Polymer Science*, **19**, p. 2033.

James, H. M. and Guth, E. (1943). *J. Chem. Phys.*, **11**, p. 455.

Johnson, A. R. and Quigley, C. J. (1992). "A Viscohyperelastic Maxwell Model for Rubber Viscoelasticity," *Rubber Chemistry and Technology*, **65**, pp. 137 - 153.

Jones, D. F. and Treloar, L. R. G. (1975). "The Properties of Rubber in Pure Homogeneous Strain," *J. Phys. D: Appl. Phys.*, **8**, pp. 1285 - 1304.

Key, Samuel W. and Krieg, Raymond D. (1982). "On the Numerical Implementation of Inelastic Time Dependent and Time Independent, Finite Strain Constitutive Equations in

Structural Mechanics," *Computer Methods in Applied Mechanics and Engineering*, **33**, pp. 439 - 452.

Malkus, David S. and Hughes, Thomas J. R. (1978). "Mixed Finite Element Methods - Reduced and Selective Integration Techniques: A Unification of Concepts," *Computer Methods in Applied Mechanics and Engineering*, **15**, pp. 63 - 81.

Malvern, L. E. (1969). "Introduction to the Mechanics of a Continuous Medium," Prentice-Hall.

Mark, James E. and Erman, Burak (1988). "Rubberlike Elasticity a Molecular Primer," John Wiley & Sons.

Marrucci, G. (1979). "A Mechanical Model for Rubbers Containing Entanglements," *Rheologica Acta*, **18**, 2, pp. 193 - 198.

McGuirt, C. and Lianis G. (1970)., "Constitutive Equations for Viscoelastic Solids under Finite Uniaxial and Biaxial Deformations,", *Trans. Soc. Rheology*, **14**, 2, pp. 117-134.

McGuirt, C. and Lianis G.,(1969). "Experimental Investigation of Non-Linear, Non-Isothermal Viscoelasticity," *International Journal of Engineering Science* , **7**, 6, pp. 579-598.

Mooney, M. (1959). "A Diffusion Theory of the Visco-Elasticity of Rubbery Polymers in Finite Elastic Strain," *Journal of Polymer Science*, **34**, pp. 599 - 626.

Ogden, R. W. (1972). "Large Deformation Isotropic Elasticity - on the Correlation of Theory and Experiment for Incompressible Rubberlike Solids," *Proc. R. Soc. Lond. A.*, **326**, pp. 565 - 584.

Ogden, R. W. (1984). "Non-Linear Elastic Deformations," John Wiley and Sons.

Onat, E. T., Leckie, F. A. (1988). "Representation of Mechanical Behavior in the Presence of Changing Internal Structure," *Journal of Applied Mechanics,* **55**, pp. 1 - 10.

Peng, S. T. J. and Landel, R. F. (1972). "Stored Energy Function of Rubbberlike Materials Derived from Uniaxial Tension," *J. Applied Physics*, **43**, pp. 3063 - 3067.

Peng, S. T. J. and Landel, R. F. (1975). "Stored Energy Function and Compressibility of Compressible Rubberlike Materials under Large Strain," *J. Applied Physics*, **46**, pp. 509 - 517.

Peng, S. T. J. and Valanis, K. C. and Landel, R. F. (1977). "Nonlinear Viscoelasticity and Relaxation Phenomena of Polymer Solids," *Acta Mechanica*, **25**, pp. 229 - 240.

Schapery, R. A. (1969). "On the Characterization of Nonlinear Viscoelastic Materials," *Polymer Engineering and Science*, **9**, 4, pp. 295 - 310.

Scholtens, B. J. R. and Henk, Booij (1986). "Nonlinear Viscoelastic Analysis of Uniaxial Stress-Strain Measurements of Elastomers at Constant Stretching Rates," *Journal of Rheology*, **30**, 2, pp. 301 - 312.

Scholtens, B. J. R. and Leblans P. R. (1986). "Nonlinear Viscoelasticity of Noncrystalline EPDM Rubber Networks,", *Journal of Rheology*, **30**, 2, pp. 313-335.

Simo, J. C. (1987). "On a Fully Three-Dimensional Finite-Strain Viscoelastic Damage Model: Formulation and Computational Aspects," *Computer Methods in Applied Mechanics and Engineering*, **60**, pp. 153 - 173.

Simo, J. C. and Taylor, R. L. (1982). "Penalty Function Formulations for Incompressible Nonlinear Elastostatics," *Computer Methods in Applied Mechanics and Engineering*, **35**, pp. 107 - 118.

Smith, T. L. (1962). *Trans. Soc. Rheol.* **6**, pp. 61-68.

Smith, T.L. and Dickie, R.A. (1969). *J. Polym. Sci.* , *Pt. A-2*, **7**, p. 635.

Stroud, A. (1971). "Approximate Calculation of Multiple Integrals," Prentice-Hall.

Sullivan, J. L. (1987). "A Nonlinear Viscoelastic Model for Representing Nonfactorizible Time-Dependent Behavior in Cured Rubber," *Journal of Rheology*, **31**, 3, pp. 271 - 295.

Sussman, Theodore and Bathe, K. J. (1987). "A Finite Element Formulation for Nonlinear Incompressible Elastic and Inelastic Analysis," *Computers and Structures*, **26**, pp. 357 - 409.

Taylor, R. L., Pister, K. S. and Goudreau, G. L. (1970). "Thermomechanical Analysis of Viscoelastic Solids," *International Journal of Numerical Methods in Engineering*, **2**, pp. 45 - 59.

Treloar, L. R. G. (1975). "Physics of Rubber Elasticity," Oxford, Claredon Press.

Treloar, L. T. G. and Riding, G. (1979). "A non-Gaussian Theory for Rubber in Biaxial Strain. I. Mechanical Properties," *Proc. R. Soc. Lond. A.*, **369**, pp. 261 - 280.

Tschoegl, N. W. (1979). "Phenomenological Aspects of the Deformation of Elastomeric Networks," *Polymer*, **20**, pp. 1365 - 1370.

Valanis, K.C and Landel, R.F. (1967). "The Strain-Energy of a Hyperelastic Material in Terms of Extension Ratios," *Journal of Applied Physics*, **38**, 7, pp. 2997-3002.

Vangerko, H. and Treloar, L. R. G. (1978). "The Inflation and Extension of Rubber Tube for Biaxial Strain Studies," *J. Phys. D: Appl. Phys.*, **11**, pp. 1969 - 1978.

Wagner, M. H. and Schaeffer, J. (1992). "Nonlinear Strain Measures for General Biaxial Extension of Polymer Melts," *Journal of Rheology*, **36**, 1, pp. 1 - 26.

Wagner, M. H. and Schaeffer, J. (1993). "Rubbers and Polymer Melts: Universal Aspects of Nonlinear Stress-Strain Relations," *Journal of Rheology*, **37**, 4, pp. 643 - 661.

Ward, I. M. (1983). "Mechanical Properties of Solid Polymers," John Wiley and Sons.

Wu, P.D. and van der Giessen, E. (1993). "On Improved Network Models for Rubber Elasticity and Their Applications to Orientation Hardening in Glassy Polymers," *J. Mech. Phys. Solids*, **41**, 3, pp. 427-456.

Yuan H. and Lianis G. (1972). " Experimental Insvestigation of Nonlinear Viscoelasticity in Combined Finite Torsion-Tension" *Trans. Soc. Rheology*, **16**, 4, pp. 615-633.

Zapas, Louis J. (1966). "Viscoelastic Behavior Under Large Deformations," *Inst. for Basic Standards, National Bureau of Standards*, **70**, 6, pp. 525 - 532.

APPENDIX A

The principle stresses are found by taking the derivative of the free energy W (Eq. 1.2.5) with respect to principle stretches such that:

$$\sigma_1 - \sigma_3 = \lambda_1 \frac{\partial}{\partial \lambda_1}\left[n \int_0^{2\pi}\int_0^{\pi} w(\lambda)\ \frac{\sin\Theta}{4\pi}\, d\Theta\, d\Phi \right] - \lambda_3 \frac{\partial}{\partial \lambda_3}\left[n \int_0^{2\pi}\int_0^{\pi} w(\lambda)\ \frac{\sin\Theta}{4\pi}\, d\Theta\, d\Phi \right] \qquad \text{(A.1)}$$

Where σ_i and λ_i are the ith principle stress and stretch respectively. Now using

$$\lambda^2(\Theta,\Phi) = \lambda_1^2\ \cos\Theta + \lambda_2^2 \sin\Theta \sin\Phi\ + \lambda_3^2 \sin\Theta \cos\Phi$$

and Eq. 1.2.6, the following derivative is found:

$$\frac{dw(\lambda)}{d\lambda_1} = \sqrt{N}\ kT\, L^{-1}(\frac{\lambda}{\sqrt{N}})\left(\lambda_1 \cos^2\Theta\right) \qquad \text{(A.2)}$$

Using A.2 and a similar expression for the λ_3 derivative in Eq. A.1 gives:

$$\sigma_1 = G\sqrt{N} \int_0^{2\pi}\int_0^{\pi} \frac{1}{\lambda} L^{-1}(\frac{\lambda}{\sqrt{N}})\left(\lambda_1^2 \cos^2\Theta - \lambda_3^2 \sin^2\Theta\, \sin^2\Phi\right) \frac{\sin\Theta}{4\pi}\, d\Theta\, d\Phi \qquad \text{(A.3)}$$

such that $\sigma_3 = 0$ and G = nkT. Exploiting symmetry, and making the change of variable $C = \cos\Theta$, Eq. A.3 is modified as such:

$$\sigma_1 = 8\, G\sqrt{N} \int_0^{\pi/2}\int_0^{1} \frac{1}{\lambda} L^{-1}(\frac{\lambda}{\sqrt{N}})\left(\lambda_1^2 C^2 - \lambda_3^2 (1 - C^2) \sin^2\Phi\right) dC\, d\Phi \qquad \text{(A.4)}$$

Modifying A.4 for uniaxial tension $\lambda_3 = 1/\sqrt{\lambda_1}$ gives:

$$\sigma_1 = 8\,G\sqrt{N}\int_0^{\pi/2}\!\!\int_0^{1} \frac{1}{\lambda} L^{-1}\!\left(\frac{\lambda}{\sqrt{N}}\right)\left(\lambda_1^2 C^2 - \frac{1}{\lambda_1}\left(1 - C^2\right)\sin^2\Phi\right) dC\, d\Phi \qquad \text{(A.5)}$$

For equibiaxial tension using the coordinate system in Fig. 1.2.4 (b), σ_2 is considered instead of σ_1 and $\lambda_1 = 1/\lambda_2$ such that

$$\sigma_2 = 8\,G\sqrt{N}\int_0^{\pi/2}\!\!\int_0^{1} \frac{1}{\lambda} L^{-1}\!\left(\frac{\lambda}{\sqrt{N}}\right)\left(\lambda_2^2 C^2 - \frac{1}{\lambda_2^2}\left(1 - C^2\right)\sin^2\Phi\right) dC\, d\Phi \qquad \text{(A.6)}$$

Figs 1.2.5 and 1.2.5 are plotted as stress per undeformed area $f = \sigma_1/\lambda_1$ while Fig. 1.2.6 is plotted as $f = \sigma_2/\lambda_2$.

Eq. A.5 and A.6 was integrated numerically by an adaptive Gauss point integration scheme. The rectangular domain is discretized into panels each containing 36 (6x6) Gauss points. The adaptive scheme is outlined as follows:

1. Discretize the domain (Φ,C) into 4 panels (1-4) and compute the integrals (I_1 - I_4) for each panel (Fig. 1a)

2. Subdivide the first panel into 4 sub-panels (1.1-1.4) and recompute the integral for the domain of panel number 1 (Fig. 1b) such that

$$I_1^s = \sum_{i=1}^{4} I_{1.i}$$

3. If $\left| I_1 - I_1^s \right| < \varepsilon$ where ε is some desired tolerance then I_1^s is used for value of the integral over the domain of panel 1 and step 2 is repeated for the panel 2 (Fig. 2a).

4. If the difference is greater than the tolerance ε, then panel 1.1 is subdivided into 4 sub-panels (1.1.1-1.1.4) (Fig. 2b) and checked, such that

$$I_{1.1}^s = \sum_{i=1}^{4} I_{1.1.i}$$

and $\left| I_{1.1} - I_{1.1}^s \right| < \varepsilon$ must be satisfied or further subdivision of 1.1 is necessary.

The subdivision process is repeated for all the panels and sub-panels and their values are summed to give the integral of the entire domain. An error tolerance 1×10^{-6} was used to calculate the integrals throughout this work.

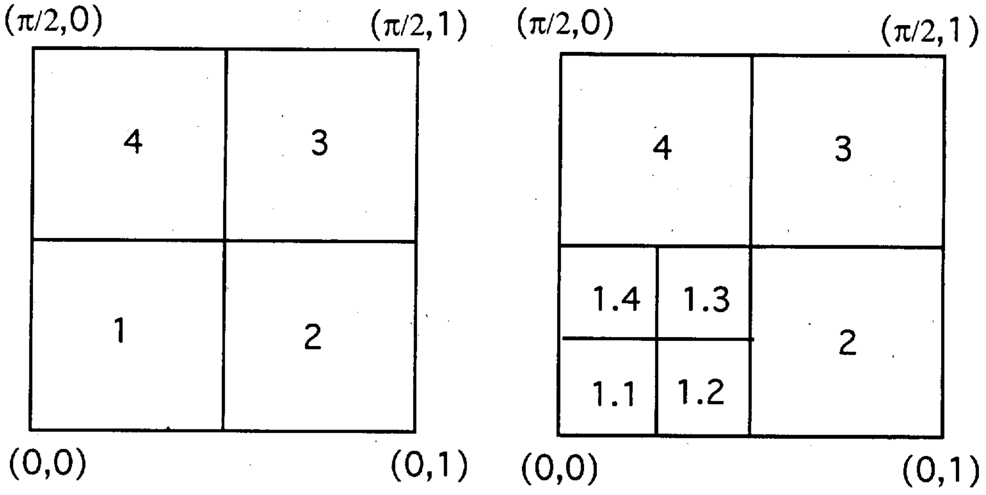
(π/2,0)
(π/2,1)
4
3
1
2
(0,0)
(0,1)
(π/2,0)
(π/2,1)
4
3
1.4
1.3
1.1
1.2
2
(0,0)
(0,1)

(a) (b)

Fig. 1 (a) First 4 panels of domain. (b) Subdivision of panel 1 into 4 sub-panels 1.1-1.4

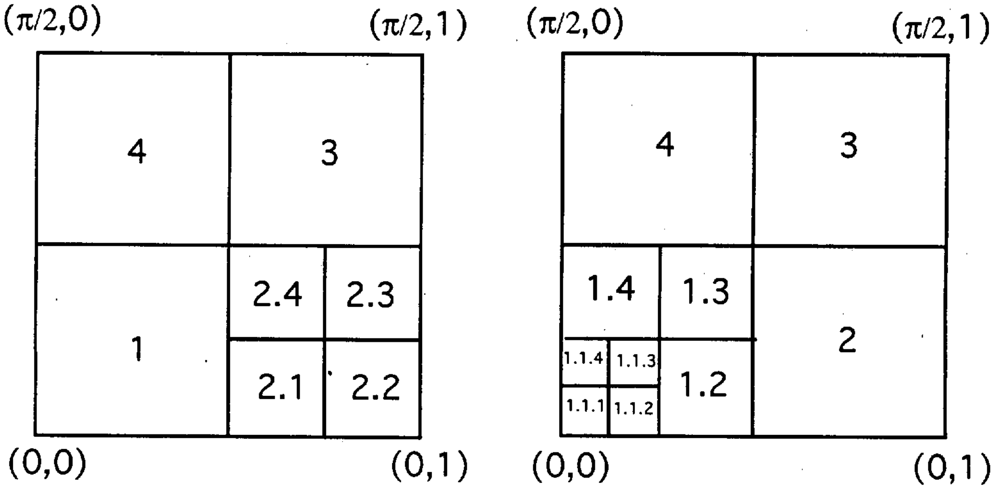
(π/2,0)
(π/2,1)
4
3
1
2.4
2.3
2.1
2.2
(0,0)
(0,1)
(π/2,0)
(π/2,1)
4
3
1.4
1.3
1.1.4
1.1.3
1.1.1
1.1.2
1.2
2
(0,0)
(0,1)

(a) (b)

Fig. 2 (a) Subdivision of panel 2. (b) Subdivision of panel 1.1

APPENDIX B

Uniaxial Tension

For uniaxial tension and compression Eq. 2.2.9 and 2.2.20 can be solved analytically. Assuming incompressibility, the following transformation is used:

$$\begin{Bmatrix} u'_1 \\ u'_2 \\ u'_3 \end{Bmatrix} = \begin{bmatrix} \lambda_1 & 0 & 0 \\ 0 & \lambda_1^{-1/2} & 0 \\ 0 & 0 & \lambda_1^{-1/2} \end{bmatrix} \begin{Bmatrix} \cos\Theta \\ \sin\Theta\cos\Phi \\ \sin\Theta\sin\Phi \end{Bmatrix} = \begin{Bmatrix} \lambda_1\cos\Theta \\ \lambda_1^{-1/2}\sin\Theta\cos\Phi \\ \lambda_1^{-1/2}\sin\Theta\sin\Phi \end{Bmatrix} \tag{B.1}$$

From Eq. B.1 the stretch is then found to be:

$$\lambda = \sqrt{u'_k u'_k} = \sqrt{\lambda_1^2\cos^2\Theta + \lambda_1^{-1}\sin^2\Theta} \tag{B.2}$$

and upon integration (Marrucci, 1979), the average stretch is:

$$\langle\lambda\rangle = \frac{1}{2}\int_0^\pi \sqrt{\lambda_1^2\cos^2\Theta + \lambda_1^{-1}\sin^2\Theta}\,\sin\Theta\, d\Theta = \frac{1}{2}\lambda_1\left(1 + \frac{\sinh^{-1}\sqrt{\lambda_1^3 - 1}}{\lambda_1^{3/2}\sqrt{\lambda_1^3 - 1}}\right) \tag{B.3}$$

For uniaxial loading $\sigma_2 = \sigma_3 = 0$. Using Eqs. 2.2.20 (b) and B.1, the longitudinal stress σ_1 is described by the following relation:

$$\sigma_1 = \sigma_1 - 1/2(\sigma_2 + \sigma_3) = G\sqrt{N_o}\, L^{-1}\left(\frac{\langle\lambda\rangle}{\sqrt{N_o}}\right) \int_0^{2\pi}\int_0^{\pi} \frac{\lambda_1^2\cos^2\Theta - \frac{1}{2}\lambda_1^{-1}\sin^2\Theta}{\lambda}\,\frac{\sin\Theta}{4\pi}\, d\Theta\, d\Phi$$

$$= \frac{3}{2}\, G\sqrt{N_o}\, L^{-1}\left(\frac{\langle\lambda\rangle}{\sqrt{N_o}}\right) \lambda_1\, \frac{\lambda_1^3 + \frac{1}{2}}{\lambda_1^3 - 1}\left(1 - \frac{4\lambda_1^3 - 1}{2\lambda_1^3 + 1}\,\frac{\sinh^{-1}\sqrt{\lambda_1^3 - 1}}{\lambda^{3/2}\sqrt{\lambda_1^3 - 1}}\right) \tag{B.4}$$

where $\langle\lambda\rangle$ is defined by Eq. B.3.

Equibiaxial Tension

Eq. B.3 and B.4 may also be used for equibiaxial tension in the 2-3 plane (i.e. $\sigma_2 = \sigma_3$, and $\sigma_1 = 0$). Substituting $\lambda_1 = (\lambda_2)^{-2}$ * into Eqs. B.3, B.4 gives the average stretch (Eq. B.5) and equibiaxial stress σ_2 (B.6).

$$\langle\lambda\rangle = \frac{1}{2}\lambda_2^{-2}\left(1+\frac{\sinh^{-1}\sqrt{\lambda_2^{-6}-1}}{\lambda_2^{-3}\sqrt{\lambda_2^{-6}-1}}\right) \qquad \text{(B.5)}$$

$$\sigma_2 = \sigma_2 - \sigma_1 = -\frac{3}{2}\, G\sqrt{N_o}\, L^{-1}\left(\frac{\langle\lambda\rangle}{\sqrt{N_o}}\right)\lambda_2^{-2}\,\frac{\lambda_2^{-6}+\frac{1}{2}}{\lambda_2^{-6}-1}\left(1-\frac{4\lambda_2^{-6}-1}{2\lambda_2^{-6}+1}\,\frac{\sinh^{-1}\sqrt{\lambda_2^{-6}-1}}{\lambda_2^{-3}\sqrt{\lambda_2^{-6}-1}}\right)$$

(B.6)

Pure Shear

For pure shear Eq. 2.2.9 and 2.2.20 cannot be solved analytically, hence the numerical quadrature method similar to that described in Appendix A was used. Again assuming incompressiblity, the following transformation is used:

$$\begin{Bmatrix} u'_1 \\ u'_2 \\ u'_3 \end{Bmatrix} = \begin{bmatrix} \lambda_2^{-1} & 0 & 0 \\ 0 & \lambda_2 & 0 \\ 0 & 0 & 1 \end{bmatrix} \begin{Bmatrix} \cos\Theta \\ \sin\Theta\cos\Phi \\ \sin\Theta\sin\Phi \end{Bmatrix} = \begin{Bmatrix} \lambda_2^{-1}\cos\Theta \\ \lambda_2\sin\Theta\cos\Phi \\ \sin\Theta\sin\Phi \end{Bmatrix} \qquad \text{(B.7)}$$

From B.7 the stretch is shown to be :

$$\lambda = \sqrt{u'_k u'_k} = \sqrt{\lambda_2^{-2}\cos^2\Theta+\lambda_2^{2}\sin^2\Theta\cos^2\Phi+\sin^2\Theta\sin^2\Phi} \qquad \text{(B.8)}$$

The equation for the average stress is:

---

* From incompressibility $\lambda_1\lambda_2\lambda_3 = \lambda_1(\lambda_2)^2 = 1$ for equibiaxial stretching in the 2-3 plane.

$$\langle\lambda\rangle = \int_0^{2\pi}\int_0^{\pi} \sqrt{\lambda_2^{-2}\cos^2\Theta+\lambda_2^{2}\sin^2\Theta\cos^2\Phi+\sin^2\Theta\sin^2\Phi}\;\frac{\sin\Theta}{4\pi}\,d\Theta\,d\Phi \tag{B.9}$$

According to the coordinate system used (Fig. 2.3.1) , $\sigma_1 = 0$ for pure shear; therefore, from Eqs. 20 and B.7, the longitudinal stress σ_1 is described by the following relation:

$$\sigma_2 = \sigma_2 - \sigma_1 = G\sqrt{N_o}\,L^{-1}\left(\frac{\langle\lambda\rangle}{\sqrt{N_o}}\right)\int_0^{2\pi}\int_0^{\pi}\frac{\lambda_2^{2}\sin^2\Theta\cos^2\Phi - \lambda_2^{-2}\cos^2\Theta}{\lambda}\;\frac{\sin\Theta}{4\pi}\,d\Theta\,d\Phi \tag{B.10}$$

Eqs. B.9 and B.10 cannot be solved analytically so the numerical quadrature technique similar to that described in Appendix A is used.

APPENDIX C

Proof of Eq. 4.4.2

The following is a proof of Eq 4.4.2 using a single exponential kernel. The proof can be easily generalized to include a Prony series kernel.

Lemma 1.

$$\frac{\partial}{\partial \lambda(t)} \int_{-\infty}^{t} c\, e^{-(t-\tau)/t_o}\, \dot{\lambda}(\tau)\, d\tau =$$

$$\frac{\partial}{\partial \lambda(t)} \lim_{\Delta t \to 0} \left[\frac{(1 - e^{-\Delta t/t_o})}{\Delta t} (\lambda(t) - \lambda(t - \Delta t)) + e^{-\Delta t/t_o} \int_{-\infty}^{t-\Delta t} e^{(t-\Delta t-\tau)/t_o}\, \dot{\lambda}(\tau)\, d\tau \right] = 1$$

Lemma 2.

The stretch $\lambda = \lambda(\Theta,\Phi,t)$ is a function of the Cauchy Green tensor $C(t)_{KL}$ and the direction cosines i.e.

$$\lambda = \lambda(\Theta,\Phi,t) = \sqrt{M_K\, C(t)_{KL} M_L}$$

therefore

$$\frac{\partial}{\partial C_{KL}} \int_0^{2\pi}\!\!\int_0^{\pi} f(\lambda) \frac{\sin\Theta}{4\pi}\, d\Theta\, d\Phi = \int_0^{2\pi}\!\!\int_0^{\pi} \frac{\partial f(\lambda)}{\partial \lambda} \frac{1}{2} \frac{M_K M_L}{\lambda} \frac{\sin\Theta}{4\pi}\, d\Theta\, d\Phi$$

Using Lemma 1. and Lemma 2., the gradient of the free energy Eq. 4.4.1 is taken to be:

$$\frac{\partial \Psi^V}{\partial E(t)_{KL}} = 2 \frac{\partial}{\partial C(t)_{KL}} \frac{1}{2} \int_0^{2\pi}\!\!\int_0^{\pi} \left(\int_{-\infty}^{t} c\, e^{-(t-\tau)/t_o}\, \dot{\lambda}(\tau)\, d\tau \right)^2 \frac{\sin\Theta}{4\pi}\, d\Theta\, d\Phi$$

$$= \int_0^{2\pi}\!\!\int_0^{\pi} \left(\int_{-\infty}^{t} c\, e^{-(t-\tau)/t_o}\, \dot{\lambda}(\tau)\, d\tau \right) \frac{M_K M_L}{\lambda} \frac{\sin\Theta}{4\pi}\, d\Theta\, d\Phi$$

Which is identical to the viscoelastic stress given by Eq. 4.3.5. with a single term exponential kernel.

Proof of $\Lambda \geq 0$

Lemma 3.

$$\frac{\partial}{\partial t}\left(\int_{-\infty}^{t} c\,e^{-(t-\tau)/t_o}\,\dot{\lambda}(\tau)\,d\tau\right) = -\frac{1}{t_o}\int_{-\infty}^{t} c\,e^{-(t-\tau)/t_o}\,\dot{\lambda}(\tau)\,d\tau + c\,\dot{\lambda}(t)$$

but $E(t)_{KL}$ is constant therefore $\dot{\lambda}(t) = 0$ and

$$\frac{\partial}{\partial t}\left(\int_{-\infty}^{t} c\,e^{-(t-\tau)/t_o}\,\dot{\lambda}(\tau)\,d\tau\right) = -\frac{1}{t_o}\int_{-\infty}^{t} c\,e^{-(t-\tau)/t_o}\,\dot{\lambda}(\tau)\,d\tau$$

By definition

$$\Lambda = -\frac{\partial}{\partial t}\frac{1}{2}\int_{0}^{2\pi}\int_{0}^{\pi}\left(\int_{-\infty}^{t} c\,e^{-(t-\tau)/t_o}\,\dot{\lambda}(\tau)\,d\tau\right)^{2}\frac{\sin\Theta}{4\pi}\,d\Theta\,d\Phi$$

Therefore using Lemma 3.

$$\Lambda = \int_{0}^{2\pi}\int_{0}^{\pi}\frac{1}{t_o}\left(\int_{-\infty}^{t} c\,e^{-(t-\tau)/t_o}\,\dot{\lambda}(\tau)\,d\tau\right)^{2}\frac{\sin\Theta}{4\pi}\,d\Theta\,d\Phi \geq 0 \qquad \text{(qed.)}$$

APPENDIX D

This Appendix includes the derivation of Eq. 4.5.2 and Eq. 4.5.3. First the derivation of 4.5.2 is considered.

Proof of Eq. 4.5.2

The definition of the viscoelastic backstress is,

$$S^{v}_{KL}(t) = \int_0^{2\pi}\int_0^{\pi}\left(\int_{-\infty}^{t} G(t-\tau)\frac{d\lambda(\Theta,\Phi,\tau)}{d\tau}\,d\tau\right)\frac{M_K M_L}{\lambda(\Theta,\Phi)}\sin\Theta\, d\Theta\, d\Phi \qquad \text{(D.1)}$$

Taking the time derivative of the following approximation for the strectch,

$$\lambda(\Theta,\Phi) \approx \sqrt{I_1/3} + \frac{1}{2}\left(\frac{I_1}{3}\right)^{-1/2}\left(\lambda^2(\Theta,\Phi) - \frac{I_1}{3}\right) \qquad \text{(D.2)}$$

gives,

$$\dot{\lambda} \approx \frac{\sqrt{3}}{6}\frac{d}{dt}(I_1)^{1/2} + \frac{\sqrt{3}}{2}M_K M_L\frac{d}{dt}\left(I_1^{-1/2}C_{KL}\right) \qquad \text{(D.3)}$$

From here on, the differential area $\frac{\sin\Theta}{4\pi}$ $d\Theta\, d\Phi$ is replaced by $d\Omega$ and the double integral is replace by the integration over Ω. Substituting Eq. D.3 into Eq. D.1 gives

$$S^{v}_{KL}(t) = \int_{\Omega}\frac{M_K M_L}{\lambda}\,d\Omega\int_{-\infty}^{t} G(t-\tau)\frac{\sqrt{3}}{6}\frac{d}{d\tau}(I_1)^{1/2}d\tau \; +$$

$$\int_{\Omega}\frac{M_K M_L M_O M_P}{\lambda}\,d\Omega\int_{-\infty}^{t} G(t-\tau)\frac{\sqrt{3}}{2}\frac{d}{d\tau}\left(I_1^{-1/2}C_{OP}\right)d\tau \qquad \text{(D.4)}$$

At this point the time and spacial integrations are decoupled. It remains to find an approximation of the spacial integrations. Many different methods were tried, the following method was the most successfull. Since $\lambda^2(\Theta,\Phi) = M_K C_{KL} M_L$ it is recognized that $\frac{\partial\lambda}{\partial C_{KL}} = \frac{1}{2}\frac{M_K M_L}{\lambda}$ and therefore:

$$\frac{1}{2}\int_\Omega \frac{M_K M_L}{\lambda}\, d\Omega = \frac{\partial}{\partial C_{KL}}\int_\Omega \lambda\, d\Omega \qquad \text{(D.5)}$$

Consequently, if the integration on the right hand side of (D.5) is approximated by invariants, the gradient of that approximation gives the desired result. This time a higher order approximation than that in Eq. 1 is used for λ is used to give better accuracy i.e.

$$\lambda \approx \sqrt{I_1/3} + \frac{1}{2}\left(\frac{I_1}{3}\right)^{-1/2}(\lambda^2 - \frac{I_1}{3}) + \frac{1}{8}\left(\frac{I_1}{3}\right)^{-3/2}(\lambda^2 - \frac{I_1}{3})^2 \qquad \text{(D.6)}$$

Substituting Eq. 6 into the spherical integral gives,

$$\int_\Omega \lambda\, d\Omega \approx \sqrt{I_1/3} + \frac{1}{2}\left(\frac{I_1}{3}\right)^{-1/2}\int_\Omega (\lambda^2(\Theta,\Phi) - \frac{I_1}{3})\, d\Omega + \frac{1}{8}\left(\frac{I_1}{3}\right)^{-3/2}\int_\Omega (\lambda^2(\Theta,\Phi) - \frac{I_1}{3})^2\, d\Omega \qquad \text{(D.7)}$$

Using the integral identities give by Eqs. 1.16 - 1.19 gives the following approximation,,

$$\int_\Omega \lambda\, d\Omega \approx \frac{\sqrt{3}}{10}(3I_1^{1/2} + \frac{I_2}{I_1^{3/2}}) \qquad \text{(D.8)}$$

Taking the derivatives of the strain invariants with respect to Greens tensor gives

$$\int_\Omega \frac{M_K M_L}{\lambda}\, d\Omega \approx \frac{\sqrt{3}}{2}(I_1^{-1/2} - \frac{3}{5}\frac{I_2}{I_1^{5/2}})\,\delta_{KL} - \frac{\sqrt{3}}{5}\, I_1^{-3/2} C_{KL} \qquad \text{(D.9)}$$

The second spacial integration in Eq. D.4 is approximated in the same fashion. It is recognized that,

$$\frac{4}{3}\frac{\partial}{\partial C_{KL}}\frac{\partial}{\partial C_{OP}}\int_\Omega \lambda^3\, d\Omega = \int_\Omega \frac{M_K M_L M_O M_P}{\lambda} d\Omega \qquad \text{(D.10)}$$

Using the same Taylor expansion method used to get (D.6) the following approximation is given for λ^3,

$$\lambda^3 \approx \left(\frac{I_1}{3}\right)^{3/2} + \frac{3}{2}\left(\frac{I_1}{3}\right)^{1/2}\left(\lambda^2 - \frac{I_1}{3}\right) + \frac{3}{8}\left(\frac{I_1}{3}\right)^{-1/2}\left(\lambda^2 - \frac{I_1}{3}\right)^2 \qquad \text{(D.11)}$$

Substitution of (D.11) into the integral and using the integral identities given by Eqs. 1.42 - 1.44 gives the following approximation,

$$\int_\Omega \lambda^3 \, d\Omega \approx \frac{13}{10}\left(\frac{I_1}{3}\right)^{3/2} - \frac{1}{10}\left(\frac{I_1}{3}\right)^{-1/2} I_2 \qquad \text{(D.12)}$$

Taking the first and second derivatives of (D.12) with respect to C_{KL} gives,

$$\int_\Omega \frac{M_K M_L M_O M_P}{\lambda} d\Omega \approx \left[\left(\frac{13}{90}\left(\frac{I_1}{3}\right)^{-1/2} - \frac{1}{90}\left(\frac{I_1}{3}\right)^{-5/2} I_2\right)\delta_{OP}\delta_{KL} + \right.$$
$$\left. \frac{1}{45}\left(\frac{I_1}{3}\right)^{-3/2}\left(\delta_{OP}C_{KL} + C_{OP}\delta_{KL}\right) + \frac{1}{15}\left(\frac{I_1}{3}\right)^{-3/2}\left(\delta_{OK}\delta_{PL} + \delta_{PK}\delta_{OL}\right)\right] \qquad \text{(D.13)}$$

Now results from (D.9) and (D.13) can be substituted into (D.4) to give,

$$S^v_{KL}(t) \approx \left[\frac{\sqrt{3}}{2}\left(I_1^{-1/2} - \frac{3}{5}\frac{I_2}{I_1^{5/2}}\right)\delta_{KL} - \frac{\sqrt{3}}{5} I_1^{-3/2} C_{KL}\right] \int_{-\infty}^{t} G(t-\tau)\frac{\sqrt{3}}{6}\frac{d}{dt}(I_1)^{1/2} d\tau \; +$$
$$\left[\left(\frac{13}{90}\left(\frac{I_1}{3}\right)^{-1/2} - \frac{1}{90}\left(\frac{I_1}{3}\right)^{-5/2} I_2\right)\delta_{IJ}\delta_{KL} + \frac{1}{45}\left(\frac{I_1}{3}\right)^{-3/2}\left(\delta_{IJ}C_{KL} + C_{IJ}\delta_{KL}\right) + \right.$$
$$\left. \frac{1}{15}\left(\frac{I_1}{3}\right)^{-3/2}\left(\delta_{IK}\delta_{JL} + \delta_{JK}\delta_{IL}\right)\right] \int_{-\infty}^{t} G(t-\tau)\frac{\sqrt{3}}{2}\frac{d}{dt}\left(I_1^{-1/2} C_{IJ}\right) d\tau$$
$$\text{(D.14)}$$

It is easily seen that,

$$\int_{-\infty}^{t} G(t-\tau)\frac{d}{d\tau}(I_1^{1/2})\, d\tau = \delta_{IJ}\int_{-\infty}^{t} G(t-\tau)\frac{d}{d\tau}(I_1^{-1/2} C_{IJ})\, d\tau \qquad \text{(D.15)}$$

Substituting (D.15) into (D.14), combining like terms and making use of the symmetry of C_{IJ} the following simplification of (D.14) results:

$$S^{v}_{KL}(t) \approx \frac{I_1^{-1/2}}{30}\left[(14 - 9\frac{I_2}{I_1^2})\,\delta_{KL}\delta_{IJ} - \frac{9}{I_1}\delta_{KL}C_{IJ} - \frac{18}{I_1}\delta_{IJ}C_{KL} + 6\,\delta_{KI}\delta_{LJ}\right]\int_{-\infty}^{t} G(t-\tau)\,\frac{d}{d\tau}(I_1^{-1/2}\,C_{IJ})\,d\tau \tag{D.16}$$

This is identical to Eq. 4.5.2. As mentioned, the derivative of (D.16) with respect to the strain gives a nonsymmetric tangent stiffness matrix. If the approximations given in Eq. D6 and Eq D.11 where one order lower (i.e. the same order as Eq. D.2), the expression for the stress would be the same as the symmetric form given by Eq. 4.5.4. It is the higher order approximations made in Eqs. D.6 and D.11 that give the additional accuracy but sacrifice the symmetry.

Proof of Eq. 4.5.2

The proof is given for a single exponential kernel function but is easily generalized for a Prony series. The derivation of Eq. of 4.5.3 starts from the definition of the scalar potential function (cf. Eq. 4.4.1)

$$\Psi^{V} = \frac{1}{2}\int_0^{2\pi}\int_0^{\pi}\left(\int_{-\infty}^{t} c\,e^{-(t-\tau)/t_o}\,\dot{\lambda}\,d\tau\right)^2 \frac{\sin\Theta}{4\pi}\,d\Theta\,d\Phi \tag{D.17}$$

Now substituting D.3 into D.17 gives,

$$\Psi^{V} \approx \frac{1}{2}\int_0^{2\pi}\int_0^{\pi}\left(\int_{-\infty}^{t} c\,e^{-(t-\tau)/t_o}\left(\frac{\sqrt{3}}{6}\,\frac{d}{d\tau}\,(I_1)^{1/2} + \frac{\sqrt{3}}{2}\,M_K M_L \frac{d}{d\tau}\left(I_1{}^{-1/2}C_{KL}\right)\right)d\tau\right)\times$$
$$\left(\int_{-\infty}^{t} c\,e^{-(t-\eta)/t_o}\left(\frac{\sqrt{3}}{6}\,\frac{d}{d\eta}\,(I_1)^{1/2} + \frac{\sqrt{3}}{2}\,M_N M_O \frac{d}{d\eta}\left(I_1{}^{-1/2}C_{NO}\right)\right)d\eta\right)\frac{\sin\Theta}{4\pi}\,d\Theta\,d\Phi \tag{D.18}$$

where the first time integration uses the dummy variable τ and the second time integration uses the dummy variable η. Now expanding terms and seperating the terms which are integrals over the spherical coordinates gives,

$$\Psi^V \approx \frac{c}{24}\left(\int_{-\infty}^{t} c\, e^{-(t-\tau)/t_o} \frac{d}{d\tau}(I_1)^{1/2}\, d\tau\right) \times \left(\int_{-\infty}^{t} c\, e^{-(t-\tau)/t_o} \frac{d}{d\eta}(I_1)^{1/2}\, d\eta\right) +$$

$$\frac{c}{4}\left(\int_{-\infty}^{t} c\, e^{-(t-\eta)/t_o} \frac{d}{d\eta}(I_1)^{1/2}\, d\eta\right) \times \left(\int_{-\infty}^{t} c\, e^{-(t-\tau)/t_o} \frac{d}{d\tau}\left(I_1^{-1/2}C_{KL}\right) d\tau\right) \times$$

$$\int_0^{2\pi}\int_0^{\pi} M_K M_L \frac{\sin\Theta}{4\pi}\, d\Theta\, d\Phi +$$

$$\frac{3c}{8}\left(\int_{-\infty}^{t} c\, e^{-(t-\tau)/t_o} \frac{d}{d\tau}\left(I_1^{-1/2}C_{KL}\right) d\tau\right) \times \left(\int_{-\infty}^{t} c\, e^{-(t-\eta)/t_o} \frac{d}{d\eta}\left(I_1^{-1/2}C_{NO}\right) d\eta\right) \times$$

$$\int_0^{2\pi}\int_0^{\pi} M_K M_L M_N M_O \frac{\sin\Theta}{4\pi}\, d\Theta\, d\Phi \tag{D.19}$$

Now the following integral identities are used,

$$\int_0^{2\pi}\int_0^{\pi} M_K M_L \frac{\sin\Theta}{4\pi}\, d\Theta\, d\Phi = \frac{1}{3}\,\delta_{KL} \tag{D.20}$$

$$\int_0^{2\pi}\int_0^{\pi} M_K M_L M_N M_O \frac{\sin\Theta}{4\pi}\, d\Theta\, d\Phi = \frac{1}{15}\left(\delta_{KL}\delta_{NO} + \delta_{KN}\delta_{LO} + \delta_{KO}\delta_{LN}\right) \tag{D.21}$$

Substitution of Eqs. D.20 and D.21 into D.19 and performing the inner products gives the desired result (cf. Eq. 4.5.3),

$$\Psi^v \approx \frac{3c}{20}\left(\int_{-\infty}^{t} e^{(t-\tau)/t_o}\frac{d}{d\tau}\left(I_1\right)^{1/2} d\tau\right)^2 +$$

$$\frac{c}{20}\int_{-\infty}^{t}\int_{-\infty}^{t} e^{(2t-\tau-\eta)/t_o}\frac{d}{d\tau}\left(I_1{}^{-1/2} C_{KL}\right)\frac{d}{d\eta}\left(I_1{}^{-1/2} C_{KL}\right) d\tau\, d\eta \qquad \text{(D.22)}$$